Alma Mater Studiorum – Università di Bologna

DOTTORATO DI RICERCA IN

Chimica

Ciclo 31°

Settore Concorsuale: 03/C2

Settore Scientifico Disciplinare: CHIM/04 CHIMICA INDUSTRIALE

Self-aggregated assembled with pre-programmed properties: nanoclusters and functional switching small molecules.

Candidato Simone Dell'Elce

Coordinatore Dottorato

Prof. Aldo Roda

Supervisore

Prof. Loris Giorgini

Cosupervisore

Dott. Vincenzo Palermo

Esame finale anno 2019

Abstract

The understanding of the role of the self-assembly mechanisms is crucial to realize molecularly precise self-organized systems at the nanoscale with a well-defined architectures and pre-programmed electronics properties. The PhD activities focused on the study of self-assembly mechanisms of model systems at liquid–solid interfaces forming meso- and macro-scopic ordered structures mainly investigated with advanced Scanning Probe Microscopies.

Two building blocks have been studied as ideal chemical models: i) synthesized metal-organic nanoclusters formed by 44 silver atoms coated by a monolayer of 30 thiol ligands (a.k.a. IBAN, intensely and broadly absorbing nanoparticles), and ii) commercial azobenzene molecules (Disperse orange 3 and Acid yellow 9).

IBANs fully monodispersed nanoparticles stable in solution used as prototype system to produce high quality macroscopic crystals. Conversely, commercially available on Sigma Aldrich, azobenzene molecules are used to produce functional architectures using scalable approaches. In particular, the integration of molecular switches with inorganic surfaces has recently shown an increasing interest to produce novel hybrid multifunctional materials.

IBANs can form 2D and 3D structures with different properties and crystals order while azobenzenes form self-assembled monolayers (SAMs). By chemical approach and solvent vapour annealing, a simple but powerful technique developed in our group, we could tune the morphology and the physico-chemical properties of such self-assembled structures with the aim of producing smart hybrid materials.

Table of Contents

Summary

List of Figures

List of Acronyms

SAM	Self Assembled Monolayer
4(FTP)	4 Fluorothiophenol
AZO	Azobenzenes
IBAN	Intensely and Broadly Absorbing nanoparticles
SVA	Solvent Vapour Annealing
SPM	Scanning Probe Microscopy
SFM	Scanning Force Microscopy
STM	Scanning Tunneling Microscopy
AFM	Atomic Force Microscopy
KPFM	Kelvin Probe Force Microscopy
FM-KPFM	Frequency Mode Kelvin Probe Force Microscopy
AM-KPFM	Amplitude Modulation Kelvin Probe Force Microscopy
TM	Tapping Mode
MFM	Magnetic Force Microscopy
CVD	Chemical Vapour Deposition
VdW	Van der Waals forces
XRD	X ray Diffraction analysis
GISAXS	Grazing Incidence Small Angle X ray Scattering
GIWAXS	Grazing Incidence Wide Angle X ray Scattering
ESCA	Electron Spectroscopy for Chemical Analysis
XPS	X ray photoemission Spectroscopy
EK	Kinetic Energy

MS	Mass Spectrometry
RGA	Residual Gas Analysis
A	Absorbance
RLS	Resonance Light Scattering
DMF	Dimethylformaamide
DCM	Dichloromethane
AgNP	Silver Nanoparticles
C1	Triclinic Crystal 3D
C2	Layered Crystal 2D
AZO1	Acid Yellow 9
AZO2	Disperse Orange 3

1.Introduction

1.1 Build-up new 2D/3D structures

Having control during the creation of fuctional nano structure is a challenge but also a target to functionalize a surface or to use metal organic framework in 2D or 3D structure with a defined shape, lateral dimension and uniformity. To this aim, supramolecular self-assembly of nanoobjects is a common approach to realize ordered structures, as example photonic crystals from colloids.
But, due to the complex interplay between covalent and supramolecular interactions control a nanostructure is tricky. The PhD period was focused on understanding the forces that govern supramolecular interactions, and how macromolecules are driven to self-assembly in ordered structures with specific properties. As models system were chosen two type of systems: one regarding silver nanoclusters, chosen inside the european project "ISWITCH" in cooperation with a switzerland partner. Nanoclusters studied, during the PhD period, in deep and with different type of instrumentation to have a complete picture of the behaviour of the aggregation system.
Second model, azobenzene, chosen due to the great knowledge got during decades on this system joined to the easy processability and manipulation of the molecules. This second model studied with less enphasis to confirm and use the knowledge and manual skills got during the first period of research.

1.1.1. Different approaches to Supramolecular Chemistry

The first term referred to nanotechnology came from Richard Feynman in 1957, with the work title "There is plenty of rooms at the bottom" in which he described the possibility to direct manipulate atoms. Inside his speech he described the idea, called "scale down", to build machine able to manipulate small object in a scale of 1:10 with the aim to build another machine smaller than before, and continuously… the new machine will be necessary for building another one but in scale 1:100 and so on.

Manipulate nano-machines or nano-objects was something that was also noticed, around ten years after by another man, Gordon E. Moore, one of the co-founders of Intel. In 1965 he observed that the number of transistors per square inch on an integrated circuit had doubled since the integrated circuit was first produced. From his initial observations, Moore then went onto predict that for every 18 months the complexity of an integrated circuit (generally proportional to the number of transistors) would double. This has been known as Moore's law. Although this law was right for a long time period today it has less impact due to the reach of a plateau in the down sizing transistors and nano-devices. Anyway it is interesting to see how just twenty years ago the dimension of transistors was around 500 nm that compared to the dimension of ten years after, 90 nm, give an idea how this law predict the story of modern technology.

Using a nanotechnology approach as top down or bottom up approach nowadays is possible to postpone the Moore's law, whose plateau is now closely to be reached. Where in the nanoworld (nanometer scale) the forces that play normally a crucial role in our life, gravity force become less prevalent, while surface tension and van der Waals forces become more active.

1.1.2. Top Down Approach

Nanotechnology is the science related to the construction of nano dimension devices. Spanning from 0.1 to 500 nm traditionally was defined from the break-down methodology. The top-down approach is the main method used in microfabrication where with an external control is possible to cut, mill, and shape a material into the desired shape and order.

An example of this classical method which use top down approach is the manipulation of a large block of silicon. During its process the starting material is cut, etched and sliced into the specific dimension. Other techniques as, Micropatterning techniques, photolithography and Inkjet printing as well as vapour treatment can be also inserted in this new top-down approaches to engineer nanostructures. To explain better how a top down approach works a briefly description of one of the most used micropatterning technique could help: photolithography, coming from the family of lithography (literally stone writing), is one of the most used in micro fabrication methodology. Using UV light as a pattern source, light carves the pattern on a photoactive organic polymer, the photoresist, which is coated onto a silicon wafer. The pattern then defines which areas of the underlying wafer are exposed for material deposition or removal. The light changes the solubility of the resist (making it more soluble or less soluble) that can be selectively removed by solvent. This

process is used to etch integrated circuits that are used in modern computer processors and memory chips.

Another fashionable top down method that became more present nowadays in particular in the world of 2D materials is scotch tape method. Starting from the piece of highly oriented graphite or another layered material, with the use the tape is possible to exfoliate the graphite thanks to its nature, producing fragments of mono- bi- tri and so on layer of graphene or related in function of the starting material.

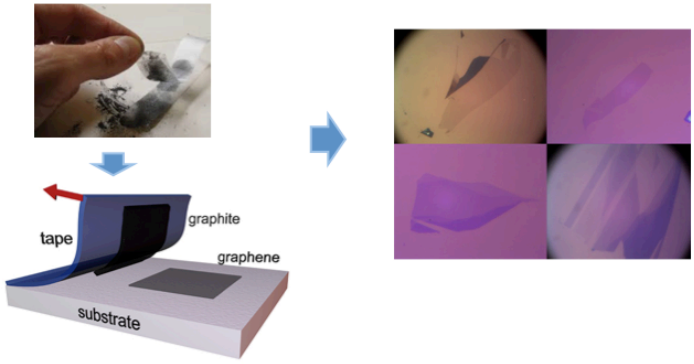

Fig 1.1 Schematic description of the scotch tape method, with optical images of mono, bi and tri layer of exfoliated graphene.

1.1.3. Bottom up approach

Top down method is not the only one to manipulate big complexes to produce nanoscopical object, bottom-up approach, another technique fully used in these years, consists of the building up of nanomaterials from smaller building blocks. This approach has given rise to nanochemistry, typically with the use of self-assembly methods for the formation of highly ordered two- and three-dimensional structures.

The idea of building nanomaterials atom-by-atom was first reported by Drexler in the mid 1980s, who envisioned the construction of 'nanorobots'.

The preparation of nanoscale components, devices or structures via the bottom-up approach my be regarded as an exercise in self-assembly in which sub-nanometre scale molecules spontaneously generate nanoscale aggregates according to their intrinsic molecular programming or as a result of the influence of a template, such as a molecule, or an aggregate, such as a micelle or bilayer of surfactants or other self-assembled structures. Example of this techniques is chemical vapour deposition (CVD), normally used to produce the best quality of graphene, where a methane gas is purged inside a vacuum chamber or with inert atmosphere and with the use of high temperature, 1000°C, the methane gas is adsorbed on copper substrate, with the time there is an increase of the graphenes island until to reach the final dimension (Fig. 1.2).[1]

Bottom up approach allows shows emergent properties that arise from the unpredictable interaction of the components of the aggregate and evolve over time, physical chemical properties that come out from the new material shows properties different to the bulk material.

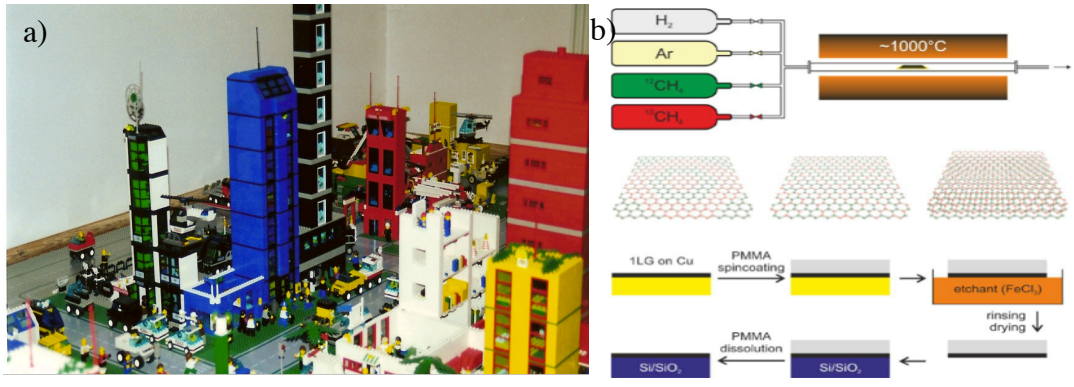

Fig 1.2 a)Building block are an example of bottom up approach because the parts are first created and then assembled without regard the final results. b) Chemical vapour deposition for the production of graphene, another example of bottom up approach using methane as building blocks.

One of the reasons why self-assembly has become a rapidly growing in chemistry is that it represents one solution to the problem of synthesizing structures larger than molecules. The stability of covalent bonds enables the synthesis of almost arbitrary configurations up to 1000 atoms. Self assembly with the bottom-up approach are in general, one strategy for organizing matter on large scales, providing one solution to the fabrication of ordered aggregates from components with sizes from nanometers to micrometers; these components fall between the sizes that can be manipulated by chemistry and those that can be manipulated by conventional manufacturing.

1.1.4. Supramolecular chemistry

To understand the role of supramolecular chemistry in self assembly of highly ordered structure is necessary to start talking about the role of the principal force which govern our universe. In nature we have the presence of four forces, two of them are characterized by short distance action, less than 10^{-5} nm and play an active role between neutrons, electrons and protons. Other two forces are instead characterized by long range distance. Gravitation force is a natural phenomena in which two mass are brought together. It was well explained by the Einsten's relativity theory where since mass and energy are equivalent, all form of energy, including light are under gravitation and can create it. Gravitation force is the weakest between the four fundamental forces. Approximately 10^{38} times weaker than the strong force, 10^{36} weaker than the electromagnetic force and 10^{28} times weaker than the weak force. Due to the weak force range gravity doesn't have influence in the subatomic particles. Instead is predominant at large scale, being responsible of the trajectory of planets, gravity, and other large object.[2]

Electromagnetic force, is another type of long range force, able to act from intermolecular distance to macroscopic systems. This force occurs typically between charged particles and in particular this force is constituted by electric fields, magnetic fields and light. The electromagnetic force plays an important role in the stabilization and creation of the internal properties of the matter whose we are surrounded. Where the ordinary matter is expression of the electromagnetic force between atoms and molecule and consequently responsible for chemical reaction in which electrons interact with other particles neighbours.

At very small distance two forces are mainly present: weak interaction and strong interaction. Strong interaction also called strong nuclear force is responsible to hold small particles as quarks together to form hadrons, like protons and neutrons. In addition, strong force is responsible to join together protons and neutrons to form nuclei. Strong force acts basically at two main distances: i) few femtometers (1-3 fm) where it is the main force that binds together protons and neutrons to form nuclei; and ii) at distance below 1 fm, where it is responsible to hold small particles as quarks together to form protons and neutrons and other hadrons particles.

Weak interaction is the second short range force. Is the force responsible for the interaction between subatomic particles that are directly involved in radioactive decay and act an important role in the nuclear fission. [3]

The complex of the natural forces explained until now are at the basis of the comprehension of the mechanisms behind supramolecular chemistry.

Unlike molecular chemistry, where all the mechanism of aggregation are covalent bond based, in supramolecular chemistry the interaction and aggregation of macromolecular system are governed by weak (non-covalent) and reversible interaction force.

The basis of the current " Supramolecular Chemistry" can be recognized mainly by Emil Fisher in 1894 where in his work explained perfectly the steric fit with his famous " lock and key" image.[4] In his work Fisher increased also the geometrical complementary, laying the basis of the modern molecular recognition.[5]

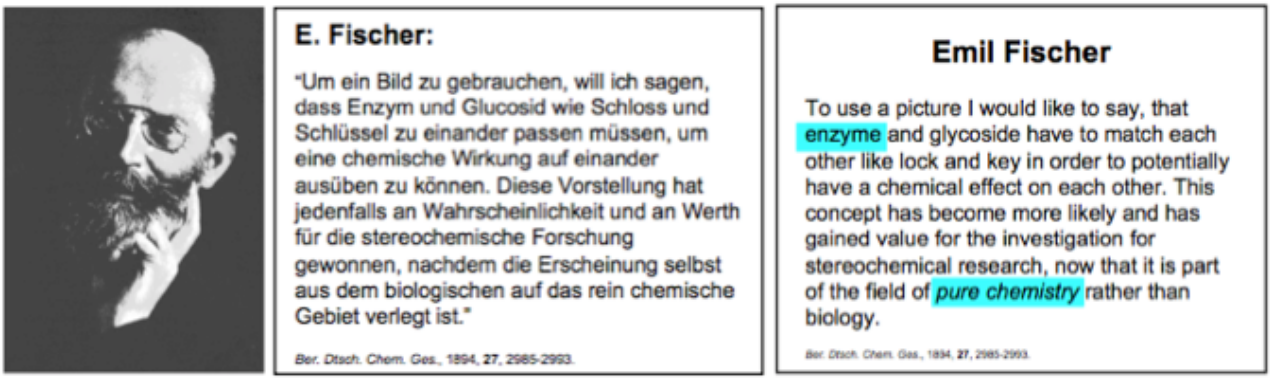

Fig 1.3 E. Fischer, one of the fathers of the supramolecular chemistry.

But the concept and the term of Supramolecular Chemistry were only introduced in 1978 with the words: "Just as there is a field of molecular chemistry based on covalent bond, there is a field of supramolecular chemistry, the chemistry of molecular assemblies and of the intermolecular bond. Noncovalent bonds play a crucial role in the biological world…",[6] with these words Jean Marie Lehn started his highly cited science article about supramolecular chemistry, but nowadays is important to add to his phrase, how noncovalent bonds play a crucial role in the whole word. An example of this was the discovering of the graphene, where different layers are joined together thanks to van der Waals forces. Through manipulation of these weak bonds, compared with the covalent one, living systems store and read information in cells, encoded as hydrogen bond network or acceptor-donors arrays or ion coordination sites. Supramolecular chemistry showed for the first time a next level of the information that can be get from chemistry.

Different topics create the basal architecture of supramolecular chemistry:

- Molecular recognition between artificial tailor made molecular receptors and their substrate to create a host guest system. While the definition of which one is host of guest is arbitrary. Using noncovalent interaction molecules are able to identify each other, with the aim to build molecular sensors and catalysis, major fields of application.

- Molecular self assembling is the spontaneous but controlled assembly of systems without guidance from an outside source. The molecules are directed to assemble through noncovalent interactions. Self-assembly can be divided into two main systems of aggregation: intermolecular self-assembly and intramolecular self-assembly. Examples are large structures such as hydrogen bonded systems,[7,8,9] micelles, membranes, vesicles, liquid crystals or also importart in the field of crystal engineering.[10]
- Mechanically interlocked architectures where molecules are blocked together due to the steric and mechanical impedance. Examples of mechanically interlocked molecular architectures include catenanes, rotaxanes,[11] molecular knots,[12] molecular Borromean rings[13] and ravels.[14]
- Adaptation, is based on the dynamic nature of supramolecular chemistry due to the ephemeral nature of the interaction that connect molecular components. The reversibility of the association allows a continuous change in constitution either by internal rearrangements or by exchange, incorporation and removal of molecules.

Different example can be shown in supramolecular chemistry: In dynamic covalent chemistry covalent bonds are broken and formed in a reversible reaction then the system is directed toward to form the lowest energy structures.[15]

Supramolecular chemistry is also a promising field to replicate biological systems. Biomimetic systems can be used to learn and replicate biological models. Examples include protein design and self-replication.[16] Using methods as molecular imprinting, there is the possibility to build the host created from small molecules using suitable species as a template. Then, after the construction, the template is removed leaving only the host. At the basis of this simple supramolecular method are: steric interactions and hydrogen bonding to improve binding strength specificity.[17]

Molecular machines are an interesting field in supramolecular chemistry, which was recognized with the award of shared Nobel prize in Chemistry to Jean-Pierre Sauvage, Sir J. Fraser Stoddart and Bernard L. Feringa 2016. Machines are able to generate movements as rotations, linear movements, switching. These architecture exist at the edge between supramolecular chemistry and nanotechnology, and prototypes have been demonstrated using supramolecular concepts.[18]

As shown until now supramolecular chemistry plays a crucial role in the growth of highly ordered materials, growth that can be induced by a template and involve molecular recognition or in oriented thin films.[19]

1.1.5. Molecular films on surfaces

The manipulation of molecules and macromolecules to form highly ordered structures such as single crystals, liquid crystalline layers, self assembled monolayers (SAMs) or ordered structures is important in many application fields from material reinforcement to molecular electronics. Therefore is more important to use the right approach to build highly ordered architectures on solid surfaces. Different method are used: Langmuir-Blodgett method, layer by layer deposition using polyelectrolyte, spin coating deposition, thermal evaporation and solvent vapour annealing.

Physically there are two ways of molecular surface adhesion: by chemisorption (chemical absorption) and physisorption (physical absorption). Usually, 0.5 eV per bond is defined as a limit to distinguish the two sorptions: upper and lower limit for molecular physisorption and chemisorption, respectively.

Chemisorption is characterized by the creation of a new type of chemical bond between the two species, adsorbate and substrate surface. Examples of chemisorption are corrosion, heterogeneous catalysis and self assembly of monolayers covalently bonded with the substrate. One of the most commonly studied SAMs are based on thiol molecules (R-SH, where R is a radical grouph) adsorbed on gold substrate forming a strong bond between noble metals (gold, silver, etc.) and sulphur groups with the release of hydrogen, the chemisorption is rarely reversible. Often, bonded molecules are removed carring out atoms of the substrate surface (e.g. chemisorbed oxygen on charcoal desorbesas carbon monoxide by thermal annealing in vacuum).

The suitable surface and surface site is a further key feature, because the reaction takes place only at certain temperature and pressure condition and not in all the surfaces. Chemical adsorption occurs only if the adsorptive makes direct contact with the active surface this means that generally the creation of the adsorbed state is often a monolayer instead of physical adsorption where multiple layers are commons.

Physisorption is the adsorption of the molecules on a surface whose interaction is characterized by the absence of a strong chemical bond. Another useful definition is the mechanism of adhesion in which the electronic structures of atoms or molecules are poorly perturbated.[20] This fundamental interacting force is constituted by van der Waals force where even if the interaction energy is very weak (~10–100meV), physisorption plays an important role in nature. For example, the nature of the gecko and its capacity to be attached to all surfaces.[21]Van der Waals forces originate from the interactions between induced, permanent or transient electric dipoles.

Although chemical adsorption can create monolayer of material this process is not exclusive, chemical and physical adsorption can happen together. It is possible to physisorbe on top of undelying chemisorbed molecules or we can have both mechanisms at the same time where physical adsorption occurs on non active sites while chemical adsorption on the other active sites.
Physisorption is also at the basis of this thesis work where highly ordered structures of silver nanoclusters and small self assembled monolayers of azo compound are prepared using different surface. Using solvent vapour annealing as method for production in the third paragraph will be show the theory behind this method.

1.1.6. Self assembling of nanoscopic structures

Self assembly consists of a group of molecules or fragments of macromolecules that interact with each other to form ordered structures. This ordered structures could be made by the same molecules or different. In fact, starting from a disordered system as a random coil, a solution or disordered aggregates they can arrive to ordered state like as crystals or layered materials.
Self assembly occurs when molecules or macromolecules interact with their self as a balance of attractive and repulsive interactions. The interactions are in general weak and no covalent, as van der Waals force, Coulomb force, hydrogen bonding, hydrophobic interaction. Although weak covalent bond are present as coordination bonding helping to stabilize the entire structure.[22]
In molecular self assembly the molecular structure determines the structure of the future assembly.[23]
Starting from the beginning where self assembly were confined only at molecular level, nowadays, with the expanding contact between chemistry, biology, material science and technology self assembling has begun to open the work field also to macro scale. Today we can define mainly three principal sizes for self-assembly: molecular level, nanoscale (nano wires, nano clusters, layered materials) and macroscopic system, until centimetre of dimensions.
The rules of self-assembly are in all cases similar but not identical. Example of new types of aggregates which find application in microelectronics,[24,25] photonics,[26,27] nearfield optics,[28] and the emerging field of nanoscience,[29,30] have attracted interest in self-assembly as a route to aggregates of components larger than molecules has grown.
Is also important to define how self aggregations enable to obtain structures that could be difficult if not impossible to obtain with molecular synthesis,[31] giving with that the possibility to play an active role in nanoscience and nanotechnology.
Therefore self assembly offer a new route in fabrication of three dimension microstructures.

An open question is still unsolved, we are able to synthesis many nanoscale structures, colloids, quantum dots, etc., but remains difficult to induce their self-assembly into functional structures at industrial scale.[32,33] Macroscopic objects can be fabricated that self-assemble well,[34] but scaling the fabrication of these structures into dimensions of microns, much less nanometers, remains an unsolved problem. Self assembly of appropriate components as a strategy for generating ordered aggregates seems likely to prove reliable and versatile method to build functional structures that show peculiar new properties.

1.1.7. Molecular films of AZO

In order to build up miniaturized devices, one of the key challenges is to control molecular function at surfaces. Switches represent a prototype of such functional molecules. The ability to integrate molecular switches with inorganic surfaces has recently become a hot topic giving rise to novel hybrid materials in which the properties of the two components are mutually affected or even enhanced in a reversible fashion. Due to its simple molecular structure and unique characteristics, azobenzene [35,36,37,38] (IUPAC name: diphenyldiazene) has arguably been the most studied photoswitch ever since its reversible isomerization was first reported some eight decades ago.[39]

In particular, azobenzene undergoing trans-cis isomerization of the N=N double bond has been well investigated in solution as well as in the gas phase.

Among photochromic molecules, azobenzenes have been extensively studied for their unique photoisomerization properties. The transition from the thermodynamically more stable trans to the cis conformation that can be induced by irradiation with UV light and reversed under heating or irradiation with visible light.

Most research has focused its attention on the preparation of SAMs[40,41,42] of azobenzene ligands on noble metals and on silicon due to the technological importance of these substrates as well as the well-established monolayer formation techniques on their surfaces. While the creation of self assembled monolayer on a metal surface is done using sulphur based ligands (in general thiols),[43] various approaches have been employed to covalently attach azobenzene onto silicon.[44,45]

SAMs are commonly used to modify the chemical properties of surfaces (i.e. polarity, chemical reactivity, or charge transfer characteristics at interfaces).[43,46,47,48] Integration of molecular switches into SAMs is an important issue since it opens the possibility to reversibly change these properties by external stimuli, e.g., light.[49,50] However, directly adsorbed on a metal surface, it exhibits strong substrate-induced quenching of the photoisomerization yield.[51,52]

The trans–cis isomerization of azobenzene involves large geometrical changes. As a consequence, steric hindrance and excitonic band formation are expected to strongly influence the photoisomerization yield.[53,54] Both effects can be analyzed and manipulated by tuning the density of the chromophores in the molecules.

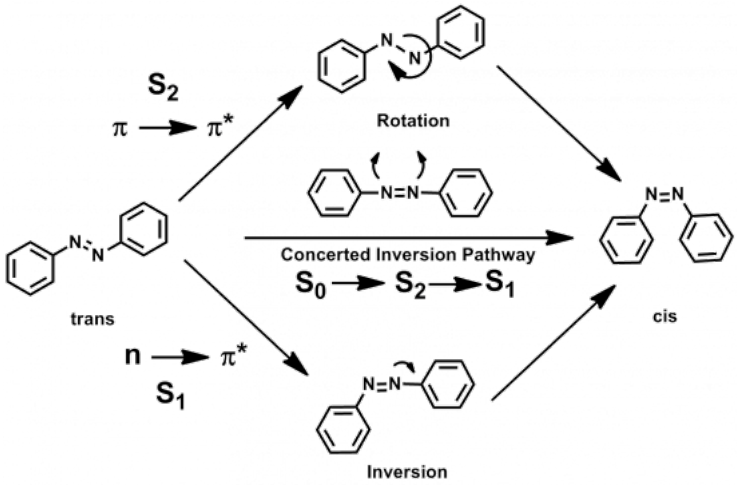

Fig 1.4 Photoisomerization mechanism of an azo benzene example.

1.1.8. Solvent Vapour Annealing

Supramolecular materials use self-assembly of molecular components to form complex architectures that may otherwise be extremely difficult to prepare. One of the fundamental aspects of this approach is that relatively weak intermolecular forces are used to direct the assembly of the subcomponents. One of the major goals in materials chemistry today is the production of highly ordered structures with low cost and up scalable technologies to give functional systems for organic electronic applications.[55,56,57] In this framework Solvent Vapour Annealing has collected a great interest as a possible candidate to be used for scalable productions.

Solvent Vapour Annealing (SVA) is an easy and versatile process that can be used to accelerate the mobility of the molecules deposited on surfaces. It is performed simply by placing a drop of the sample material on a specific substrate closed into a vessel where a vapour-liquid equilibrium is attainable for the chosen solvent. Using SVA is possible to obtain a great control on the amount of solvent condensing on the substrate, and that forming a continuous layer with a thickness of a few nanometres. This very thin layer is sufficient to allow the molecules pre absorbed on the surface to move for hundreds of mm producing macroscopic structures. The resulting reorganization of the functional materials at the surfaces is due to a partial re-solubilization of the deposited layers, allowing the molecules to rearrange into structures characterized by a higher degree of order as compared to the starting samples, and a significant improvement of the performance.[58,59]

The molecules will thus have a rather high lateral diffusion, while being at the same time constrained in close proximity to the surface, in the thin layer of liquid, which can thus be described as a quasi-2- dimensional solution.

This choice requires consideration of all the interactions playing a role in the organization of a molecule from solution on a surface such as molecule–solvent, molecule–substrate, molecule–molecule, and solvent–substrate interactions. If the annealing is carried out with a good solvent for the deposited species, the expected degree of rearrangement will be notably higher due to strong molecule–solvent interactions.

SVA is usually used to increase the level of order within pre organized architectures for improving the performance of the associated devices. In fact this method help materials to reorganize in more stable and ordinate system, they give at the system an activated energy to win a barrier between two different states (**Fig. 1.5**). The possibility to the experimental conditions makes it possible to promote reorganization from nanoscale up to several hundreds of micrometers, leading to the formation of crystalline functional architectures.

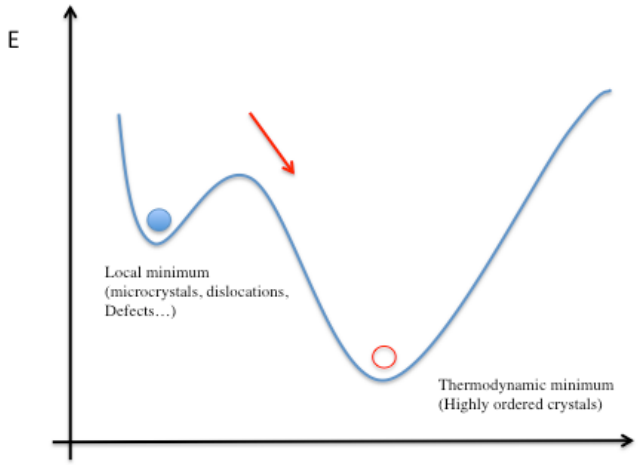

Fig 1.5 Schematic representation of energy state of materials in vapour annealing process.

SVA treatment allows to tune the morphology of the self-assemblies, are reported in Fig. 1.6. HBC-PEO molecules arrange on silicon oxide forming different assemblies increasing the SVA time. [60]

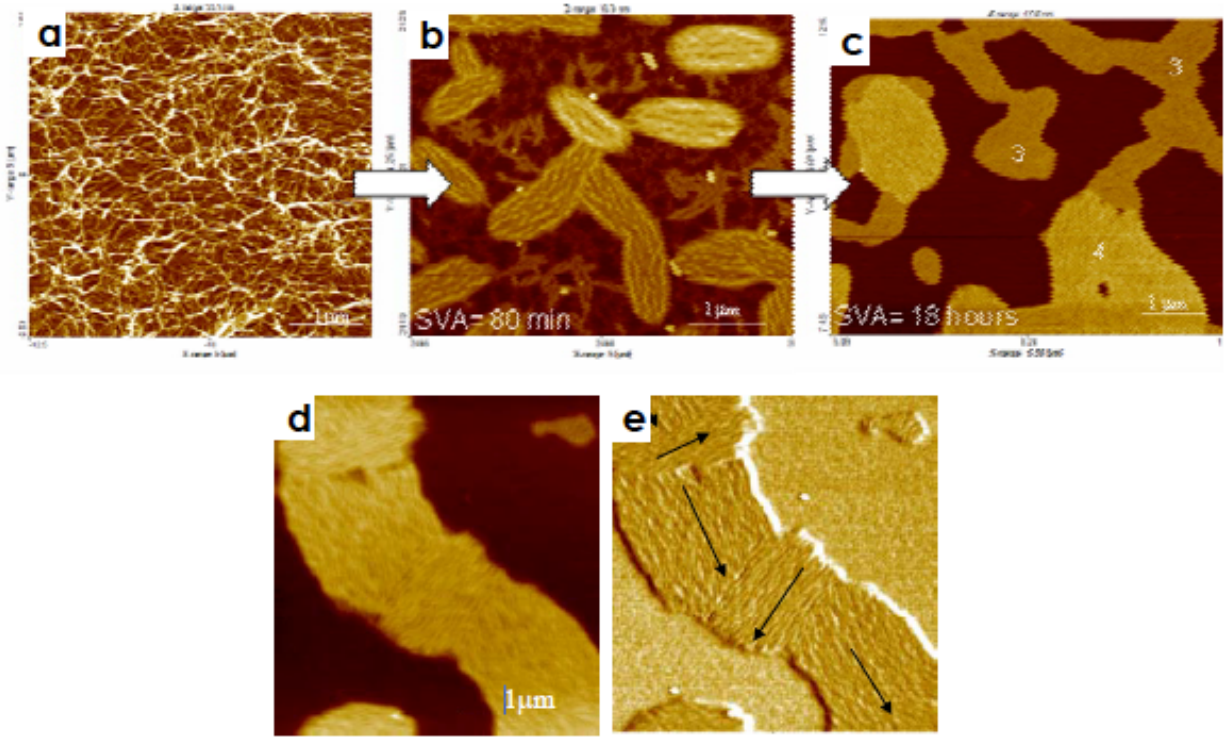

Fig 1.6 AFM images of HBC-PEO deposited on Si/SiOx a) Original morphology after spin-coating. b) After 80 min of SVA. c,d) After 18 h of SVA. e) Phase image of the area shown in d. 3 and 4 marks indicate islands formed by three and four layers, respectively.

SVA treatment allows to move and to rearrange small amounts of material on a surface in a controlled way, at ambient conditions and without the use of vacuum setups, paving the way to a new class of experiments.

References

1. Top-down and bottom-up design. *Wikipedia* (2018).
2. Bernal, P. Scientific Laws, Principles and Theories: A Reference Guide (Krebs, Robert E.). *J. Chem. Educ.* **78,** 1026 (2001).
3. B. Povh, K. Rith, C. Scholz, F. Zetsche. *Particelle e nuclei. Un'introduzione ai concetti fisici*. (Bollati Boringhieri, 1998).
4. Fischer, E. Synthesen in der Zuckergruppe II. *Berichte Dtsch. Chem. Ges.* **27,** 3189–3232 (1894).
5. Mayer Roland. Aus meinem Leben: Von Emil Fischer (with a Proloque and an Epiloque by Bernhard Witkop); Reprint from „Emil Fischer, Gesammelte Werke, edited by M. Bergmann, 1922"□; Berlin, Heidelberg, New York, Springer-Verlag, 1987; XXVIII, E XVII und 201 S. mit 3 Bildern, Vor- und Nachwort (engl.); Format 16,0 cm × 23,5 cm, Kart. 78,- DM; ISBN 3-540-18002-8. *Z. Für Chem.* **29,** 229–230 (1989).
6. Lehn, J.-M. Toward Self-Organization and Complex Matter. *Science* **295,** 2400 (2002).
7. Whitesides, G. M. *et al.* Noncovalent Synthesis: Using Physical-Organic Chemistry To Make Aggregates. *Acc. Chem. Res.* **28,** 37–44 (1995).
8. Fyfe, M. C. T. & Stoddart, J. F. Synthetic Supramolecular Chemistry. *Acc. Chem. Res.* **30,** 393–401 (1997).
9. Lehn, J.-M. Perspectives in Supramolecular Chemistry—From Molecular Recognition towards Molecular Information Processing and Self-Organization. *Angew. Chem. Int. Ed. Engl.* **29,** 1304–1319 (1990).
10. Ariga, K. *et al.* Challenges and breakthroughs in recent research on self-assembly. *Sci. Technol. Adv. Mater.* **9,** 014109 (2008).
11. Philp, D. & Stoddart, J. F. Self-Assembly in Natural and Unnatural Systems. *Angew. Chem. Int. Ed. Engl.* **35,** 1154–1196 (1996).
12. J.-P. Sauvage, C. Dietrich-Buchecker. *Molecular Catenanes, Rotaxanes and Knots: A Journey Through the World of Molecular Topology*. (WILEY-VCH Verlag GmbH, 2007).
13. Ikeda, T. & Stoddart, J. F. Electrochromic materials using mechanically interlocked molecules. *Sci. Technol. Adv. Mater.* **9,** 014104 (2008).
14. Li, F., Clegg, J. K., Lindoy, L. F., Macquart, R. B. & Meehan, G. V. Metallosupramolecular self-assembly of a universal 3-ravel. *Nat. Commun.* **2,** 205 (2011).
15. Rowan, S. J., Cantrill, S. J., Cousins, G. R. L., Sanders, J. K. M. & Stoddart, J. F. Dynamic Covalent Chemistry. *Angew. Chem. Int. Ed.* **41,** 898–952 (2002).
16. Zhang, S. Fabrication of novel biomaterials through molecular self-assembly. *Nat. Biotechnol.* **21,** 1171 (2003).
17. Dickert, F. L. & Hayden, O. Molecular imprinting in chemical sensing. *TrAC Trends Anal. Chem.* **18,** 192–199 (1999).
18. Balzani, V., Gómez-López, M. & Stoddart, J. F. Molecular Machines. *Acc. Chem. Res.* **31,** 405–414 (1998).
19. Wittmann, J. C. & Smith, P. Highly oriented thin films of poly(tetrafluoroethylene) as a substrate for oriented growth of materials. *Nature* **352,** 414 (1991).
20. Oura, K., Lifshits, V.G., Saranin, A., Zotov, A.V., Katayama, M. *Surface Science*. (Springer-Verlag Berlin Heidelberg, 2003).
21. Autumn, K. *et al.* Adhesive force of a single gecko foot-hair. *Nature* **405,** 681 (2000).
22. Olenyuk, B., Whiteford, J. A., Fechtenkötter, A. & Stang, P. J. Self-assembly of nanoscale cuboctahedra by coordination chemistry. *Nature* **398,** 796 (1999).
23. Whitesides, G. M. & Boncheva, M. Beyond molecules: Self-assembly of mesoscopic and macroscopic components. *Proc. Natl. Acad. Sci.* **99,** 4769 (2002).

24. Sirringhaus, H. *et al*. High-Resolution Inkjet Printing of All-Polymer Transistor Circuits. *Science* **290,** 2123 (2000).
25. Rogers, J. A. *et al*. Paper-like electronic displays: Large-area rubber-stamped plastic sheets of electronics and microencapsulated electrophoretic inks. *Proc. Natl. Acad. Sci.* **98,** 4835 (2001).
26. Jenekhe, S. A. & Chen, X. L. Self-Assembly of Ordered Microporous Materials from Rod-Coil Block Copolymers. *Science* **283,** 372 (1999).
27. Xia, Y., Gates, B., Yin, Y. & Lu, Y. Monodispersed Colloidal Spheres: Old Materials with New Applications. *Adv. Mater.* **12,** 693–713 (2000).
28. Wu, M.-H. & Whitesides, G. M. Fabrication of arrays of two-dimensional micropatterns using microspheres as lenses for projection photolithography. *Appl. Phys. Lett.* **78,** 2273–2275 (2001).
29. Lieber, C. M. The incredible shrinking circuit. *Sci. Am.* **285,** 58–64 (2001).
30. Klimov, V. I. *et al*. Optical gain and stimulated emission in nanocrystal quantum dots. *Science* **290,** 314–317 (2000).
31. Whitesides, G. What Will Chemistry Do in the Next Twenty Years? *Angew. Chem. Int. Ed. Engl.* **29,** 1209–1218 (1990).
32. Xia, Y., Gates, B. & Li, Z.-Y. Self-Assembly Approaches to Three-Dimensional Photonic Crystals. *Adv. Mater.* **13,** 409–413 (2001).
33. Bachtold, A., Hadley, P., Nakanishi, T. & Dekker, C. Logic circuits with carbon nanotube transistors. *Science* **294,** 1317–1320 (2001).
34. Bowden, N. B., Weck, M., Choi, I. S. & Whitesides, G. M. Molecule-Mimetic Chemistry and Mesoscale Self-Assembly. *Acc. Chem. Res.* **34,** 231–238 (2001).
35. Dürr, H. & Bouas-Laurent, H. *Photochromism : molecules and systems*. (Elsevier ; Distributors for the U.S. and Canada, Elsevier Science Pub. Co., 1990).
36. Kumar, G. S. & Neckers, D. C. Photochemistry of azobenzene-containing polymers. *Chem. Rev.* **89,** 1915–1925 (1989).
37. Crecca, C. R. & Roitberg, A. E. Theoretical Study of the Isomerization Mechanism of Azobenzene and Disubstituted Azobenzene Derivatives. *J. Phys. Chem. A* **110,** 8188–8203 (2006).
38. Fliegl, H., Köhn, A., Hättig, C. & Ahlrichs, R. Ab Initio Calculation of the Vibrational and Electronic Spectra of trans- and cis-Azobenzene. *J. Am. Chem. Soc.* **125,** 9821–9827 (2003).
39. Krollpfeiffer Friedrich, Pötz Hans & Rosenberg Albrecht. Über N-Alkyl-benzotriazole und die Konstitution des Benzotiazols. *Berichte Dtsch. Chem. Ges. B Ser.* **71,** 596–603 (2006).
40. Dariusz Witt, Rafal Klajn & Piotr Barski and Bartosz A. Grzybowski. Applications, Properties and Synthesis of ω-Functionalized n-Alkanethiols and Disulfides - the Building Blocks of Self-Assembled Monolayers. *Curr. Org. Chem.* **8,** 1763–1797 (2004).
41. Bain, C. D. *et al*. Formation of monolayer films by the spontaneous assembly of organic thiols from solution onto gold. *J. Am. Chem. Soc.* **111,** 321–335 (1989).
42. Sagiv, J. Organized monolayers by adsorption. 1. Formation and structure of oleophobic mixed monolayers on solid surfaces. *J. Am. Chem. Soc.* **102,** 92–98 (1980).
43. Love, J. C., Estroff, L. A., Kriebel, J. K., Nuzzo, R. G. & Whitesides, G. M. Self-Assembled Monolayers of Thiolates on Metals as a Form of Nanotechnology. *Chem. Rev.* **105,** 1103–1170 (2005).
44. Siewierski, L. M., Brittain, W. J., Petrash, S. & Foster, M. D. Photoresponsive Monolayers Containing In-Chain Azobenzene. *Langmuir* **12,** 5838–5844 (1996).
45. Hamelmann, F. *et al*. Thin molybdenum oxide films produced by molybdenum pentacarbonyl 1-methylbutylisonitrile with plasma-assisted chemical vapor deposition. *Thin Solid Films* **446,** 167–171 (2004).
46. Ulman, A. *Chem Rev* **96,** 1533 (1996).
47. DiBenedetto Sara A., Facchetti Antonio, Ratner Mark A. & Marks Tobin J. Molecular Self-Assembled Monolayers and Multilayers for Organic and Unconventional Inorganic Thin-Film

Transistor Applications. *Adv. Mater.* **21,** 1407–1433 (2009).
48. Yang, H., Yuan, B., Zhang, X. & Scherman, O. A. Supramolecular chemistry at interfaces: host-guest interactions for fabricating multifunctional biointerfaces. *Acc. Chem. Res.* **47,** 2106–2115 (2014).
49. Feringa, B. L. & Browne, W. R. *Molecular switches*. **42,** (Wiley Online Library, 2001).
50. Ferri, V. *et al.* Light-Powered Electrical Switch Based on Cargo-Lifting Azobenzene Monolayers. *Angew. Chem.* **120,** 3455–3457 (2008).
51. Wolf, M. & Tegeder, P. Reversible molecular switching at a metal surface: A case study of tetra-tert-butyl-azobenzene on Au (1 1 1). *Surf. Sci.* **603,** 1506–1517 (2009).
52. Schmidt, R. *et al.* On the electronic and geometrical structure of the trans-and cis-isomer of tetra-tert-butyl-azobenzene on Au (111). *Phys. Chem. Chem. Phys.* **12,** 4488–4497 (2010).
53. Gahl, C. *et al.* Structure and excitonic coupling in self-assembled monolayers of azobenzene-functionalized alkanethiols. *J. Am. Chem. Soc.* **132,** 1831–1838 (2010).
54. Utecht, M., Klamroth, T. & Saalfrank, P. Optical absorption and excitonic coupling in azobenzenes forming self-assembled monolayers: a study based on density functional theory. *Phys. Chem. Chem. Phys.* **13,** 21608–21614 (2011).
55. Hagen Klauk. *Organic Electronics: Materials, Manufacturing, and Applications*. (Hagen Klauk, 2006).
56. Yan, H. *et al.* A high-mobility electron-transporting polymer for printed transistors. *Nature* **457,** 679 (2009).
57. Yang, Y. & Wudl, F. Organic Electronics: From Materials to Devices. *Adv. Mater.* **21,** 1401–1403 (2009).
58. Bull, T. A., Pingree, L. S. C., Jenekhe, S. A., Ginger, D. S. & Luscombe, C. K. The Role of Mesoscopic PCBM Crystallites in Solvent Vapor Annealed Copolymer Solar Cells. *ACS Nano* **3,** 627–636 (2009).
59. Miller, S. *et al.* Investigation of nanoscale morphological changes in organic photovoltaics during solvent vapor annealing. *J. Mater. Chem.* **18,** 306–312 (2008).
60. Treossi, E. *et al.* Temperature-Enhanced Solvent Vapor Annealing of a C3 Symmetric Hexa-peri-Hexabenzocoronene: Controlling the Self-Assembly from Nano- to Macroscale. *Small* **5,** 112–119 (2009).

1.2. Scanning Probe Microscopy

Since the discovery of Scanning Probe microscopies (SPMs) family by Binning, Roher and Gerber for Scanning tunnelling microscopy (STM)[1] in 1982 and Atomic force microscopy (AFM) by Binning, Quate and Gerber[2] in 1986, a big step forward has been done to understand the physical and chemical properties of the nano world Thanks to a nanometric tip size architecture was possible to see identify architecture and self assembly structure down to the atomic and molecular scale.

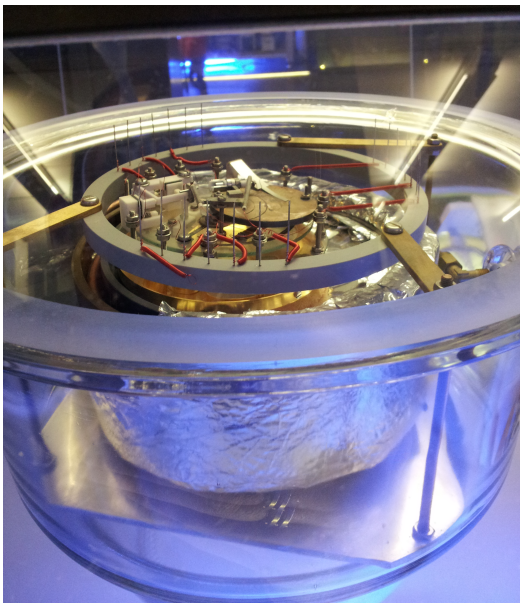

Fig 1.2.1 First scanning tunnelling microscope by Gerd Binning and Heinrich Robrer IBM Research GmbH, Rüschlikon (Schweiz) Deutsches Museum München, Germany.

STM was the first technique of the SPM family providing a new approach of analysis of different conducting, semiconducting or insulating samples, giving the possibility to visualize[1] and manipulate the single atom. The principle of the STM is simple: constituted by a sharp metallic tip approaching to the surface and probing the local physico-chemical properties. For the sake of simplicity, we can imagine for a moment to lose our possibility to see, without our eyes the only way that we have to check the environment are our arms, fingers, touch. Tapping around objects with our fingers and moving with our legs we register the position and the shape of the objects.

[1] STM provides to map the electronic density of state of the single atom.

Scanning probe microscopies resemble in this case the human analogy, where in case of the instrument, the probe is constituted by a nanometrically sized tip.

Scanning force microscope consists of major four components: a cantilever mounted tip, a piezoelectric motor, deflection sensor and a feedback control system. The tip-sample interaction is very sensible to the distance, automatically the piezoelectric circuit will making movement in Z, X, Y, direction with a precision of Ångstroms. Consequently the feedback system controls the tip-sample distance. The image is created from a raster scan. At a discrete point in the raster scan a value is recorded (when and where depends from type of SPM). All the data recorded are finally showed in a heat map to produce the final image, in general with different shade of orange and black.

Through these techniques we can obtain a high resolution in vertical direction (≤ 0,1 nm for STM and SPM) and in lateral resolution a high precision (≤ 1 nm for SPM and STM). Conductive, semiconductive and insulating samples are normally analized with these type of instruments, as in not invasive or mildly invasive conditions. Scanning probe microscopy give the possibility instead of TEM or SEM to analyse sample in environment condition or also at solid-liquid interfaces.

The analisis mode of scanning probe microscopy are mainly classified in two method: constant interaction mode and constant height mode.

In constant interaction mode or feedback mode, a feedback loop is used to maintain the interaction constant to the surface or closely to the surface. The type of interaction depends on which type of SPM is in use, example: for atomic force microscopy is the tip deflection, for scanning tunnelling microscopy is the tunnelling current.

In constant height mode the z axis is fixed and is not moved during the scan. The interaction instead of the height is always recoded, in case of STM the tunnelling current, cantilever deflection in case of AFM. This second system of analysis gives less resolution respect to the previous method due to the weak interaction with the sample, although the interaction is not strong enough in non contact mode there are less possibility to perturb the sample.

1.2.1. Scanning Force Microscopy

Only from 30 years ago answer are coming to us thanks to the discovery of scanning probe microscopies. The earliest success of investigation of the nano world were atom by atom spacing of Si(111) – (7x7) reconstruction,[1] Au (111),[3] the molecular spacing of organized organic films,[4-5] and the topography of the DNA[6]. All the earliest publication have in common the presence of a conductive substrate, the invention of Scanning force microscopy or Atomic force microscopy in 1986[2] solved this problem giving the possibility to analysis without any preference on semiconducting or insulating substrate. The most popular operating mode for scanning force microscopy to detect deflection in cantilever is to use an optical detection system constituted by a tip, laser and a four quadrant photodiode. The work principle is simple: a laser is focused on a cantilever tip (with a general length of 100 μm) which is deflected on four quadrant photodiode, during the analysis the interactions of the tip with the sample produce deflection or torsions, depends in which type of analysis mode we are operating, A four quadrant photodiode detect the deflection of the tip (vertical direction) and torsional movement (X-Y directions) simultaneously. Then a software collect the raster data showing the image in heat graph. In fig. 1.2.2 is shown a scanning electron microscopy image of a Silicon nitride cantilever with a pyramid tip.

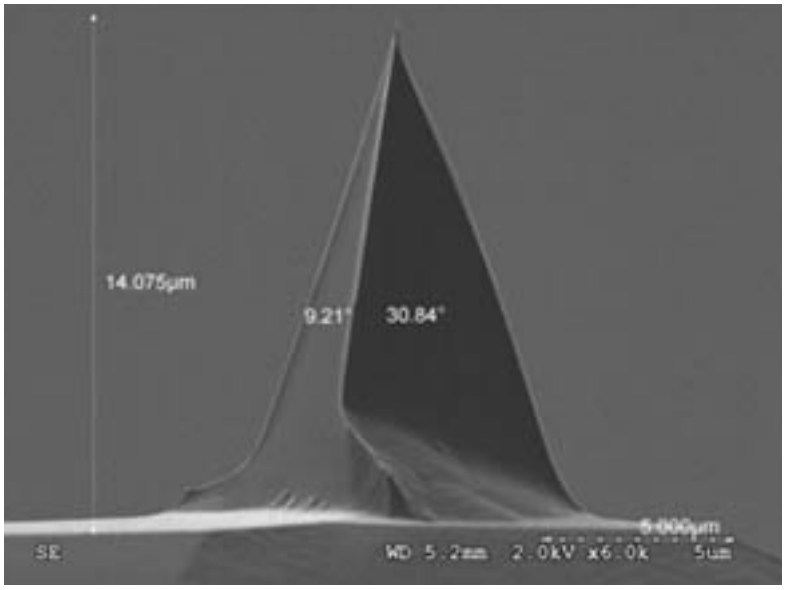

Fig 1.2.2 AFM tip with approximate values for pyramidal-shaped AFM tips.
Ref Nanoscience Instruments

Depending on the nature and the shape of the probe, a huge variety of information is possible to get in Scanning force microscopy. Here a briefly list of the major SFM mode:

Instrument	Interaction	Substrate Used	Tips	Lateral Resolution	Discovery	Ref
STM	Tunnelling Current	Conductors, semiconductors	W, Pt/Ir	1 Å	Binning, Rohrer et al. (1981)	[1]
AFM	Long and short range Forces	Conductors, semiconductors, insulators	W, Pt/Ir, Si_3N_4	1 Å	Binning, Gerber, Quate (1986)	[2]
MFM	Magnetic Forces	Ferromagnetic materials	AFM coated tips, Ni	5 Å	Martin, Wickra-masinghe (1987)	[7]
EFM	Electrostatic Forces	Conductors, semiconductors	AFM coated tips	5 Å	Terris, Stern,Rugar (1989)	[8]
KPFM	Electrostatic Forces	Conductors, semiconductors, Insulators	AFM coated tips	5 Å	Weaver, Abraham (1991)	[9]
SCM	Electrostatic Forces	Conductors, semiconductors, Insulators	AFM coated tips	5 Å	Mattey, Blanc (1985)	[10]
SNOM	Evanescent Waves	Conductors, semiconductors, Biological films	Optical fiber	10 Å	Pohl (1984)	[11]
STOM	Photon emission	Conductors, semiconductors	AFM coated tips + photodiode	5 Å	Coombs, Gimzewski (1988)	[12]
SNTM	Heat Transfer	Conductors, semiconductors,	Thermocouple	30 Å	William, Wickra-	[13]

		Biological films			Masinghe (1986)	

STM: Scanning Tunneling Microscopy
AFM: Atomic Force Microscopy
MFM: Magnetic Force Microscopy
EFM: Electrostatic Force Microscopy
KPFM: Kelvin Probe Force Microscopy
SCM: Scanning Capacitance Microscopy
SNOM: Scanning Near field Optical Microscopy
STOM: Scanning Tunneling Optical Microscopy
SNTM: Scanning Near filed Thermal Microscopy

In SPM another classification can be based on the system of scanning, scanning probe, scanning sample, fixed or tip and sample scanning system. In general the conformation of scanning sample is the most common, giving the possibility of less noise and production of artefact. Depending of the scanning system architecture different lengths are possible to measure, arriving in the best case to thousands of mm in large area to few Å in case of STM in ultra high vacuum.[14-15] Although a great flexibility in dimensions analysis Scanning force instruments are really sensible to the environment condition and to the design. Temperature, humidity, electrical noise, turbulence can influence significantly the measurement and is important to take in account all this factors. Calibration play an important role trying to reduce the problem that affect these microscopies. Piezoelements, photodiode, cantilever must be calibrated to reduce noise or artefact that can affect the image. For piezoelement the calibration is performed using reference surface with specific patter (Microgrid, steps, cone etc…) commercially available. In general highly oriented pyrolitic graphite (HOPG), patterned silicon Nitride, mica are used as a calibration systems. Another important value is the normal and torsional spring constant of the tip, commonly given by the producers with an average value. Mainly we can consider two way to get the spring constant value: a geometrical calculation which consider also the chemical nature of the cantilever itself[16-17] or experimentally. The first method consider not only the geometry and the chemical nature of the cantilever but also the coating applied to it. The second method more empirically include shifts check at different frequency of mass loaded cantilever,[18] measuring of a thermally induced vibration of a free standing

cantilever,[19] estimation of the spring constant can be obtained also by cantilever deflection by applying a known load.[20] These procedure in addition of the spring constant give information also about mechanical properties of the cantilever, Young modulus,[21] or also the thickness.[22] Photodiode also need to be calibrated using optical lever detection system.

For a quantitative analysis, is important to define all the possible physical phenomena that can occur. During the scan the interaction between the tip and the sample is object of a variety of forces. Long and short range of forces affect the atomically nature of the tip. The tip also is influenced by the environment condition due to capillary force which create a neck of water giving a false result in topography or other information. Pressure of the tip on the surface can produce plastic deformation and nanoindentation. Know which type of force mainly govern the interaction permit to know the best work condition.

1.2.2. Classification of Forces

Forces are typically distinguish as i) long- and ii) short- distance.

Long Distance Forces:

- Van der Waals forces (VdW). In honour of the Dutch scientist Johannes Diderik Van der Waals, such forces can be attractive and repulsive between atoms and molecules or also surfaces. Proportional to $1/R^6$ distance between atoms, respect to the ionic or covalent bond is a weak force and easily perturbated by the environment. More important for supramolecular chemistry as well as biology and condensed matter they are at the base of AFM interactions.

  VdW are ascribed to three principal phenomena: i) permanent dipole-permanent dipole interaction (Keesom interaction), ii) induced dipole-permanent dipole interaction (Debye interaction) and iii).instantaneous dipole-dipole (London interaction).
- Electrostatic forces (EF) due to permanent dipoles, charge density are important not only in the biological field but also in chemistry and condensed physics. EFM and KPFM are the mainly instrument which investigate this category of force. Electrostatic force comes from the force which happens with opposite charges and is described by Coulomb's Law.
- Capillary phenomena. Working at environment conditions is important to take in account the phenomena of the capillarity and the creation of a bridge between the tip and the sample

created normally by the humidity in the air.[23-24-25] Depending on the relative humidity, capillary force due to the neck created between tip and sample can vary in the range of 1 – 100 nN, modifying drastically the contrast and the resolution of the scanning probe analysis.

Short Distance forces

- Repulsive forces. Commonly at distance of few Angstrom, constituted by charge overlapping between tip and sample. It is referred only to a small number of atoms. The origin of this force comes from two phenomena: nuclei clouds overlapping which produce a repulsion effect due to the production of a coulombic effect. And a second phenomena, Pauli repulsion, referred to electrons with same spin that try to occupy the same orbital in contrast with the Pauli exclusion principle. They are proportional to $1/R^n$ with $n > 8$.
- Chemisorption and Physisorption. Forces created between solute and substrate, depending on which type of interaction we are in presence of. In case of physisorption is characterized by weak intermolecular interaction (van der Waals etc..). In chemisorption the interaction is due to the creation of a chemical bond (ionic or covalent). With this type of interaction the range of value in enthalpy ΔH going from 20 Kj mol^{-1} for the physisorption to 200 Kj mol^{-1} for the chemisorption.
- Friction force. Friction is highly depended on the surface interaction (few atomic layers). Hard, soft, smooth, rough, viscoelastic of plastic, dry or lubricated, etc. surface can be of different nature and made with different chemicals. When two shearing objects coming into and out contact they produce a local pressure that can fluctuate between a wide rage of pressure, from 1 Pa to GPa.[26]

In first approximation the forces who act actively and in large part to the deflection of the cantilever can be described in terms the Lennard-Jones potential:

$$V(r) = 4\varepsilon \left(\left(\frac{\sigma}{r}\right)^{12} - \left(\frac{\sigma}{r}\right)^{6} \right) \quad (1)$$

where r is the surface-probe distance, ε is the depth of the potential wall, σ is a finite distance where the inter-particle potential is zero. At large distance the probability that the probe interacts with surface is minimal and consequently the potential energy is closely to be zero. Reducing the distance the interaction increases, with a decreasing of the potential energy reaching a minimum (maximum interaction). At the minimum the two systems are at the equilibrium as long as the

equilibrium is perturbated. Changing the equilibrium and try to get closer the tip to the surface corresponds to the increasing of the potential (high repulsion), (i.e. similar to the Pauli exclusion principle in the case of two particles). In the formula (1) the two contribution of attractive and repulsive force are shown with the powered r^{-12} for the repulsive force and r^{-6} for the attractive force.

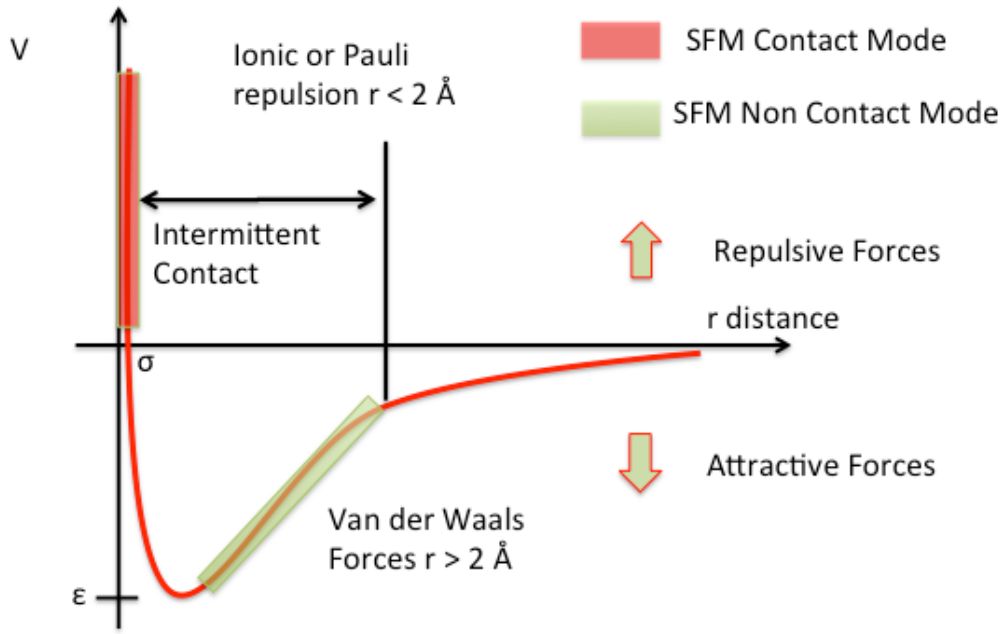

Fig 1.2.3 Graph representation of the Lennard Jones potential who act actively in the tip deflection and interaction.

In the graph are highlighted two operational part in scanning probe microscopy. In contact mode the tip-sample interaction is placed in the repulsion zone, where the distance between this two object is less than 2 Å. While in non contact mode the distance between the tip and the surface is over 2 Å. In intermittent contact mode, also known as Tapping Mode, the tip-surface interaction is instead placed between the repulsive and attractive forces. In the next chapter will be discussed different mode of analisis.

1.2.3. Contact Mode

Contact Mode was the first method developed where the tip is physically in contact with the surface. The tip is strongly associated to the feedback electronic to maintain a pre set imaging value (ex. Force). Is performed at distance where play an important role the repulsive and capillary force producing the so called "snap in" effect. In contact mode low stiffness cantilevers are normally used. The reason is to reach a good contact with the surface and having a stiffness of few N/m to avoid "nanolithography" phenomena. Furthermore a cantilever with more deflection can give a better resolution. In contact mode crucial role is leaved to the force of the tip on the sample. In general forces applied to samples are in the range from tens to hundreds of nanoNewton. Moreover all the surface, at environment condition are covered with water and other contaminants, whose surface tension pull the tip and probe downwards. For this purpose measuring tip- sample forces is useful to be performed with force curves (deflection vs distance). The examination of force curve permit to identify the best condition of working in contact mode. This analysis mode, give also the possibility to obtain other information from the sample, not only the topography. During the scan the force generated by the tip when is moved laterally can be used to get information. The lateral force applied to the tip causes torsion to the cantilever, automatically detected by the photodiode (as shown fig. 1.2.4) with the lateral segments of the photodetector.

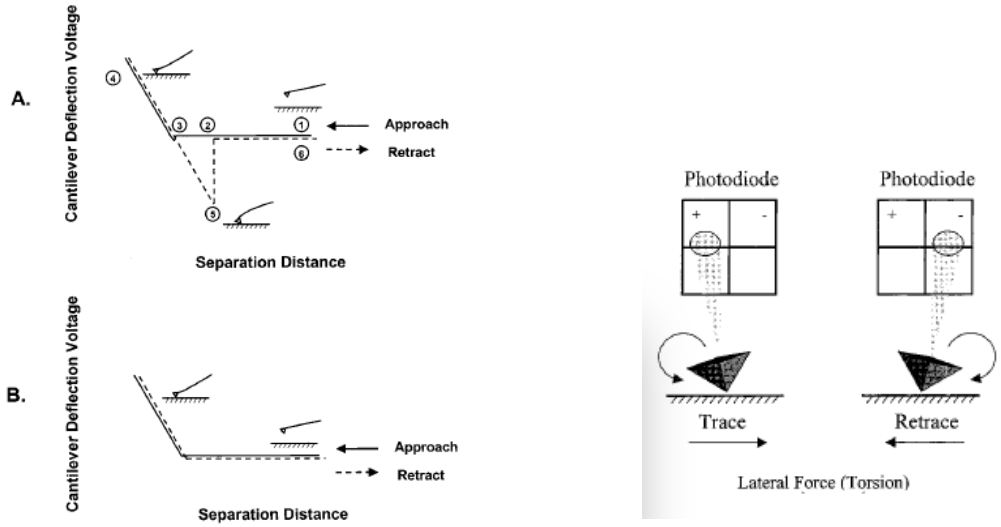

Fig 1.2.4 Schematic representation of tip surface interaction and how the photodiode response during lateral movements.

1.2.4. Tapping mode

Touching continuously the surface, contact mode provides a large lateral resolution. However, tip can damage or modify the physical and chemical nature of the sample surface. In particular, with soft sample (i.e. DNA, cells, polymers etc.), the friction force between tip and sample can be strong enough to cut the material destroing the sample. For that reason, Intermittent contact mode[27] was depeloped also providing to minimize the contribution of the capillary forces. In this mode the tip is oscillated at a frequency closed to its resonance frequency and the oscillating amplitude is monitored. At the beginning, the tip start with a free oscillation, approaching to the surface the tip become to hit the surface and to change the oscillation amplitude. Recording the feedback signal required to keep the oscillating amplitude constant is possible to know the topography. In intermittent contact mode or Tapping mode (TM) the tip goes through attractive and repulsive force (as shown fig 1.2.3). The tip-sample forces can be also manipulated to select in which part is preferable to work, attractive o repulsive, having the best performance. Working mainly in attractive force, is reduce the shearing force to the sample with a reduction in this case of contrast, on the other hand working with a setpoint near the repulsive forces gives better resolution with a major interacting force. The advantages of this method is the drastically reduction of the shearing force during the scan respect to contact mode.[28]

Basically, there are two methods for oscillate the tip[29]: acoustically and magnetically. Acoustically the tip is oscillated by the piezo-actuators in the contact with the cantilever supporting chip. In the second method, an alternating magnetic field is applied to the tip, which is covered in the backside with a susceptible magnetic film. Furthermore, another important comes from the detection of the phase. In particular, phase shift is strictly related to the energy dissipated to the tip- sample contact and mapping the phase shift on the surface permit to identify regions with different interactions.

The development of TM was a breakthrough in biological imaging giving the possibility to analyse living cell in liquid or DNA filaments with a resolution of 1 nm.

1.2.5. Non Contact Mode

Despite of TM minimises the contact between tip and surface, this technique cannot be used to study very soft samples. A further technique is developed, called non contact mode, where tip is forced to oscillate at a given frequency (free oscillation). Interacts with the surface sample, the given frequency will change, inducing a shift in the resonance frequency due to the VdW forces. The signal can be detected or via frequency fluctuation onto the surface in direct signal or via feedback loop, in constant frequency shift. Characteristic of this mode analysis is the use of strength tips (high spring constant) to minimize the attractive forces close to the surface, avoiding excessive bending.

In the few decades the evolution of AFM-combined techniques allowed a detailed description of the process and structures at the nanoscale. In particular the possibility to cover tips with conductive film open up the possibility to combine scanning probe techniques and conductive analysis. In this thesis we will describe the SPM techniques which combine topological and electrostatic information: Kelvin probe force microscopy (KPFM).

1.2.6. Kelvin Probe Force Microscopy (KPFM)

Developed in 1991,[30] KPFM is rapidly improved itself in velocity and lateral resolution. This analysis method takes its nature from an experiment of Lord William Thomson, as known as Lord Kelvin, who explained the build in contact potential difference in metals.[31] The technique was initially applied to visualize the metal surface with low resolution.[30] Few year later came the use of this technique in self assembled monolayers[32] and biological cell membrane.[33] Nowadays, KPFM gives the possibility to combine electrical and topological information with a resolution closely to few nanometer. In deep this technique combined with topological information from AFM gives, thanks to the conductive tip, informations about the distribution of contact potential difference (CPD) at nanoscale resolution. What is measured in this technique is not the conduction but the electrostatic interaction created between the tip and the sample.

Electrostatic forces, being a long range interaction force, do not require a contact between the two surface. KPFM is not a contact mode, AFM based on a vibrating capacitor set up where the two electrodes of the capacitor are the surface and the oscillating AFM tip. Being a no contact and no destructive techniques, it doesn't have the risk of damaging or removing weak species from the surface.

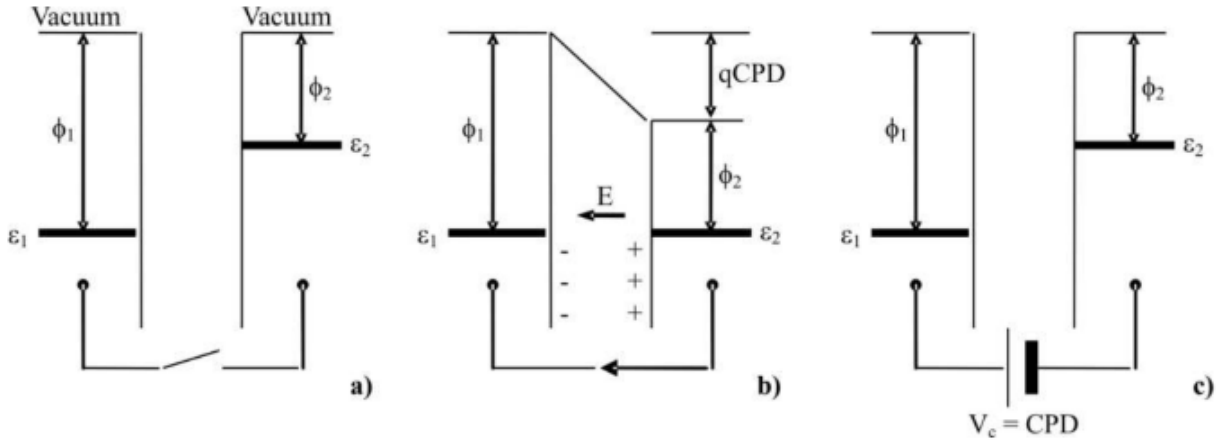

Fig 1.2.5 Schematic diagram of Kelvin Probe physics. a) Two materials 1 and 2 with different work functions ε_1 and ε_2, corresponding to the energydifference between the Fermi level e and the vacuum level. b) When the two materials are electrically contacted, electrons flow from 2 to 1 until theFermi levels are aligned, leading to a contact potential Vb. The charges present in the two materials causes an electric field E. q: electron charge; CPD:contact potential difference. c) The electric field is removed by applying an external potential Vcwhich equals the contact potential.

In the modern set up, a conductive tip scan the surface in a non-contact mode following its topography. An applied alternating voltage V_{ac} with a specific frequency ω is applied to the tip during the scan. The tip interacts during the scan with the surface with attractive and repulsive

forces at the same frequency of V_{ac}. During the interaction the electrostatic forces induces a mechanical oscillation of the cantilever at ω frequency. The oscillation of the tip then is recorded by a photodiode, which send a signal to the lock in amplifier that try isolating the oscillation ω. Where the amplitude of the oscillation is proportional to the surface potential between tip and surface. In order to get a precise value of the work function is positioned another feedback loop. A given direct current V_{dc} is applied to the tip in system, in order to minimize the electrostatic interactions. In this configuration both, the alternating V_{ac} and direct current V_{dc}, are applied to the cantilever and the sample. The electrical configuration can be expressed as follow:

$$\Delta V = \Delta\phi - V_{dc} + V_{ac} \sin(\omega t) \tag{2}$$

where,

$\Delta\phi$ is the contact potential (difference in work function between tip and sample);

V_{dc} is the direct current applied to the tip;

V_{ac} is the alternating current with ω amplitude and a specific frequency.

The previous equation can be used to derive the electrostatic force present during the interaction between tip and sample. Assuming a parallel plane capacitor, created by the tip and the sample, the energy between the two plate can be expressed:

$$U = \frac{1}{2} C \Delta V^2 \tag{3}$$

Where C is the Capacitance between the tip and the sample. The force generate during the approach between the due object can be derived as follow:

$$F = -\frac{\partial U}{\partial z} = -\frac{1}{2}\frac{\partial C}{\partial z}\Delta V^2 \tag{4}$$

Where

$$F = F_{dc} + F_{\omega} + F_{2\omega} \tag{5}$$

Adding the direct current V_{dc} component inside the equation:

$$V_{dc} = -\frac{1}{2}\frac{\partial C}{\partial z}\left[(\Delta\phi - V_{dc})^2 + \frac{V_{ac}^2}{2}\right] \tag{6}$$

Adding also the two frequencies ω and 2ω:

$$F_{\omega} = -\frac{\partial C}{\partial z}[(\Delta\phi - V_{dc})V_{ac}\ \sin(\omega t)] \quad (7)$$

$$F_{2\omega} = -\frac{1}{4}\frac{\partial C}{\partial z}[V_{ac}^2 \cos(2\omega t)] \quad (8)$$

The information on the electrical properties of the sample can be obtained analysing separately the three terms F_{dc}, F_{ω} and $F_{2\omega}$.

Alternatively, another measuring method can be applied in Kelvin force microscopy. In frequency modulation (FM-KPFM) the detected signal is the gradient of the force, $\nabla F = \partial F/\partial z$. The measurement of such signal can be achieved in two different ways: detecting the frequency shift or the phase shift at a given frequency (ω).

When lifted, the tip is oscillating and the change in frequency and phase shift is recorded. In the limit of small force gradient the resonant frequency shift and phase shift are given by::

$$\Delta\omega = \frac{\omega_0}{2\kappa}\frac{\partial F}{\partial z} \quad (9)$$

and

$$\Delta\phi = \arcsin\left(\frac{Q}{k}\frac{\partial F}{\partial z}\right) \quad (10)$$

where ω_0 is the resonance frequency, k is the spring constant, Q the quality factor of the cantilever.

Considering tip-sample systems as a parallel capacitor, the gradient can be written as:

$$\frac{\partial F}{\partial z} = -\frac{1}{2}\frac{\partial^2 C}{\partial z^2}(\Delta V)^2 \quad (11)$$

Combining the equations 9, 10 and 11 we obtained:

$$\Delta\omega = -\frac{\omega_0}{4\kappa}\frac{\partial^2 C}{\partial z^2}(\Delta V)^2 \quad (12)$$

$$\Delta\phi = -\arcsin\left(\frac{Q}{2\kappa}\frac{\partial^2 C}{\partial z^2}(\Delta V)^2\right) \quad (13)$$

Thus, the resonance frequency and phase shift are squared function of the potential between the tip and the sample. The resolution of this mode is determined by the lateral variation of the gradient $\partial^2 C/\partial z^2$.[34]

KPFM principally work using two modes. The first one scans at the beginning in topography (AFM), then in a second scan, a mechanically lift is applied to the cantilever. The lift is required to

reduce the contribution in the signal of the short range forces. Then when the tip in far enough to the surface a second scan is performed recording the electrostatic forces.

1.2.7. Applications of SPM

Nowadays the progress regarding scanning force microscopy gives the possibility to analyze any kind of samples from insulating to conductive one. Born at the beginning as an instrument for surface characterization with the years become essential as instrument for the nano-world. Principally the classification of scanning probe can be done not in regard which type of sample we would like to analyse but in function of which type of information we want to get from the sample.

Scanning tunnelling Microscopy/ Spectroscopy (STM/STS), first microscope discovered, [1] mainly used for electrical and topological characterization. Thanks to its lateral resolution is mainly applied to visualization and manipulation of molecules and atoms in different environments.

Atomic force Microscopy (AFM), second microscope discovered in time line,[2] developed during the years in different conformation with different lateral resolution. Is used for surface characterization, where nowadays with the possibility to tune the instrument easily can be used for: topological information, friction, adhesion information, tribological information (Peak force Quantitative Nanomechanical Mapping PFQNM)[14].

Kelvin Force Microscopy (KPFM), used for measuring surface potential difference (CPD) in conductive samples. KPFM gives the possibility, knowing the work function of the tip, to detect the work function of the sample giving information also about the density of states.

Magnetic Force Microscopy (MFM), used for measuring magnetic sample. It is based on magnetic tip that scans magnetic samples. Based on the interaction between the two magnetic sample-tip is possible to reconstruct the magnetic topology of the sample.

Near field scanning optical microscopy (SNOM) is a microscopy technique which investigate nanostructures with the use of evanescence waves. The excitation laser is focused through an aperture with a diameter smaller than the excitation wavelength. In particular the resolution achieved is a function of the distance between the tip and the sample where the optical resolution of the transmitted or reflected light is limited by the diameter of the aperture.

References

1. G. Binnig, H. Rohrer. Scanning tunneling microscopy. **55,** 726 (1982).
2. Binnig, G., Quate, C. F. & Gerber, C. Atomic Force Microscope. *Phys. Rev. Lett.* **56,** 930–933 (1986).
3. Hallmark, V. M., Chiang, S., Rabolt, J. F., Swalen, J. D. & Wilson, R. J. Observation of Atomic Corrugation on Au(111) by Scanning Tunneling Microscopy. *Phys. Rev. Lett.* **59,** 2879–2882 (1987).
4. Walczak, M. M., Chung, C., Stole, S. M., Widrig, C. A. & Porter, M. D. Structure and interfacial properties of spontaneously adsorbed n-alkanethiolate monolayers on evaporated silver surfaces. *J. Am. Chem. Soc.* **113,** 2370–2378 (1991).
5. Poirier, G. E. Characterization of Organosulfur Molecular Monolayers on Au(111) using Scanning Tunneling Microscopy. *Chem. Rev.* **97,** 1117–1128 (1997).
6. Clemmer, C. & Beebe, T. Graphite: a mimic for DNA and other biomolecules in scanning tunneling microscope studies. *Science* **251,** 640 (1991).
7. Martin, Y. & Wickramasinghe, H. K. Magnetic imaging by '"force microscopy"' with 1000 Å resolution. *Appl. Phys. Lett.* **50,** 1455–1457 (1987).
8. Terris, B. D., Stern, J. E., Rugar, D. & Mamin, H. J. Contact electrification using force microscopy. *Phys Rev Lett* **63,** 2669–2672 (1989).
9. Weaver, J. M. R. & Abraham, D. W. High resolution atomic force microscopy potentiometry. *J. Vac. Sci. Technol. B Microelectron. Nanometer Struct. Process. Meas. Phenom.* **9,** 1559–1561 (1991).
10. Matey, J. R. & Blanc, J. Scanning capacitance microscopy. *J. Appl. Phys.* **57,** 1437–1444 (1985).
11. Pohl, D. W., Denk, W. & Lanz, M. Optical stethoscopy: Image recording with resolution λ/20. *Appl. Phys. Lett.* **44,** 651–653 (1984).
12. Coombs, J. H., Gimzewski, J. K., Reihl, B., Sass, J. K. & Schlittler, R. R. Photon emission experiments with the scanning tunnelling microscope. *J. Microsc.* **152,** 325–336 (1988).
13. Williams, C. C. & Wickramasinghe, H. K. Scanning thermal profiler. *Appl. Phys. Lett.* **49,** 1587–1589 (1986).
14. High-performance scientific instruments and solutions for molecular and materials research, as well as for industrial and applied analysis | Bruker. *Bruker.com* Available at: https://www.bruker.com/. (Accessed: 28th September 2017)
15. Atomic Force Microscopy for Nanotechnology & Scientific Research | NT-MDT. Available at: http://www.ntmdt-si.com/. (Accessed: 28th September 2017)
16. Dror Sarid. *Scanning Force Microscopy With Applications to Electric, Magnetic and Atomic Forces*. (Oxford University Press, 1994).
17. Wetsel, G. C. & Drummond Roby, M. A. Dynamic scanned-probe lateral-force determination. *Appl. Phys. Lett.* **67,** 2735–2737 (1995).
18. Cleveland, J. P., Manne, S., Bocek, D. & Hansma, P. K. A nondestructive method for determining the spring constant of cantilevers for scanning force microscopy. *Rev. Sci. Instrum.* **64,** 403–405 (1993).
19. Walters, D. A. *et al.* Short cantilevers for atomic force microscopy. *Rev. Sci. Instrum.* **67,** 3583–3590 (1996).
20. BUTT, H.-J. *et al.* Scan speed limit in atomic force microscopy. *J. Microsc.* **169,** 75–84 (1993).
21. Hazel, J. L. & Tsukruk, V. V. Friction Force Microscopy Measurements: Normal and Torsional Spring Constants for V-Shaped Cantilevers. *J. Tribol.* **120,** 814–819 (1998).
22. Lüthi, R. *et al.* Nanotribology: an UHV-SFM study on thin films of C60 and AgBr. *Surf.*

Sci. **338,** 247–260 (1995).
23. Thundat, T., Zheng, X.-Y., Chen, G. Y. & Warmack, R. J. Role of relative humidity in atomic force microscopy imaging. *Surf*. *Sci*. **294,** L939–L943 (1993).
24. Weisenhorn, A. L., Hansma, P. K., Albrecht, T. R. & Quate, C. F. Forces in atomic force microscopy in air and water. *Appl*. *Phys*. *Lett*. **54,** 2651–2653 (1989).
25. Jacob Israelachvili. *Intermolecular and Surface Forces 3rd Edition*. (Academic Press, 2011).
26. Urbakh, M., Klafter, J., Gourdon, D. & Israelachvili, J. The nonlinear nature of friction. *Nature* **430,** 525–528 (2004).
27. Zhong, Q., Inniss, D., Kjoller, K. & Elings, V. B. Fractured polymer/silica fiber surface studied by tapping mode atomic force microscopy. *Surf*. *Sci*. **290,** L688–L692 (1993).
28. Tamayo, J. & García, R. Deformation, Contact Time, and Phase Contrast in Tapping Mode Scanning Force Microscopy. *Langmuir* **12,** 4430–4435 (1996).
29. Revenko, I. & Proksch, R. Magnetic and acoustic tapping mode microscopy of liquid phase phospholipid bilayers and DNA molecules. *J*. *Appl*. *Phys*. **87,** 526–533 (1999).
30. Nonnenmacher, M., O'Boyle, M. P. & Wickramasinghe, H. K. Kelvin probe force microscopy. *Appl*. *Phys*. *Lett*. **58,** 2921–2923 (1991).
31. Kelvin, Lord. V. Contact electricity of metals. *Philos*. *Mag*. **46,** 82–120 (1898).
32. Lü, J. *et al*. Kelvin Probe Force Microscopy on Surfaces: Investigation of the Surface Potential of Self-Assembled Monolayers on Gold. *Langmuir* **15,** 8184–8188 (1999).
33. Knapp, H. F., Mesquida, P. & Stemmer, A. Imaging the surface potential of active purple membrane. *Surf*. *Interface Anal*. **33,** 108–112 (2002).
34. Palermo, V., Palma, M. & Samorì, P. Electronic Characterization of Organic Thin Films by Kelvin Probe Force Microscopy. *Adv*. *Mater*. **18,** 145–164 (2006).

2. Aim of the work

Self-assembly is a bottom-up process in which components (molecules, nanoparticles, etc) spontaneously form ordered aggregates from nano- to macro- scale.[1] In the last decades it is emerged as an attractive route to nanostructured materials with programmed complex morphologies and dedicated properties (i.e. shape and functional groups).

One of the fundamental aspects of this approach is that relatively weak intermolecular forces are used to direct the assembly of the subcomponents. One of the major goals in materials chemistry today is the production of highly ordered structures with low cost and up scalable technologies to give functional systems for organic electronic applications.[2,3,4] The manipulation of molecules and macromolecules to form highly ordered structures such as single crystals, liquid crystalline layers, self-assembled monolayers (SAMs) or ordered structures is important in many application fields from material reinforcement to molecular electronics. Therefore is more important to use the right approach to build highly ordered architectures on solid surfaces.

Is also important to define how self aggregations enable to obtain structures that could be difficult if not impossible to obtain with molecular synthesis,[5] giving with that the possibility to play an active role in nanoscience and nanotechnology.

Therefore self-assembly offer a new route in fabrication of three dimension microstructures.

Actually, several efforts are devoted to exploit the self-assembly as a scalable process. In general, we are able to synthesis many nanoscale structures, colloids, quantum dots, etc. but remains difficult to induce their self-assembly into functional structures at the industrial scale.[6,7] Macroscopic objects can be fabricated that self-assemble well,[8] but scaling the fabrication of these structures into dimensions of microns, much less nanometers, remains an unsolved problem in particular for industrial scale up. Self-assembly of appropriate components as a strategy for generating ordered aggregates seems likely to prove reliable and versatile method to build functional structures that show peculiar new properties.

The understanding of the role of the self-assembly mechanisms is crucial to realize molecularly precise self-organized systems at the nanoscale with well-defined architectures and pre-programmed electronics properties. For this reason, the PhD activities was focused on the study of self-assembly mechanisms of model systems at liquid–solid interfaces.

Two systems have been studied:

i) silver nanoclusters $Ag_{44}(4FTP)_{30}$ (a.k.a. IBAN, intensely and broadly absorbing nanoparticle),

ii) azobenzene molecules (Disperse Orange 3, Acid yellow 9) with conformational isomerization driven by external stimulus (cis- LIGHT freq, trans, LIGHT freq). Both systems consisted of monodisperse building blocks with simple geometry: planar and spherical, respectively, which do not interact with the substrate. In both cases the self-assembly mechanisms were not assisted by the surface being only governed by the geometry and the chemistry of the bricks.

All the activities have been performed in collaboration with European partners involved within the EU Marie Sklodowska-Curie project "ISwitch" (G.A. 642196).

Synthetized by the group of Prof. Stellacci (SUNMIL lab, EPFL, Losanne), IBANs are fully monodispersed nanoparticles stable in solution used as prototype systems to produce high quality macroscopic crystals. Conversely, commercially available on Sigma Aldrich, azobenzene molecules are used to produce functional architectures using scalable approaches. In particular, the integration of molecular switches with inorganic surfaces has recently shown an increasing interest to produce novel hybrid multifunctional materials.

Self-assembly processes have been driven tuning the stability of the silver nanocluster suspensions and exploiting the solvent vapour annealing approach (SVA).[9] In this way, tuning the supramolecular interactions between the nanoparticles, with solvent and substrate, we obtained in controlled way self-aggregated structures with different morphologies and properties, ranging from low-density fractal aggregates, to close-packed but amorphous aggregates or even highly-ordered crystals.[10]

It is important to underline that the SVA method allows its thermodynamic driven. The building blocks (molecules or particles) are firstly deposited on the substrate forming an amorphous layer, corresponding to the case of the maximal disorder. In this way, the presence of solvents can allow the system to evolve quickly from such high-energy morphology to a most favourable uniform, crystalline layer.

Tuning the environment conditions (solvent, temperature, time of exposure, pressure) we were able to produce crystals with different morphologies (3D crystals and 2D layered structures) with corresponding different physico-chemical properties (Figure 2.1).

Also in the case of azobenzene molecules we can neglect the interaction between the molecule and the substrate. For this reason, due to the higher degrees of freedom, the obtained structures show a lower ordering, as depicted in 3D-AFM, Figure 2.2.

It is noteworthy to underline that SAM deposition on surfaces is currently used as a fast and cheap approach to tune the surface properties such as polarity, chemical reactivity, or charge transfer characteristics at interfaces.[11,12,13] The possibility to drive a conformational switch directly in SAMs opens the way to induce a reversibly change of the surface properties by using external stimuli, e.g., light.[14,15]

All the produced structures have been characterized using microscopic, spectroscopic and diffraction techniques.

Most of the experimental activities of the PhD have been devoted to use of Scanning Probe techniques (AFM, KPFM) to achieve a quantitative analysis of the morphological and electronic properties (i.e. work function, dipoles density, dipole alignment due to conformational switching, etc.) of the produced self-assemblies with nanometric resolution. Image analysis have been performed using SPIP 6 allowing to manage automatically hundreds of different samples. AFM/KPFM measurements have been performed using Multimode 8 microscope (Bruker).

A dedicated analysis has been performed to characterise the starting building block materials (i.e. dimension, monodispersity, stability of suspensions, etc.) pot life. In particular, UV-vis and Fluorescence spectroscopies and Fluorimetry were used to investigate the solution stability and as well as, the mechanism involved to create different ordered structures.

A dedicated study of the structural properties of the produced crystals have been performed using X-ray scattering techniques: *ex-situ* X-Ray Diffraction (XRD) measurements performed at CNR-IMM and *in-situ* Grazing Incidence Wide/Small Angle X-ray Scattering (GISAXS/GIWAXS) performed at Electra synchrotron in Trieste. Chemical analysis and thermal stability are monitored combining X-ray Photoemission (XPS) and Mass (MS) spectrometries.

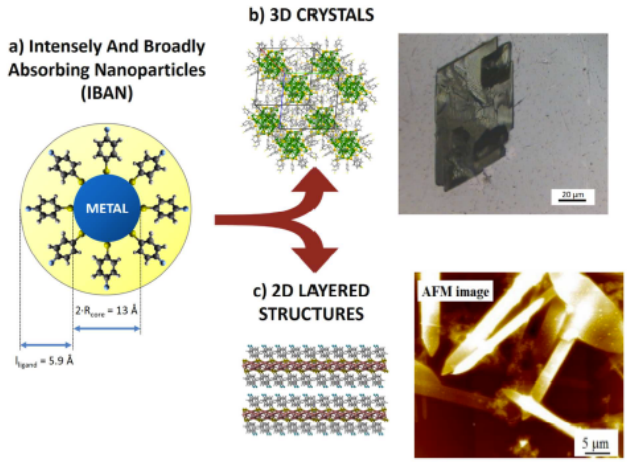

Fig 2.1. a) Cartoon of Silver Nanocluster, b) rearrangement in 3D structure in optical microscopy, c) 2D self assembly in AFM image and molecular simulation.

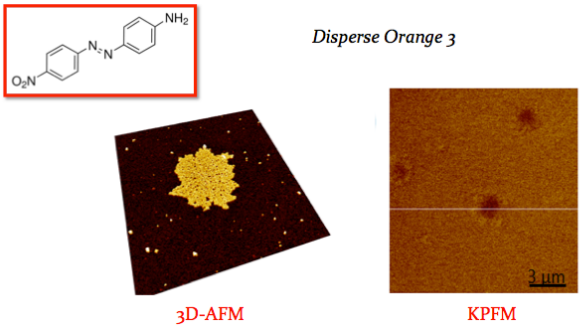

Fig. 2.2 3D AFM of Azobenzene Disperse Orange 3 SAM not covalently bonded on silicon oxide 300 nm. KPFM after light stimulus.

References

1. Whitesides, G. M. & Boncheva, M. Beyond molecules: Self-assembly of mesoscopic and macroscopic components. *Proc. Natl. Acad. Sci.* **99,** 4769 (2002).
2. Hagen Klauk. *Organic Electronics: Materials, Manufacturing, and Applications*. (Hagen Klauk, 2006).
3. Yang, H., Yuan, B., Zhang, X. & Scherman, O. A. Supramolecular chemistry at interfaces: host-guest interactions for fabricating multifunctional biointerfaces. *Acc. Chem. Res.* **47,** 2106–2115 (2014).
4. Yan, H. *et al*. A high-mobility electron-transporting polymer for printed transistors. *Nature* **457,** 679 (2009).
5. Whitesides, G. What Will Chemistry Do in the Next Twenty Years? *Angew. Chem. Int. Ed. Engl.* **29,** 1209–1218 (1990).
6. Xia, Y., Gates, B. & Li, Z.-Y. Self-Assembly Approaches to Three-Dimensional Photonic Crystals. *Adv. Mater.* **13,** 409–413 (2001).
7. Bachtold, A., Hadley, P., Nakanishi, T. & Dekker, C. Logic circuits with carbon nanotube transistors. *Science* **294,** 1317–1320 (2001).
8. Bowden, N. B., Weck, M., Choi, I. S. & Whitesides, G. M. Molecule-Mimetic Chemistry and Mesoscale Self-Assembly. *Acc. Chem. Res.* **34,** 231–238 (2001).
9. De Luca, G. *et al*. Solvent vapour annealing of organic thin films: controlling the self-assembly of functional systems across multiple length scales. *J. Mater. Chem.* **20,** 2493–2498 (2010).
10. Palermo Vincenzo & Samorì Paolo. Molecular Self-Assembly across Multiple Length Scales. *Angew. Chem. Int. Ed.* **46,** 4428–4432 (2007).
11. Love, J. C., Estroff, L. A., Kriebel, J. K., Nuzzo, R. G. & Whitesides, G. M. Self-Assembled Monolayers of Thiolates on Metals as a Form of Nanotechnology. *Chem. Rev.* **105,** 1103–1170 (2005).
12. Ulman, A. *Chem Rev* **96,** 1533 (1996).
13. DiBenedetto Sara A., Facchetti Antonio, Ratner Mark A. & Marks Tobin J. Molecular Self-Assembled Monolayers and Multilayers for Organic and Unconventional Inorganic Thin-Film Transistor Applications. *Adv. Mater.* **21,** 1407–1433 (2009).
14. Feringa, B. L. & Browne, W. R. *Molecular switches*. **42,** (Wiley Online Library, 2001).
15. Ferri, V. *et al*. Light-Powered Electrical Switch Based on Cargo-Lifting Azobenzene Monolayers. *Angew. Chem.* **120,** 3455–3457 (2008).

3. Experimental techniques

In this chapter we will describe the work of principle of the other experimental techniques used to characterize the two model systems, IBANs and azobenzenes. XPS was mainly used to characterize chemically the silver nanoclusters, both in disperse form that in self assembled in highly ordered structure. XPS was useful to get information about the different mechanism of degradation which involve oxidation process of the silver nanocluster species.

UV-Vis spectroscopy used to confirm the quality of the silver nanoclusters batches, in monodispersity and time life. On the other hand this technique was mandatory to be used when we treated azobenzene. Irradiating in situ and ex situ with UV-light, spectrophotometry was the right choice to understand the switching behaviour or the azo molecules in solution.

Resonance light scattering (RLS) performed with a classical fluorescence spectrophotometer and analized in comparison with UV-Vis spectra gave informations about aggregation mechanism and formation of cromophore species.

XRD performed at IMM department of CNR of Bologna, to understand the grade of self assembling of the different systems. XRD was in particular a useful technique for the layered material where found immediately the inter layer spacing, it also gave information about the disposition of the atoms between the layers.

Grazing Incidence Small/Wide Angle X Ray Scattering used at ELECTRA Synchrotron facility of Trieste act to understand, due to the complexity of the systems that we produced in solvent vapour annealing, the different crystals lattice. Furthermore GISAXS gave also the possibility to apply temperature trends to investigate in situ the changing of the different morphology and stability with temperature.

3.1. X ray photoemission spectroscopy

X-ray photoelectron spectroscopy (XPS), also called electron spectroscopy for chemical analysis (ESCA) is a very suitable technique for investigating thin surface layers. In XPS, the substrate is bombarded with *X*-rays with a well-defined energy. The X-rays interact with core electrons present around the nucleus of the different atoms present in the sample, and these electrons, if they escape the sample, is emitted at a well-defined kinetic energy, EK, given by:

$$Ek=hv-Eb-\Phi \quad (14)$$

Where *hv* is the *X*-ray photon energy, E_b is the electron binding energy, and Φ the work function that is the energy needed for the electron to free itself from the surface. Where all the values depends on the spectrometer and the substrate.

In fact the kinetic energy of the photoelectrons emanating from different types of atoms and orbitals, and even the same type of atom and orbital in different binding states, have different binding energies. Thus, by separating the electrons with different kinetic energy in an analyser and displaying the results in a spectrum showing the photoelectron intensity different types of atoms present on the surface and their abundance can be easily determined. XPS is surface sensitive due to the short inelastic mean free path, λ, of electrons in Condensed materials. Typical values are 1–2 nm for metals, 1.5–4 nm for oxides and down to 3 nm for organic materials.

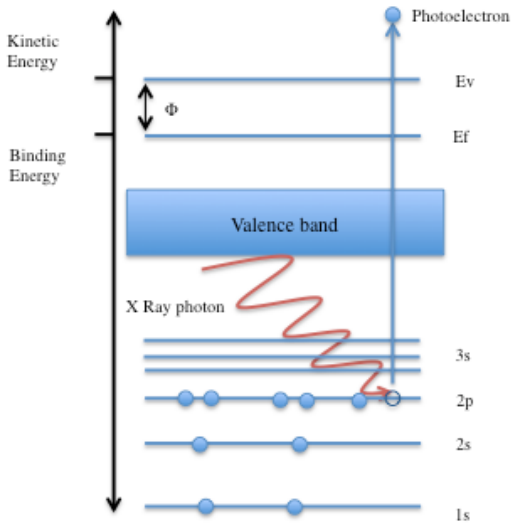

Fig 3.1 Schematic representation of the XPS process.

The quantification of the ESCA results can be carried out in different ways and to different degrees of sophistication. The most common method is to present the results in atom%, where the relative abundance of the different types of atoms in the surface layer is calculated by dividing the photoelectron intensity for a given element with the sensitivity factor of that element. In cases where the adsorbed layer contains an element that is not present in the substrate, a more detailed analysis can be carried out.

The main problem with using XPS as a tool for studying cleaning processes at surfaces is that it is a high vacuum technique. Thus, the sample has to be transferred from the solution to vacuum prior to analysis. This can lead to unwanted deposition (of Langmuir–Blodgett type) or desorption when the sample is removed from the solution. Although XPS analysis is a non-destructive technique, however, some care should be taken since X-ray degradation followed by evaporation of low molecular fragments may occur. The best way to control if this is the case is to record the ESCA spectrum a few times to determine if the peak intensities are changing or not.

In summary, XPS provides important information on surface composition, and it is a useful technique for investigating adsorption and removal processes. However, care should be taken when preparing the sample in order to minimize the chemical changes occurring during transfer from solution to high vacuum. The technique has not been extensively used for studying removal of particulate soil, but this is certainly possible provided the particles contain some element that makes it easily distinguished from the substrate. Modern XPS instruments are equipped with scanning possibilities, which allows surface maps of the elements to be created. Thus the distribution of particles over the surface can also be investigated.

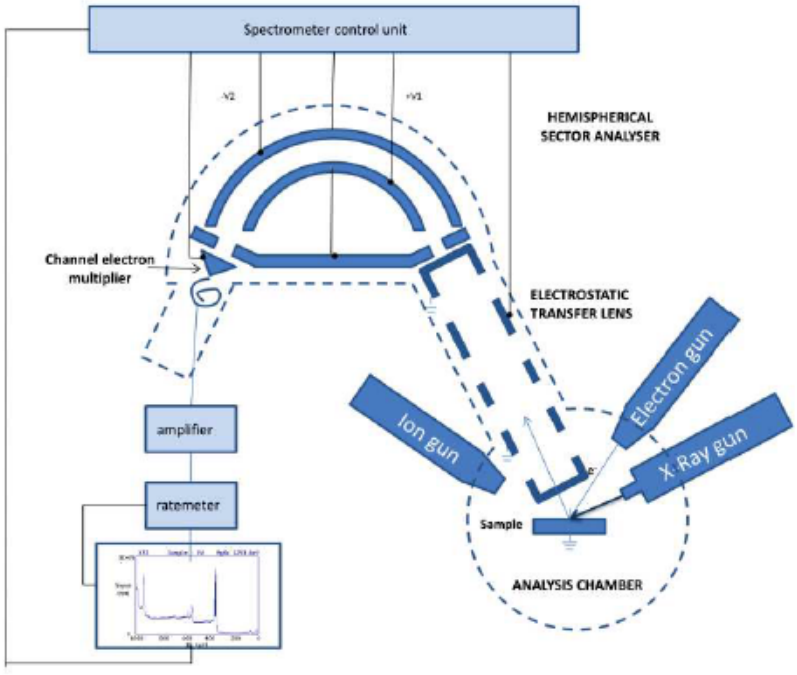

Fig 3.2 Schematic representation of the principal working blocks of the XPS.

All the work done on XPS in this thesis were performed on each deposit with a Phoibos 100 hemispherical energy analyser (Specs), using Mg Kα excitation source (XR-50, Specs) (photon

energy = 1253.6 eV). The X-ray power was 250 W. The base pressure in the analysis chamber during analysis was 2×10^{-10} mbar.

3.2. UV-Vis Spectrometry

UV-Vis is a fast, simple method to determine the concentration of an analyte in solution. It can be used for relatively simple analysis as well as in combination with different instrument as HPLC in the detector part. The principle is based on the ability of the analyte to absorb or reflect the incident light giving consequently information about its concentration.

The Beer-Lambert Law is at the base of the working principle of the instrument where the absorbance of a solution is directly proportional to the concentration of the species in the solution and also functional of the path length.[1] At the same time is mandatory to know the velocity of the absorbance changing with the concentration and this information is only given by molar extinction coefficients. The Lambert-Beer law (or Beer's law) is a linear relationship between absorbance and concentration of an absorbing species. The general Beer-Lambert law is usually written as:

$$A = \varepsilon * b * c \tag{15}$$

Where ε is the molar extinction coefficient, b is the path length and c the concentration of the analyte in solution. Sometimes Beer's law can deviate from the linearity due to high concentration of the analyte that saturate the signal producing an absorption flattening.

The UV-Vis instrument measures the intensity of the light passing through a sample (in general a cuvette) comparing the intensity of the light before and after passing the sample. The value detected can be expressed, generally in two ways, Transmittance (T), expressed as a percentage (%T) or Absorbance (A), function of transmittance.

$$A = - \log T \tag{16}$$

The spectrophotometer can be also configured in reflectance where in this case is measured the light reflected from the sample, as transmittance reflectance is expressed as percentage (%R).

A spectrophotometer is mainly constituted by a light source, a sample holder, a prism to separate the different wavelengths and a detector. The radiation is emitted with different source, in general Tungsten filament (300-2500 nm), deuterium arc lamp to reach also a small part of the ultraviolet radiation (190-2000) or nowadays also LED lamp in the visible part of the spectra.

The detector normally are photodiodes, charge coupled device or photomultiplier. Spectrophotometer normally has two configurations: single beam or double beam. Single beam,

first configuration to be developed present only in old instruments. Double beams, where the light, is split in two beam before reach the sample or the blank.

Samples in UV/Vis are in general liquids but gases and solid can be also analysed. Fused silica, quartz glass, common glass or plastic are the principal sample holders used in function of the spectra analysed.[2]

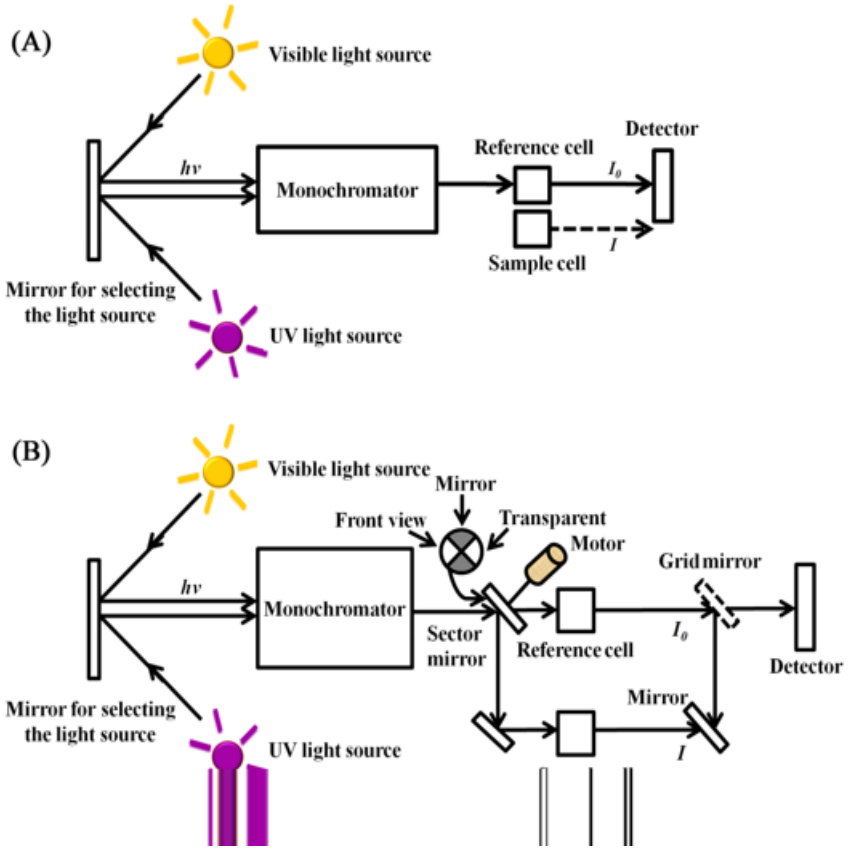

Fig 3.3 Working principle of (A) single beam spectrophotometer and (B) double beam spectrophotometer.

UV-vis spectroscopy measurements were performed using Perkin Elmer LAMBDA 650 spectrophotometer (deuterium and tungsten light sources), a high-performance double-beam dual monochromator spectrometer with microcomputer electronics. Its wavelength range extends from 900 to 190 nm. Spectral band width in the UV-vis range is from 0.17 to 5.00 nm. Range of wavelength tested from 900 to 300 nm. The 24h solution monitoring were performed with Agilent CARY 100, double beam, dual chopper, ratio recording, Czerny-Turner 0.278 m monochromator UV-vis spectrophotometer, centrally controlled by a computer.

3.3. Resonance light scattering (RLS)

Resonance light scattering is a useful technique discovered by Pasternack and collaborators in 1993.[3] Pasternack observed that using synchronous scanning in a classical fluorescence spectrophotometer the light scattering signal increased of several order of magnitude when self assembling with DNA samples.

The theory behind this techniques and in accordance with electromagnetic theory, scattered light, is radiated by electrons in scatterers of a scattering system, which are accelerated and set into oscillatory motion with the excitation of an incident electromagnetic wave.[3,4] Since all systems, with the exception of a vacuum, are more or less heterogeneous, light scattering thus exists widely in the universe, and this phenomena is at the basis of resonance light scattering (RLS).[4]

Resonante light scattering is a techniques normally used for bio assemblies analysis, aggregation of inorganic species and different analytical purpose where aggregates are normally formed.

Some features that gives to RLS the characteristic to be unique and very powerful in aggregates analysis:

- Good selectivity and sensitivity due to the RLS detections on light scattering signals at or near the absorbing region of the scatterer system.
- Easy to use. RLS signals can be easily measured with a conventional fluorospectrophotometer without using complex instrumentation or expensive light source.
- Great potential in analytical chemistry, due to the ability to detect agglomeration giving information also about the nature of the analytes and dimension.

All the measurements presented in this thesis were performed using Steadystate photoluminescence synchronous spectra in deaerated and air-equilibrated solutions, using an Edinburgh FLS920 fluorimeter, (300–850 nm), at the excitation wavelength of 340 nm.

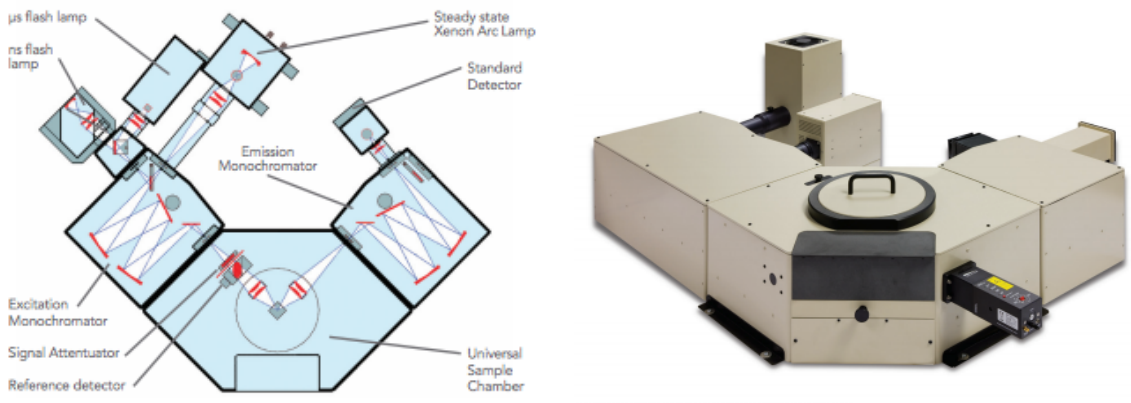

Fig 3.4 Standard layout for an FLS920 Series spectrophotometer.

3.4. X ray diffraction analysis

X-ray diffraction (XRD) is a useful technique and a non-destructive method to analyse all kinds of materials from liquids to powders and crystals. With the Bragg reflection associated to the crystal structure is possible to correlate the properties of a material with its crystal structure.

Additionally XRD can be used to get information about the unit cell parameter and other quantitative information, as the percentage of different minerals in a powder mixture and crystalline phases.

X ray are used to produce a diffraction pattern because their wavelength λ are the same order of magnitude of the d spacing of the crystal lattice.

The working principle is based on the Bragg equation:

$$N\lambda = 2d\sin\theta \tag{17}$$

Where n is an integer, λ is the wavelength, d is the interplanar crystalline distance, θ is the incident angle of the beam.

When the equation is satisfied, the scattered radiation that coming from atoms of a periodic structure is in phase obtaining a diffraction pattern with a direction defined by the angle θ.

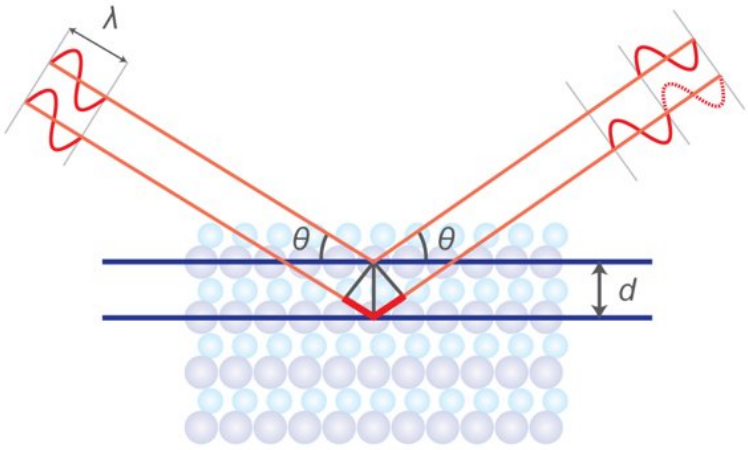

Fig 3.5 Cartoon representing the Scattering diffraction coming from a periodic crystalline structure with a direction of diffracted light of θ.

Diffraction pattern can be easily considered as the fingerprint of an ordered materials and can be used as a map for chemical identification of different coumpounds and properties of material.

Nowadays most of the diffractometers present in laboratories are configured in reflection geometry where the radiation produced by the x ray source are reflected off by the sample onto the detector. This configuration is generally known as Bragg-Brentano geometry.

The Bragg-Brentano geometry is also divided into two types:

In the θ-2θ geometry, the X-ray source and primary optics are fixed, while the sample holder moves around θ and the secondary optics and detector moves around 2θ.

In the θ-θ geometry the sample is fixed while the X-ray source and primary optics, and the secondary optics and detector both move around θ°.

The characteristics of the two geometries are: the relationship between θ (the angle between the incident X-ray beam and the sample surface) and 2θ (the angle between the incident X-ray beam and the receiving slit-detector) is maintained throughout the analysis.

The distance between the x-ray source and the sample, and the sample and the receiving slit-detector is fixed and equal and define the diffractometer circle in which the sample is always at the center.

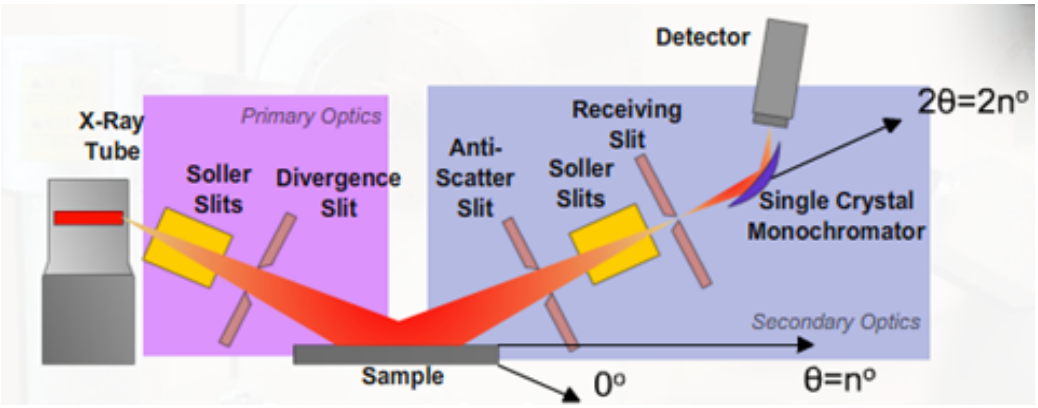

Fig 3.6 Scheme of X ray diffraction instrument and the principal components.

3.5. Grazing incidence small angle/ wide angle x-ray scattering (GISAXS/GIWAXS)

Small Angle X ray scattering is a non distructive and highly versatile method for analyzing nostructures and any type of material spanning from inorganic materials to biological ones.

X rays or neutron trasmission geometry are very well established and normally used in micro scale characterization with a high grade of precision.[5] While for investigation at mesoscale level small angle x ray scattering (SAXS) and down to molecular level, wide angle x ray scattering are the perfect candidate to be used.[67]

The combination of GISAXS/GIWAXS offer an exceptional tool for study and probing the molecular orientation in soft matter, in particular nowaday find a large use in the field of organic electronics (OLEDs, OFETs, OSCs, OPDs) where know orientation and arrangements of molecules is the key factor in the building step.[8,9]

Thanks to the technological progress and the development of x ray beams there has been an increase in molecular scale resolution joined with the reduction of data acquisition, due basically to the latest generation of synchrotron sources. This opened the door also to in situ and in operando studies.

In parallel, a revolution in detector technology has replaced traditional CCD detectors with fast single-photon counting detectors capable of collecting hundreds of frames per second with up to 90% efficiency in the hard X-ray range.

A common feature of all these experiments, whether GISAXS and GIWAXS the X-ray beam impinges on the sample surface at a very shallow angle $\alpha_i < 1°$ (measured with respect to the sample surface), while the scattering is probed with a two-dimensional detector as a function of the exit angle (or out-of-plane angle) α_f and the in-plane angle ψ.

Generally the detectors are at distances, for GISAXS, in the order of 130–500 cm, and for GIWAXS, about 10–50 cm, depending on range and detector size.[10]

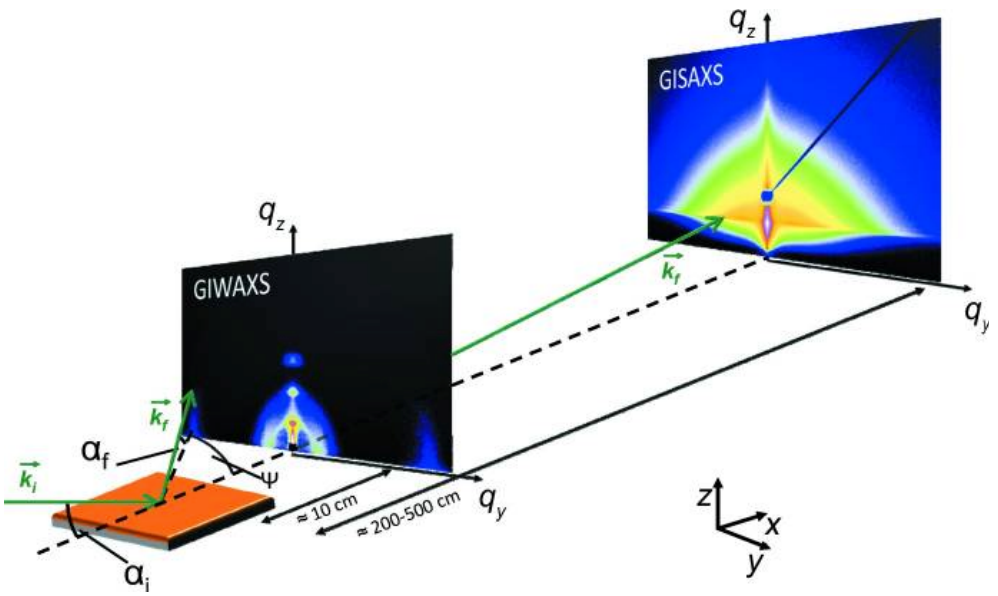

Fig 3.7 Cartoon of the scattering geometry used in GISAXS and GIWAXS. The sample surface is inclined by an incident angle αi with respect to the horizon. The exit angle is denoted αf and the in-plane angle ψ.

All the analysis performed in this thesis in regard GIWAXS and GISAXS were done at Elettra Synchrotron of Trieste, in highflux SAXS beamline. The systems has been built by the Institute of Biophysics and Nanosystems Research (IBN), Austrian Academy of Sciences, and since September 1996 is in operation. On October 2012 the beamline was transferred from the IBN to Graz University.

The beamline was mainly intended for time-resolved studies on fast structural transitions in the sub-millisecond time region in solutions and partly ordered systems with a SAXS-resolution of at least 100 nm in real-space. But increasingly also grazing-incidence (GISAXS) measurements are performed to study self-assembly processes on surfaces, or to perform structural characterisations of thin films. Additionally SAXS measurements can be coupled to simultaneous Differential Scanning Calorimetry (DSC) and Wide Angle X-ray Scattering (WAXS) recordings.

In-situ real time GISAXS measurements were performed at the beamline SAXS of ELETTRA synchrotron facility (Trieste, Italy) by using a wavelength of 1.54 Å and an incident angle, αi, of 0.4°. GISAXS images were recorded for 30 seconds every minutes during the thermal annealing in nitrogen atmosphere and after the cooling. Different thermal ramps were carried out from room temperature up to 128°C, 180°C and 300°C. 2D camera (Pilatus detector) were placed normal to the incident beam direction at 600 mm from the sample.

Ex-situ XRD measurements. 2D-GIWAXS images were collected on the pristine and annealed samples at the beamline XRD1 of ELETTRA synchrotron facility by using a wavelength of 1.542

Å. αi was chosen slightly larger than the critical angle for total reflection of the crystals (0.3°), in order to penetrate through the full crystals depth.

The diffraction patterns were recorded using a 2D camera (Pilatus detector) placed normal to the incident beam direction at 200 mm from the sample. XRD measurements, both in specular and grazing incidence geometries, were performed using a SmartLab Rigaku diffractometer in a parallel beam geometry equipped with a CuKα (λ = 1.5418 .) rotating anode followed by a parabolic mirror to collimate the incident beam and a series of variable slits (placed before and after the sample position) to obtain an acceptance of 0.02° and 0.114°, respectively.

References

1. Verhoeven J. W. Glossary of terms used in photochemistry (IUPAC Recommendations 1996). *Pure Appl. Chem.* **68,** 2223 (1996).
2. Bower, N. W. Principles of Instrumental Analysis. 4th edition (Skoog, D. A.; Leary, J. J.). *J. Chem. Educ.* **69,** A224 (1992).
3. Pasternack, R. F., Bustamante, C., Collings, P. J., Giannetto, A. & Gibbs, E. J. Porphyrin assemblies on DNA as studied by a resonance light-scattering technique. *J. Am. Chem. Soc.* **115,** 5393–5399 (1993).
4. Yguerabide, J. & Yguerabide, E. E. Light-scattering submicroscopic particles as highly fluorescent analogs and their use as tracer labels in clinical and biological applications. *Anal. Biochem.* **262,** 137–156 (1998).
5. Higgins, J. S. & Stein, R. S. Recent developments in polymer applications of small-angle neutron, X-ray and light scattering. *J. Appl. Crystallogr.* **11,** 346–375 (1978).
6. E, W. C., P, M. R. & André, G. Small-Angle Scattering of X-Rays and Neutrons. in *X-ray Characterization of Materials* 211–254 (Wiley-Blackwell, 2007). doi:10.1002/9783527613748.ch4
7. Fratzl, P. Small-angle scattering in materials science - a short review of applications in alloys, ceramics and composite materials. *J. Appl. Crystallogr.* **36,** 397–404 (2003).
8. Chen, W., Nikiforov, M. P. & Darling, S. B. Morphology characterization in organic and hybrid solar cells. *Energy Environ. Sci.* **5,** 8045–8074 (2012).
9. Müller-Buschbaum Peter. The Active Layer Morphology of Organic Solar Cells Probed with Grazing Incidence Scattering Techniques. *Adv. Mater.* **26,** 7692–7709 (2014).
10. Hexemer, A. & Müller-Buschbaum, P. Advanced grazing-incidence techniques for modern soft-matter materials analysis. *IUCrJ* **2,** 106–125 (2015).

4. Solvent-dependent structure and stability of 2D and 3D metal-organic super-structures made of silver atoms and thiol ligands

4.1. Characterization of single IBAN dissolved in solution

4.1.1. Poly dispersity index (D_R)

Atomic force microscopy was used to characterize the polydispersity of silver nanocluster to avoid any possible aggregation that could damage the formation of highly ordered structures.
Spin coated a very diluted solution on silicon substrate is possible to check a population of hundreds of nanocluster to give a good picture of the particle size and distribution.

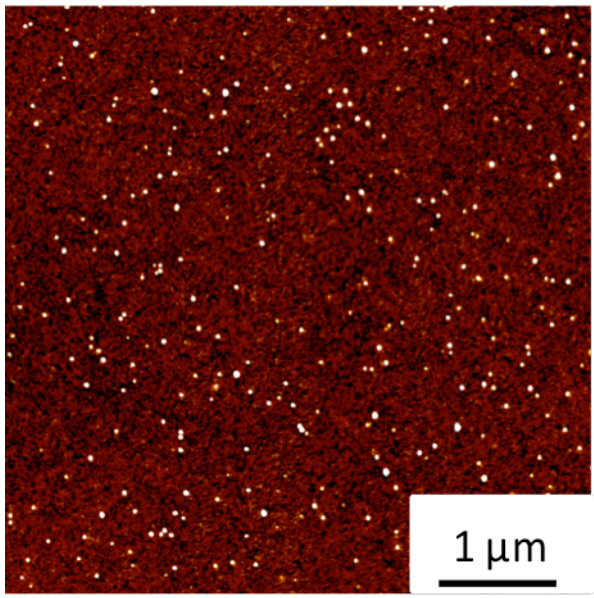

Fig 4.1 AFM image of Ag NPs deposited from dichloromethane solution on native silicon oxide substrate. Z range = 2 nm

AFM images are usefull also to calculate the size histogram $f(R_i)$, with the use of standard image analysis software (SPIP from Image Metrology and Gwyiddion by Czech Metrology Institute).
$f(R_i)$ is the number of measured objects having a given radius (R_i), so that $\sum_i f(R)_i = N_i$, for example the total numer of particles counted.

We defined the discrete distribution (p_i) and the corresponding moment $\langle R^\alpha \rangle$ as

$$p_i = \frac{f(R_i)}{N} \text{ and } \langle R^\alpha \rangle = \sum_i R_i^\alpha \cdot p_i \quad (18)$$

where $\langle \dots \rangle$ indicates the expectation value of the moment of order α of the size discrete distribution. Among these moments, the most important ones are of order one (α=1) and two (α=2).

α=1 corresponds to the average radius $\langle R \rangle$ and α=2 to the average of the radius squared $\langle R^2 \rangle$.

Polydispersity is a measure of the heterogeneity of sizes of particles. Thus, we defined the size polydispersity index (D_r) in terms of momentum distributions:

$$D_R = \langle R^2 \rangle / \langle R \rangle^2 \quad (19)$$

In case of monodispersed objects, D_R is equal to the unit. In real samples, the higher the value, the larger the radius distribution.

AFM images were studied using an automatic image processing analysis performed on >600 NP. The analysis yielded an average radius of 15±8 Å and D_R 1,2 ± 0,3 wich is comparable to the value expected for monodispersed objects ($D_R = 1$).

The measured D_R is intrinsically higher than 1 because of the noise level of the AFM measurements and the finite size of the tip $R_{tip} \geq R_{IBAN}$.

4.1.2. IBAN characterized in UV-Vis

AFM gives a good amout of data regarding size distribution and state of aggregation but precise information about the chemical nature and extend of degradation mechanism is still lacking.
UV-Vis absorption, a well established and user frendly instrument, instead can gives information about the nature of the nanocluster and the time life of the material in solution. In Fig. 4.2 is shown the UV-vis absorption spectra of IBAN solutions in different solvents. This is the simplest system to study, where each particle is well-dispersed in solution, with no perturbations due to the substrate or to other IBAN.

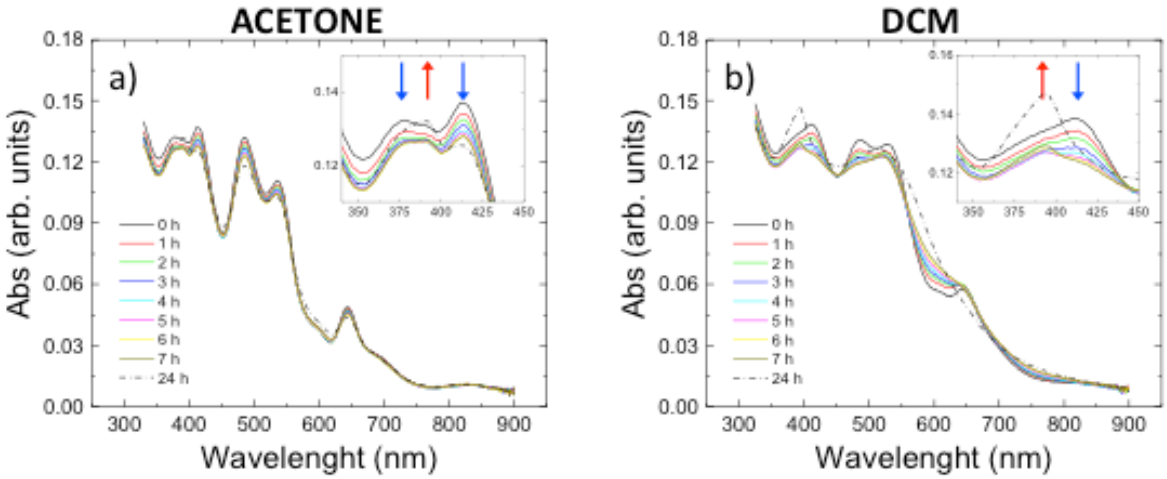

Fig 4.2 Time evolution of UV-vis absorption spectra of IBAN suspensed in (a) acetone and (b) dichloromethane solution for 24 hours. All the spectra are acquired at RT.

A highly-structured spectrum was observed in all the cases, with strong molecule-like absorption displaying several well-defined peaks, corresponding to the typical features of IBAN.[4] Althoght at t zero the spectra displayed the tyical feature of IBAN significant changes in absorption during the time were observed at room temperature when the IBANs were dissolved in (a) acetone or (b) dichloromethane (DCM).
In acetone solution the spectrum was similar to what already reported in ref 3. Though, small spectral changes showed a hypochromic effect for the peaks centered around 377 nm, 390 nm, 414 nm, 485 nm, 537 nm and 644 nm, a slight hyperchromicity of the 390 nm peak, as well as a small rise of the baseline and the possible appearance of weak new features at ca. 450 and 600 nm. The relative differences between the spectra acquired over 7h were relatively small, <7%, see fig. 4.3.

The most significant changes were mainly localized at wavelengths around 400 nm, corresponding to the contribution of the electron-rich ligands in the collective excitations di the silver core.[5,6]

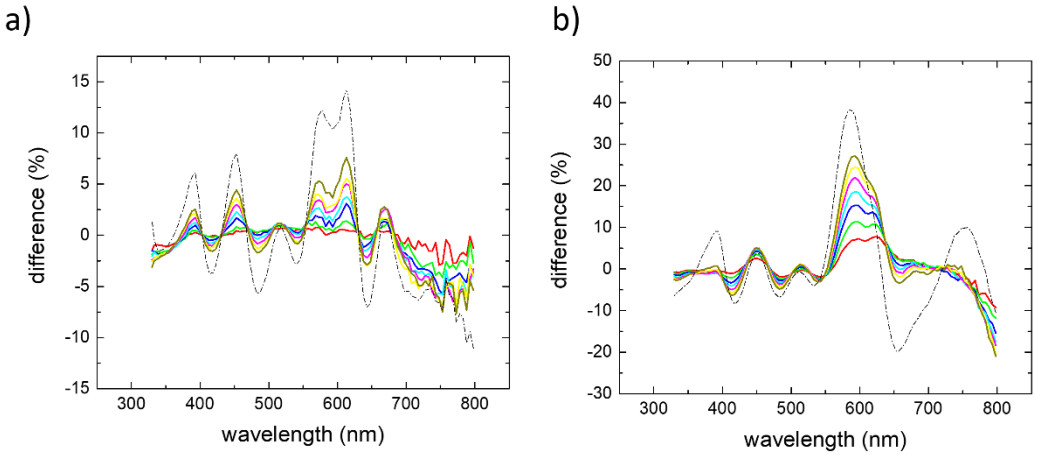

Fig 4.3 Percentage variation of the spectra shapes acquired on a) acetone and b) dichloromethane within 24 hours.

The spectral changes observed in dichloromethane, Fig. 4.3b, were more substantial and appeared faster than in acetone, leading in about 7h to the disappearance of most of the bands typical of IBAN.

A significant hypochromicity was observed in the 350-550 nm range. The final absorption profile was characterized by the presence of a peak at 390 nm and by a very broad band at 520 nm which could be explained by the transformation of the isolated IBAN into larger structures with a single plasmon-like resonance.[5] This changes are a consequence of the solvent used, as comparison, IBAN was also suspensed in the same synthesis solvent, dimethylformalamide, where it did not show any spectral changes when stored at room temperature, see fig. 4.4. We observed a decrease of the absolute values and a variation of the intensities lower that 3%. IBANs showed only changes of the spectra only when they were irradiated with light or the external temperature increased until 90°C.

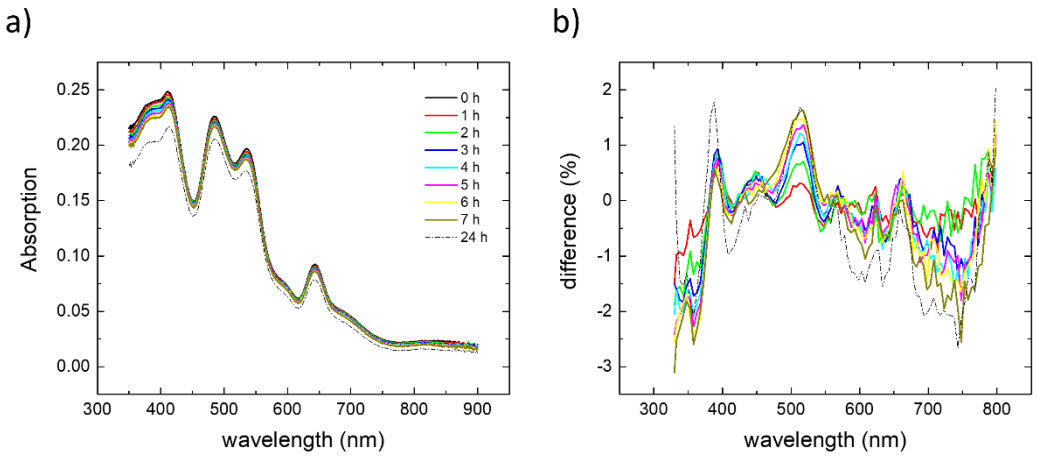

Fig 4.4 a) UV-vis absorption measurements of Ag NPs in dimetylformalamide solution acquired at different times: from 0 (pristine) to 24 hours. b) Percentage of variation of the spectra at different wavelengths. All the graphs showed the same color code: (black) 0h, (red) 1h, (green) 2h, (blue) 3h, (cyan) 4h, (magenta) 5h, (yellow) 6h, (dark yellow) 7h, (dot line) 24h.

The spectral changes observed in dichloromethane and, to a minor extent, in acetone could be explained by decomposition of the IBAN and formation of aggregates. The formation of larger structures in dichloromethane was confirmed by resonance light scattering RLS, a powerful technique sensitive to the formation of aggregates in solution particularly in the case of electronically coupled chromophores.

All spectroscopic evidence indicated a slight solvent-dependent instability of the IBAN in acetone, and a greater instability in dichloromethane. The changes present in the spectra gives information about the presence of two species, with different shape and dimensions, responsible to the creation of different highly ordered structures. In both cases, IBANs solution in acetone and in dichloromethane showed the presence inside the same solution of both species. One species more pronunciated in acetone, (major quantity of natural IBAN respect to denaturazed form), opposite in dichloromethane.

4.1.3. Resonance light scattering characterization

Resonance light scattering was used in combination with UV-Vis spectrophotometer. Thanks to the ISOF-CNR facilities was possible to measure, at the same time, the sample in UV-Vis and Fluorimetry. This opportunity gave us the possibility to check, with two instruments, what happen in solution without any possible influence from outside. The stability of the nanocluster was mainly evaluated in UV-Vis spectrometry and the information coming from the resonance light scattering was used to confirm the degration mechanism in regard aggregation phenomena. Being UV-Vis spectrophotometer and Fluorimeter two instruments present in our group and in the same room was considered the right choise to get information about the degradation mechanism without a particular emphasis on the study. For this reason DLS and SEM was not applied, also because Atomic force microscopy was a "daily" instrument used in our lab.

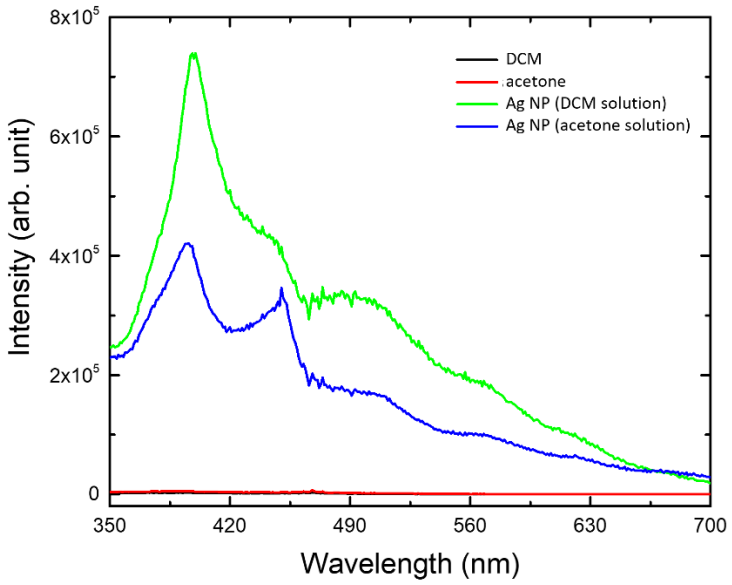

Fig 4.5 RLS spectra measured in dichloromethane (DCM) (green) and acetone (blue) solution. Reference measurements were performed on pure solvents (black and red, respectively).

In resonance light scattering the intensity of the spectra of freshly prepared Ag NP solutions in acetone and dichloromethane was about 70-fold higher than the neat solvents spectra, in line with the presence of noble metal nanoparticles in solution.[1] In time, both Ag NP solutions displayed an increase in the intensity of the scattered light, these phenomena being more prominent in dichloromethane indicates the growth of aggregated species.

4.2. Supramolecular self-assembly of IBAN on a solid substrate

In general, (meta)stable suspensions of nanoparticles (or clusters) become unstable when deposited on a substrate and the solvent slowly evaporates (drop casting). The structure of the aggregates depends on the supramolecular interactions between the nanoparticles, with solvent and substrate, yielding structures ranging from low-density fractal aggregates, to close-packed but amorphous aggregates or even highly-ordered crystals.

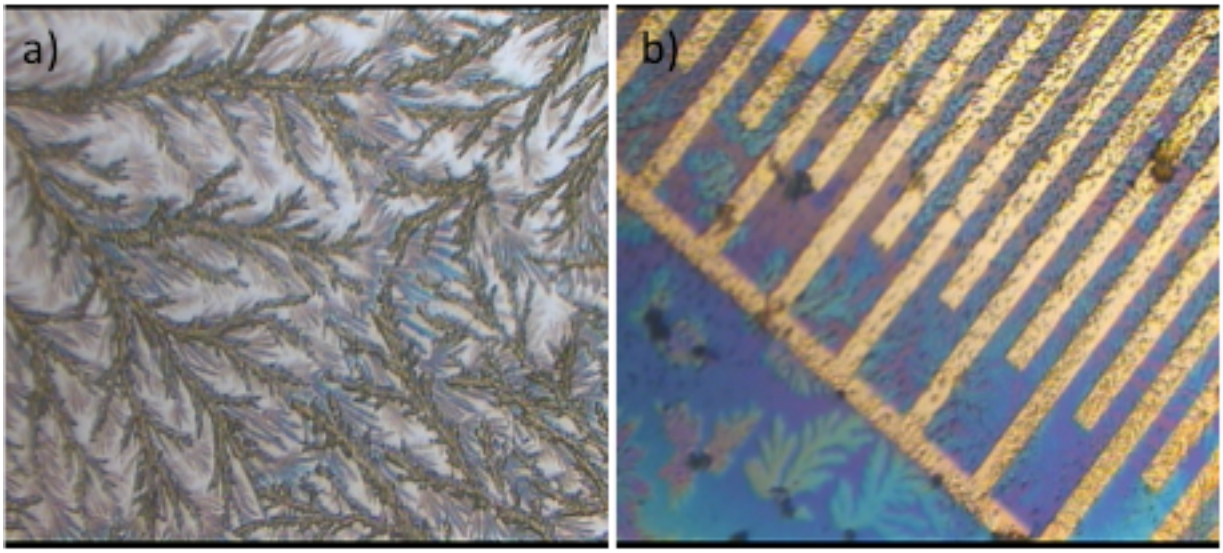

Fig 4.6 Low energy ordered structures of IBAN dissolved in acetone with a low time exposure to SVA treatment: a) Fractals on SiO_2, b) fractals on organic field effect transistor (OFET).

In the work of Yang et al., large crystals of IBAN were grown in about 3 days by drop casting from dimethylformalamide solutions and with a very slow evaporation of the solvent. We obtained a much faster and bigger size than the previous work using solvent vapour annealing (SVA), improving in this way the control of the self-assembling process.

The key of SVA approach is that the target molecules or particles are pre-deposited on the substrate in an amorphous layer, trying to achieve maximal disorder, and thus high thermodynamic energy. In this way, the presence of solvents can allow the system to evolve quickly from such high-energy morphology to a most favorable uniform, crystalline layer.

The method used constituted for the first step: to deposit a drop of IBAN in acetone on a silicon substrate, yielding an amorphous layer due to the fast evaporation of the solvent; then promote the IBAN self- assembly using a SVA treatment in acetone or DCM.[1,2,7] Using this approach, large

ordered structures of IBAN could self-assemble in few hours instead than few days, allowing to have a much larger density of crystals respect to previous works to perform statistical analysis.

Large ordered structures could be observed already after 7h of SVA at room temperature using either acetone or dichloromethane as solvent, instead of dimethylformalamide where due to the high boiling point solvert vapour annealing was difficult to use. With SVA was possible to produce large ordered structures spanning from few nm in height until few micron in lateral dimension giving the possibility to be analized also with optical microscopes.

Using SVA were observed the formation of two different species: polygonal crystals with size of hundreds of microns (called C1) and needle-like crystals (called C2). SVA in acetone yielded the formation of both structures, C1 with lateral sizes spanning from 300 nm–100 μm surrounded by C2 with a typical length of 1–10 μm. SVA in dichloromethane gave instead only C2 (due to the high denaturation grade) with length up to 100 μm. XRD measurements showed that the two structures had a different out-of-plane periodicity (19.01±0.01 Å for C1 and 14.67±0.01 Å for C2, respectively) suggesting a different packing of the silver atoms and thiol groups in the crystals.

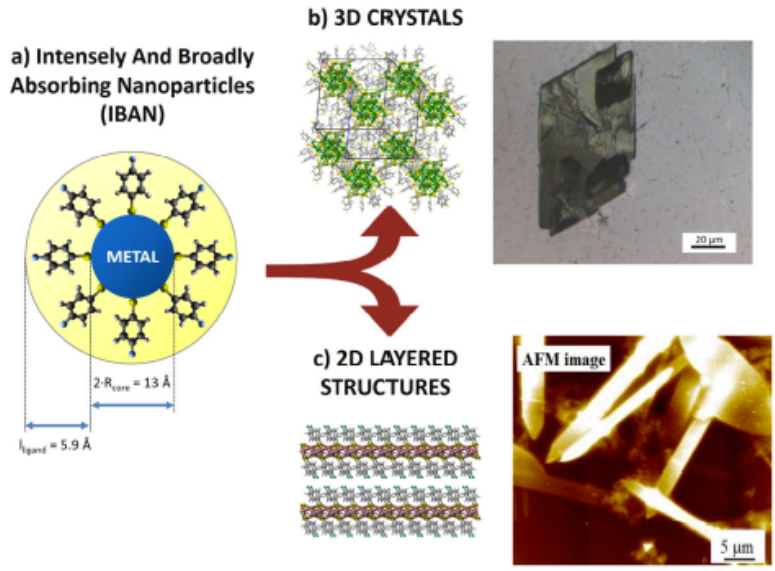

Fig 4.7 a) Schematic representation of an IBAN. b) optical microscopy image of 3D crystal of IBAN. c) AFM image of layered structures obtained by IBAN structural rearrangement.

4.2.1. Clustering in acetone solution - AFM measurements

Silver nanoclusters are fairly stable in acetone within 24h from the preparation, as confirmed by UV-Vis spectroscopy. As previously explained for longer time, more than 7h, layered structures were found also in acetone solutions.

An experiment was performed using a 3 week-old solution. A drop of the solution was laid on silicon oxide then after 7h of SVA was brought to the AFM. The acquired AFM images, Fig. 4.8 showed the presence of aggregates of 2D sheets having similar lateral size (ca 500 nm) and thickness (ca 2 nm). Moreover, the interfacial angle of the 2D sheets amounted to ca 55°.

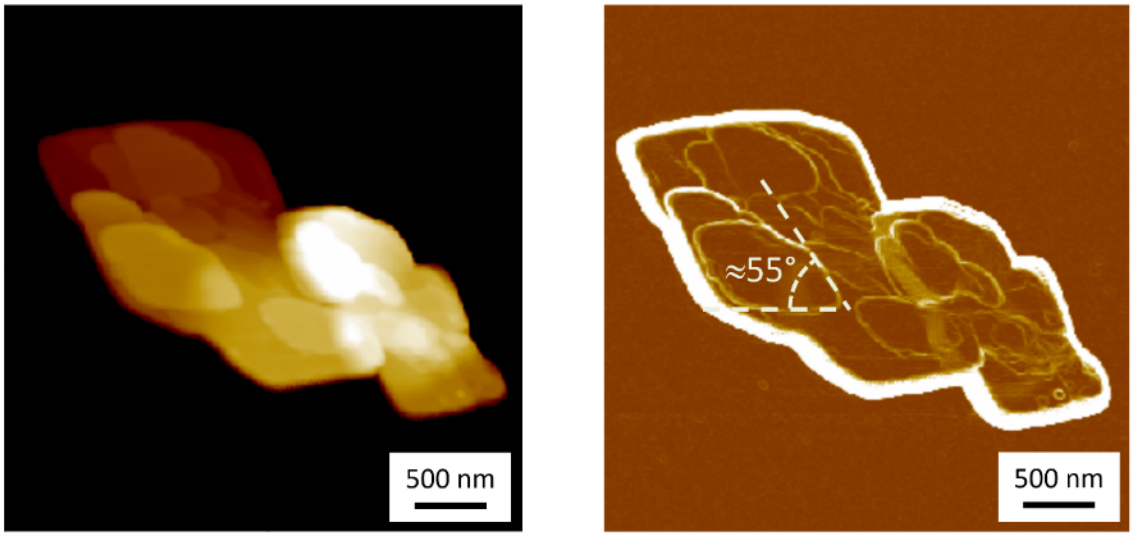

Fig 4.8 Topographic (a) and corresponding gradient (b) AFM image of clusters deposited on native silicon oxide. Acetone solution few-days old. Z-range: (a) 60 nm.

AFM images suggested that the observed 2D sheets are single layers C_2 layered structures.

4.2.2. C1 crystals (3D superlattices of IBAN)

Upon SVA in acetone were obtained large, mesoscopic C1 crystals, always together with C2 needle like structures (Fig. 4.9a). Although single crystal XRD gave information only for a single crystalline structure (thanks to the dimensions of the crystals easily detached by hand) XRD measurements performed on the same substrate (silicon oxide) gave on the other hand information of both structures.

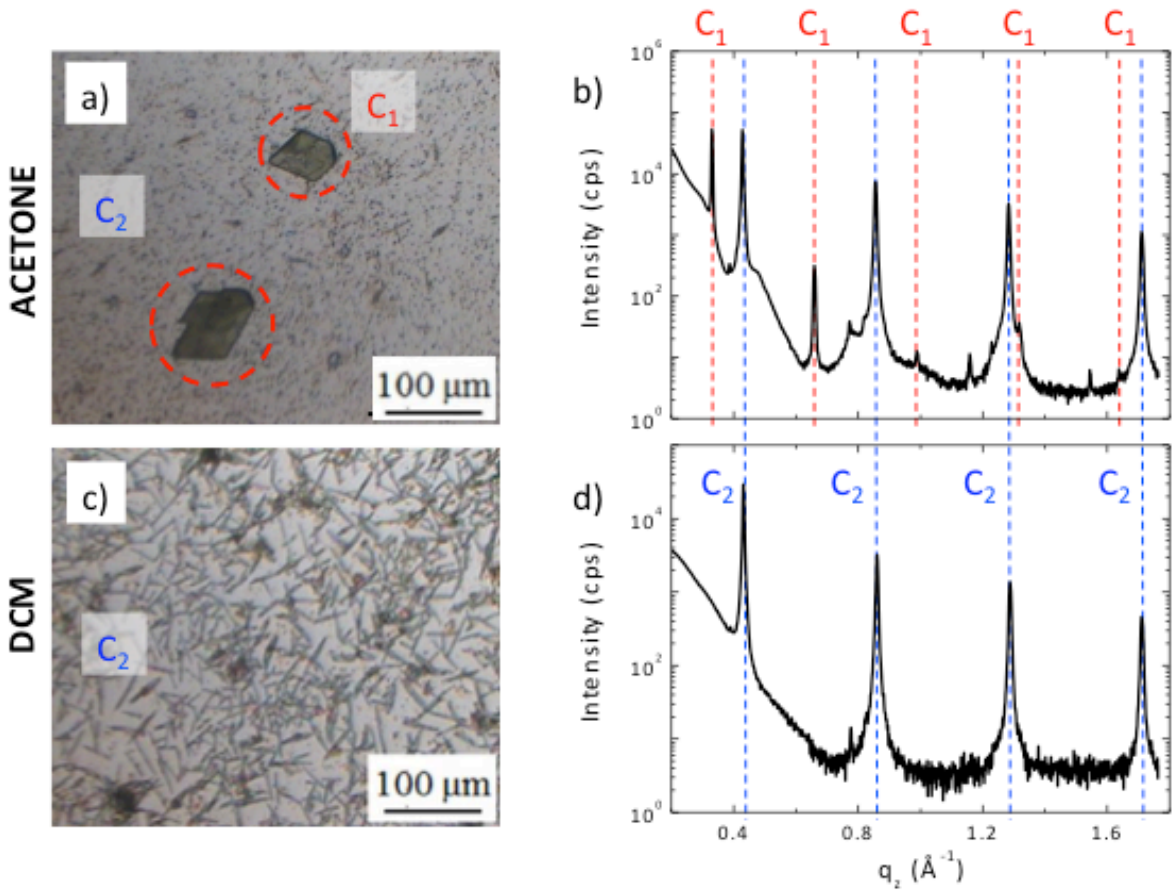

Fig 4.9 Optical images of self-assembled structures obtained by SVA in (a) acetone and (c) DCM, and corresponding (b, d) XRD patterns. SVA in acetone yielded two crystalline structures: large triclinic (C1) and layered (C2) crystals. SVA in DCM yielded only large C2 crystals.

The dimension of the C_1 crystal, previously synthetized, was analized using single crystal x ray analysis. It showed a triclinic structure with a high-density packing of Ag NPs.

Empty volume, corresponding to ca 4% of the unit cell, was divided into 11 small cavities (and ≈10 e-/cell, as calculated from PLATON SQUEEZE[8] routine) where counterions are housed. The Kitaigorodskii packing index[9] amounts to 66% and it strongly suggests that there is no solvent inside

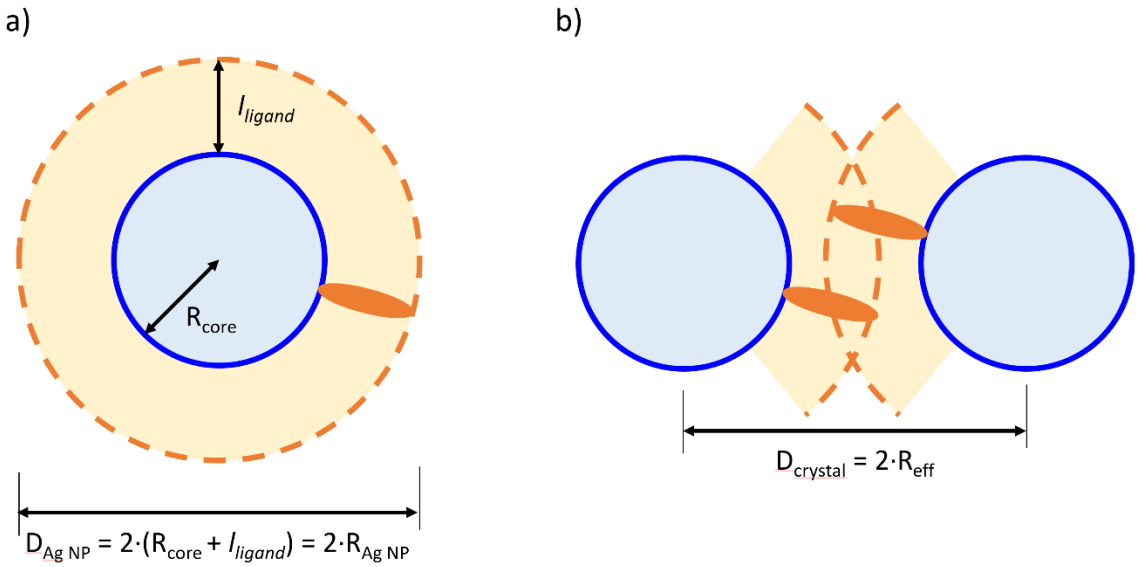

Fig 4.10 Packing of ligands in C_1 superlattices. Sketches of (a) single Ag NP and (b) interdigitating ligands coronas between two Ag NPs showing core radius $R_{Ag\ NP}$, ligand length l_{ligand}, and effective radius R_{eff}..

In the analysis of the C_1 crystal was found that the distances between Ag NP are lower than Ag NP diameter: $D_{crystal} < D_{Ag\ NP}$, due to the interdigitation of ligands. Where was possible to define the effective radius as half the distance between two nanoparticles: $R_{eff} = D_{crystal}/2$. R_{eff} corresponded to the radius of NPs using the rigid spheres model.

The distances and geometrical displacements measured by single crystal XRD corresponded to the values: $R_{eff}/R_{core} \approx 1.6$ and $l_{ligand}/R_{core} \approx 0.9$. These two values are in excellent agreement with the description obtained by the Optimal Packing Model (OPM)[10] which postulated that the space-filling of ligands is placed along the bond axis.

XRD of the C1 single crystals showed that they were composed by undamaged IBAN. Other confirmation of the real nature of the silver nanoclusters was the dissolution of the single crystal previously detached and analyzed in XRD.

Crystal was dissolved in 3ml of acetone solution and analyzed immediately in spectrophotometry. The new solution obtained analyzed in UV-Vis did not show Tyndall effect or the presence of precipitates visible by eye, and as well as that the UV-vis absorption spectra measured on the obtained solution clearly showed the five features observed in the pristine solution, as depicted in figure 4.11.

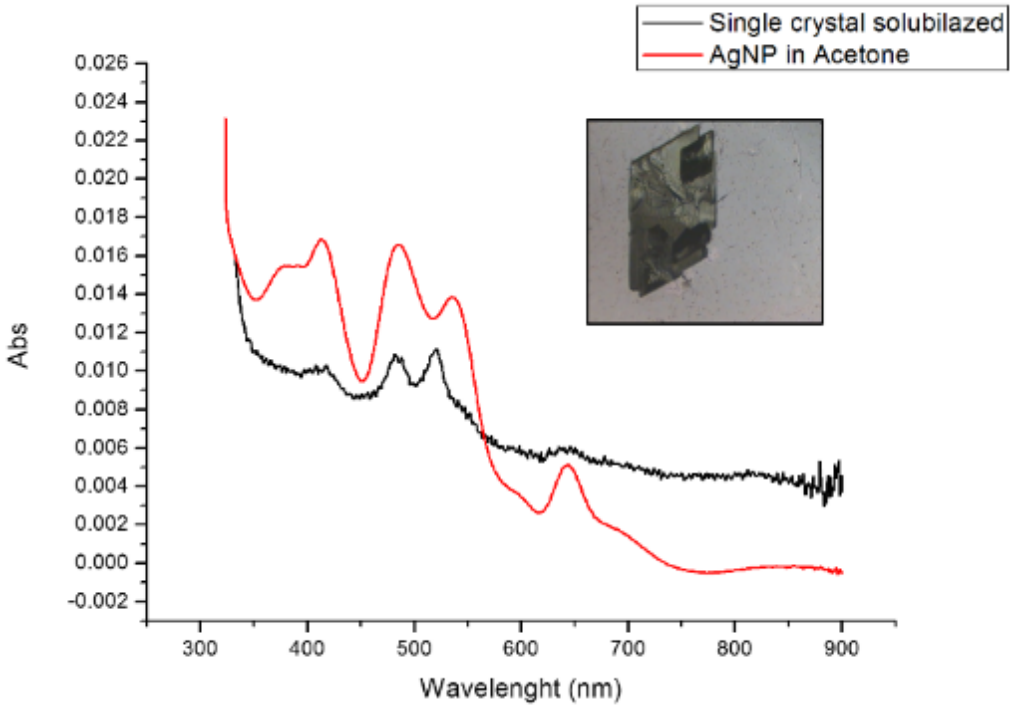

Fig 4.11 UV-vis absorption spectra acquired on acetone solution before the SVA treatment (red) and after the dissolution of the C_1 crystal in acetone (black).

The C1 single crystal dissolved in acetone and observed by optical spectroscopy, confirm that the IBAN did not undergo any chemical rearrangement. The UV-vis absorption spectrum of this solution was comparable to the one of pristine IBAN solution in acetone, even if less intense due to the tiny amount of material contained in the single crystal dissolved.

Moreover XPS analysis performed on the sample, revealed as well that the value of the Ag/S ratio measured on the single crystals (1.7±0.2 Å) was comparable to that expected from the stoichiometry of IBAN (44/30≈1.47). C1 crystals had a solvent-free triclinic structure shown in Fig. 4.12.

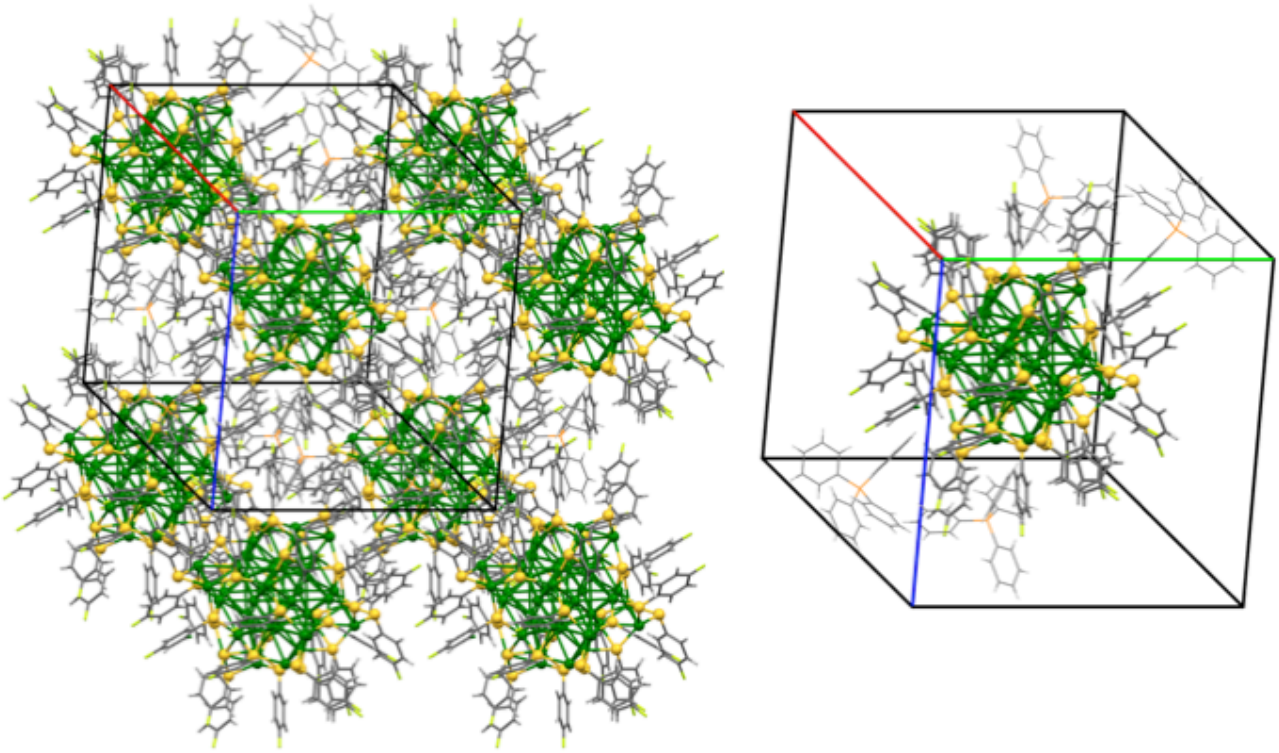

Fig 4.12 C1 unit cell reconstructed by XRD of single crystals at RT. Lattice parameters: (red line) a = 20.746(4) ., (green line) b = 21.188(4) ., (blue line) c = 22.462(4) ., α = 94.71(3)°, β = 115.14(3)° and γ = 117.54(3)° (space group 1, volume 7,433(4)Å^3). The total volume of solvent accessible voids amounts to 289 Å^3.

According to this model, thiol ligands from adjacent nanoparticles are in close contact only within a narrow volume along the plane between nearest neighbors. Similar triclinic structures were previously reported in the literature, with IBAN having different S-R ligands or with intermetallic Ag/Au nanoclusters having a total "magic number" of 44 metal atoms.[6]

In general, these triclinic crystals can be modelled as hard metallic cores separated by relatively soft ligands. In such structure, the van der Waals interactions between the outer layer of thiols play a crucial rule to form and to stabilize the crystal structure.

4.2.3. GIWAXS measurements

C_1 crystals are not the only product of the SVA in acetone as previously reported. GIWAXS images recorded before removing the big crystals on the substrate, reveals the coexistence of both layered and nanoclusters superlattices where the intense and narrow spots come from the C_1 structure.
Their position and intensity can be reproduced by assuming that crystals grow mainly having [001] texturing and being almost in-plane randomly oriented. The simulation of the Bragg spots in the small angle region is reported in Fig. 4.13d. The appearance and disappearance of Bragg spots in GIWAXS images, when collected at different positions, arises from the absence of all the possible in-plane orientations of single-crystals

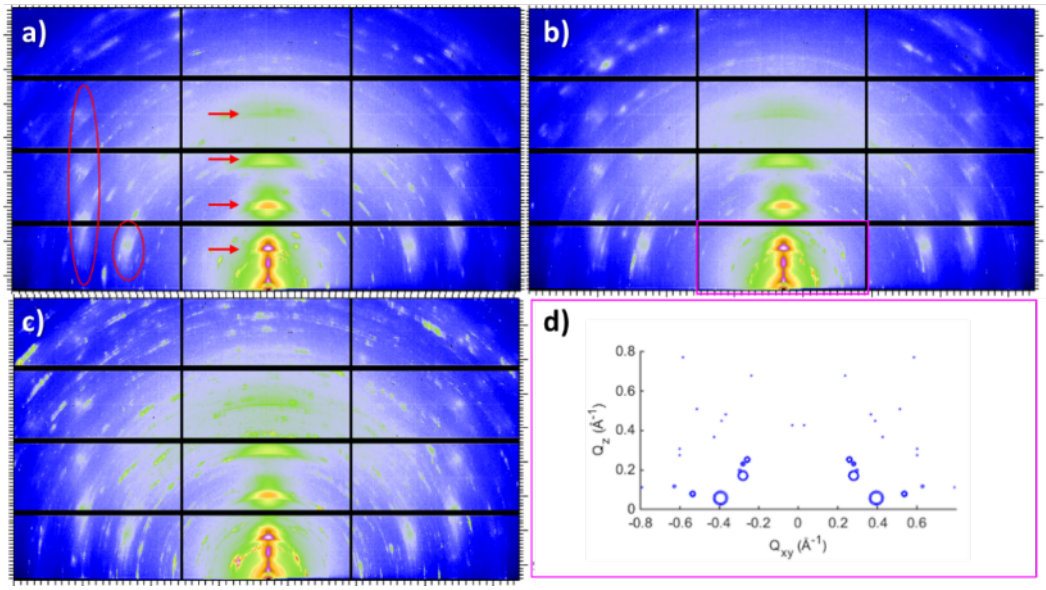

Fig 4.13 2D-GIWAXS image of crystals formed by SVA in acetone recorded at different position of the substrate (a-c). The Bragg spots coming from the C_2 structures are highlighted by red lines only in the first image. d) Calculated positions of Bragg peaks, in the small angles region of the reciprocal space, from 1the C_1 structure of nanoclusters crystals assuming a [001] texturing and a random orientation in the plane parallel to the surface. The areas of the circles are proportional to the peak intensity.

4.2.4. C2 needle-like crystals (2D layered structures)

Differently from the C1 crystals, the C2 needle-like ones could not be re-dissolved in any solvent, suggesting that in this case the IBAN aggregated irreversibly into these clusters on the substrate surface.

A report of the structure found with different techniques, XRD, GIWAXS and AFM is shown.

	Interlayer spacing (Å)	Unit cell (a) (Å)	Unit cell (b) (Å)	Interfacial angle (°)
AFM	18 ± 4			
XRD	14.67 ± 0.01		3.632	55.58
2D GISAXS	14.6 ± 0.5	5.588		55 ± 2

Table 1 Structural values of C2 crystals obtained by different techniques.

XRD measurements of samples obtained by SVA in dichloromethane showed a clear periodicity of 14.67±0.01 Å demonstrating the presence of the layered structure. 2D-GIWAXS provided more detailed information, showing the typical features of a decoupled periodicity along different directions, as expected in a layered structure. On the other hand out-of-plane scans (Fig. 4.14b) showed a z periodicity of 14.6±0.5 Å, in excellent agreement with the specular XRD plots (Fig. 4.14b,d). Noteworthy, in-plane scans indicated also the presence of lateral order in the stack giving a possible unit cell a = 5.588 Å b = 3.632 Å γ = 55.58°, significantly different form the one observed for C1 and also not observed in previous work.[11] Instead, a small signal from residual, pristine IBAN was observed as a ring at $q \approx 0.4$ Å^{-1}, corresponding to the nearest neighbor distance for IBAN. (label A in Fig 4.14a).

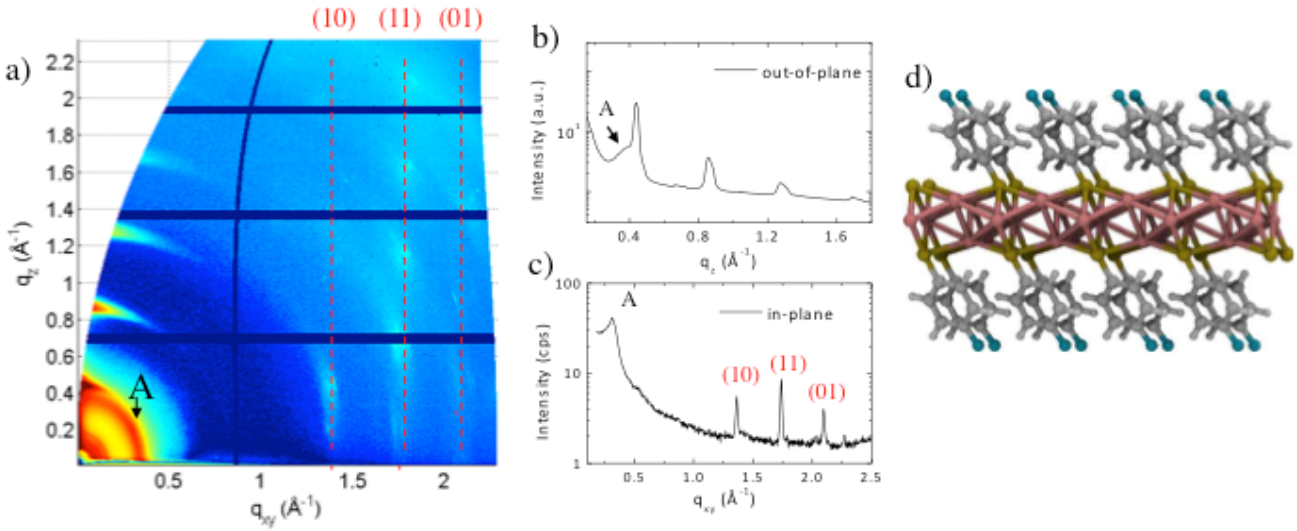

Fig 4.14 a) 2D-GIWAXS image of C_2 crystals and corresponding (b) out-of-plane and (c) in-plane scans. The presence of clusters formed by a small amount of residual Ag NPs is indicated by a diffraction ring at small q (labeled A). (d) The proposed C_2 structure, as calculated by DFT using the X-ray scattering measurements.

Other confirmation were performed in AFM where was found C2 crystals with a wide range of thickness (50 – 500 nm) and length (0.5 – 100 μm), as well as a constant angle between crystal facets of 55±2° corresponding to the γ angle found by GIWAXS. AFM also confirmed that the layered, C2 crystals, showing defects such as steps, holes and terraces, indicating a heterogeneous nucleation growth similar to the Terrace-Ledge-Kink model[12] suggesting that the kinetics of C2 crystal selfassembly is given by the interplay of nucleation events occurred both in bulk solution and under 2D confinement.

The spacing between different terraces in atomic force microscopy analysis was found in 18±4 Å, as measured by statistical histogram analysis, in agreement with the distance measured with XRD and GIWAXS; all the structural values obtained by the different techniques showed an excellent agreement.

Such layered structure is similar to what observed by Dance et al.,[11] who modelled it as a periodic stack of 2D layers, where the thiol substituents extend perpendicular to both sides of a central slab of Ag and S atoms. Evaporating Ag clusters on the substrate surface, also Hu et al.[13] produced and characterized similar organic single-layers of Ag lamellae functionalized with alkyl thiols, with uniform thickness (≈3 nm) and in-plane ordering (i.e. 2D crystals). Because of their peculiar organization, this layered materials have been also defined “covalent soaps”.[14]

XPS analysis was also performed on the layered structures giving infomation about the relative abundance ratio of silver sulfur atoms Ag/S = 1.6±0.2, comparable with the stoichiometric one

(Ag/S = 1.47) and indicated that the silver layer is mainly formed by oxidized Ag atoms, covalently bound to sulfur ones.

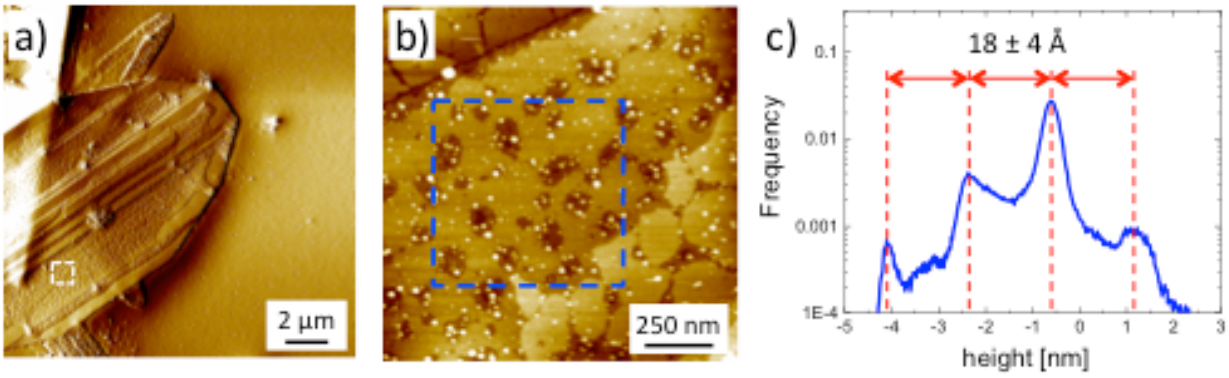

Fig 4.15 (a) Large scale AFM image of C2 crystals, gradient-filtered to better show the surface structure of the crystal. b) zoom-in of the white box in (a), topographic image. (c) Histogram analysis calculated from the blue box in (b), showing that different steps have a constant thickness of 18 Å.

4.2.5. Qualitative analysis of MFM images

Magnetic maps of all the samples were performed by using a Smena Head microscope (NT-MDT, Russia). BudgetSensors Multi75M-G cantilevers with a resonance frequency of about 75 kHz, coated with a cobalt/chromium magnetic layer (BudgetSensors, Bulgaria), were used to image crystalline 3D superlattice and stacked assemblies of 2D layers. Any external magnetic field was applied on both sample and tip in order to measure the spontaneous magnetization of samples. All samples were topographically imaged by using AFM in intermittent contact mode, while Magnetic Force Microscopy (MFM) images were collected in lift mode at fixed distance (50 nm).

The contrast observed in the MFM images is due to different magnetic interaction between the MFM probe and the sample leading to a shift in the phase of the oscillating tip.[15]

Using acetone (Fig 4.16) both C_1 (marked by box) and C_2 crystals were obtained. Only C_2 crystals showed a negative magnetic contrast with respect to the SiO_2 substrate (darker using false color scale). In the case of dichloromethane solvent (Fig 4.16c) topography,d) magnetic signal) only C_2 crystals were produced showing a similar magnetic contrast, confirming that the electrostatic contribution can be neglected. This is peculiar for magnetic contrast; for a fixed direction of the magnetization moment of the tip (along z, up or down[13]), the average direction of the magnetization moment of the sample can be antiparallel respect to the tip, causing a repulsive interaction – positive shift phase – , or parallel, causing an attractive interaction – negative shift phase –.

Being the substrate diamagnetic, the measured contrast suggested the paramagnetic behaviour of most of the C_2 crystals. The presence of diamagnetic Ag NP assemblies of few hundreds of nm covering the crystals prevented a more quantitative analysis.

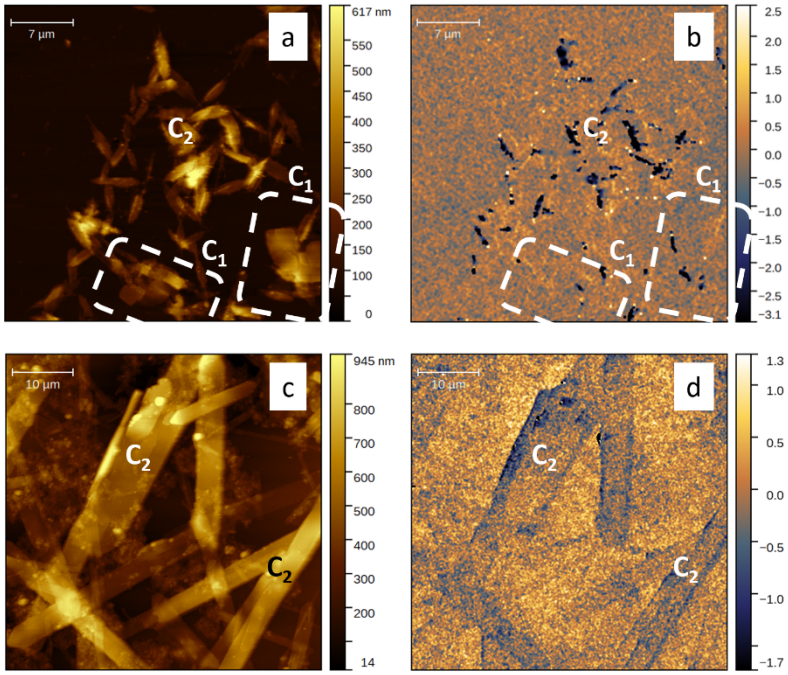

Fig 4.16 Topographic (a, c) and MFM (c, d) images of C_1 and C_2 crystals. Sample a) produced in acetone, b) in dichloromethane.

4.2.6. DFT calculation for C_2 crystal

Detailed modelling of the atomic structure of the layer and of the role of the thiol ligands was done using DFT calculations. Taking into account the geometries proposed for the layered structure,[11] were constructed several test structures using the basic stoichiometry $Ag_3(S\text{-}R)_2$.

The calculated structure showed a complete atomic reorganization of the IBAN which implies an oxidative mechanism where one silver atom is added to each silver nanocluster, with the loss of four electrons. The resulting neutral structure was optimized by constraining the lattice vectors to the best experimental estimation of the unitary cell, as obtained by GIWAXS. A P-1 symmetry was imposed to the crystal structure, which constrains one Ag atom to the (0 1/2 0) position where it is fully coordinated to the surrounding S and Ag atoms. The other two Ag atoms form a bridge between the sulfur sub-lattice, defining the upper and lower surfaces of a 2D layer. Each S atom is capped with a ligand, which is tilted about 60° respect to the plane of Ag_3S_2. A picture of the theoretical structure is shown in Fig. 4.17.

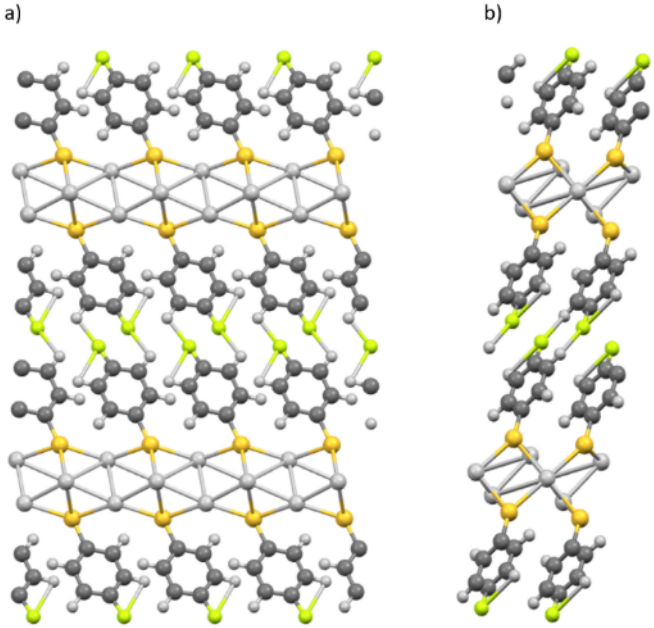

Fig 4.17 Structure of C_2 crystal along the planes generated by vectors: a) *a*,*c* and b) *b*,*c*

The calculated structures indicates that dichloromethane molecules trigger the silver atoms to undergo an oxidative transformation, losing the stability given by the "magic number" 18 electrons

closed shell and transforming it into a more stable layered structure where the two Ag atoms maintain their formal oxidation state, while one atom of Ag is in a neutral state.

Noteworthy, the electron count of the resulting crystal structure leaves an unpaired electron per unit cell, suggesting the C2 crystal to be paramagnetic. Qualitative magnetic force microscopy (MFM) measurements performed at room temperature confirmed a paramagnetic behaviour of C2 structures, not observed in C1 crystals.

The molecular packing was determined by optimizing a handful of trial structures, generated with the program GDIS[16] based on the experimentally determined crystal cell. Each structure was first optimized by keeping constant the cell, followed by a second optimization. The crystal structures obtained were ranked by their relative energy, which never exceeded 10 kcal/mol. At the end the best structure was determined by comparison with the XRD data.

The results obtained indicate thus that, with simple exposure to DCM solvent, the silver atoms undergo an oxidative transformation, losing the stability given by the "magic number" 18 electrons closed shell and transforming into a layered structure in which two Ag atoms maintain their formal oxidation state, while one atom of Ag is in a formal neutral state.

4.3. Thermal stability and degradation mechanisms of C1 and C2 crystals

Thermal stability is an important properties to be investigated with the idea of using smart materials in the future nano devices. Thermal stability was monitored using two approach in situ and ex situ analysis to avoid any possible risk of the temperature decrease giving also at the same time informations real time about the crystalline changes.

The thermal stability of these crystalline structures were performed with temperature ex situ in specular XRD, while in an hot stage for GIWAXS/GISAXS anaysis, in situ. Samples were prepared using sovent vapour annealing, in acetone, in this way was possible to generate, on the same substrate, both structures, C1 and C2, in order to get a direct comparison of the thermal stability of the two structures.

The XRD analysis discoverd for the C1 crystals, orange areas in Fig. 4.18, significantly changes for T≤150 °C with a clear shift of their diffraction peaks while the peaks related to C2 needle-like structures, blue areas in Fig. 4.18, did not show any change in intensity and position at the same temperature, indicating an higher stability respect the C1 crystals.

Both C1 and C2 crystals were completely dissolved at T>200°C where no more reflections were detectable in the diffraction pattern.

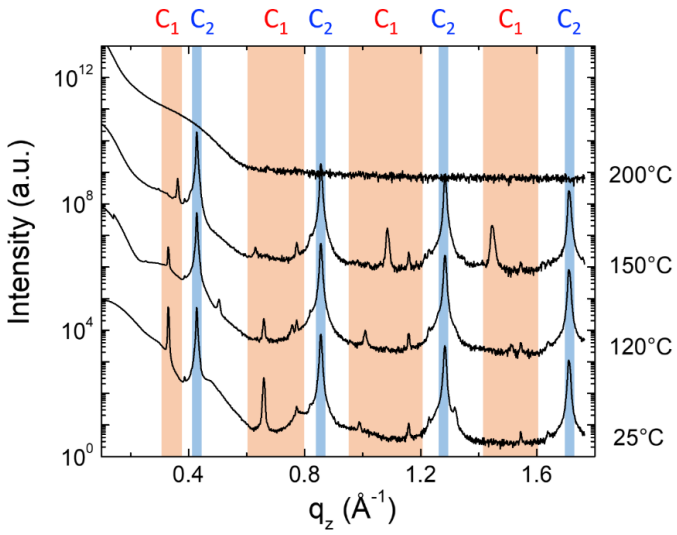

Fig 4.18 XRD measurements acquired at different annealing temperatures. Features marked in orange boxes are ascribable to small phases of C_1 crystals

In-situ GISAXS measurements performed during the thermal treatment (27 – 238 °C) in nitrogen atmosphere showed the evolution of the C2 crystal structure obtained by dichloromethane.

Unfortunately, the presence of small aggregated of pristine IBAN, discussed before, could not be avoided, giving an additional signal in the GISAXS measurements; the lack of a corresponding peak in the XRD patterns suggests that such nanoclusters were very small, composed of few IBAN particles.

Fig. 4.19a shows the evolution of the GISAXS intensity along the out-of-plane direction; fig. 4.19b,c shows the variation in normalized intensity and position of the main features, respectively. The main peak (P1) corresponded to the interlayer spacing of the C2 structure, i.e. the distance between the Ag-rich planes=14.6 . (Table 1 in the chapter *4.2.4*).

P1 intensity increased between 80°C and 160°C due to the combination of the crystal ordering and the Debye-Waller effect. Where P1 disappeared at T≈210°C.

In the whole temperature range tested, the peak position did not change indicating the strong stability of the interlayer distance and, similarly, of the ligands packing. Peak P2 is attributed to aggregates of residual IBAN, which arranged in more ordered structure at T>100°C, then degraded at around 170°C, as also suggested by the disappearance of the ring A in 2D-GIWAXS measurements.

Above this temperature, the IBAN structure changed, giving peaks P3 and P4 at T>160°C. Given that, in this temperature range, the chemical state of silver did not change and the Ag/S ratio remained constant, these changes in GIWAXS signal are ascribed to a re-arrangement of the packing of ligands, which tended to be perpendicular to the plane (i.e. increasing of the interlayer distance). At T> 200°C, the structures melted completely, and no periodicity was observed anymore. All the transitions observed were irreversible.

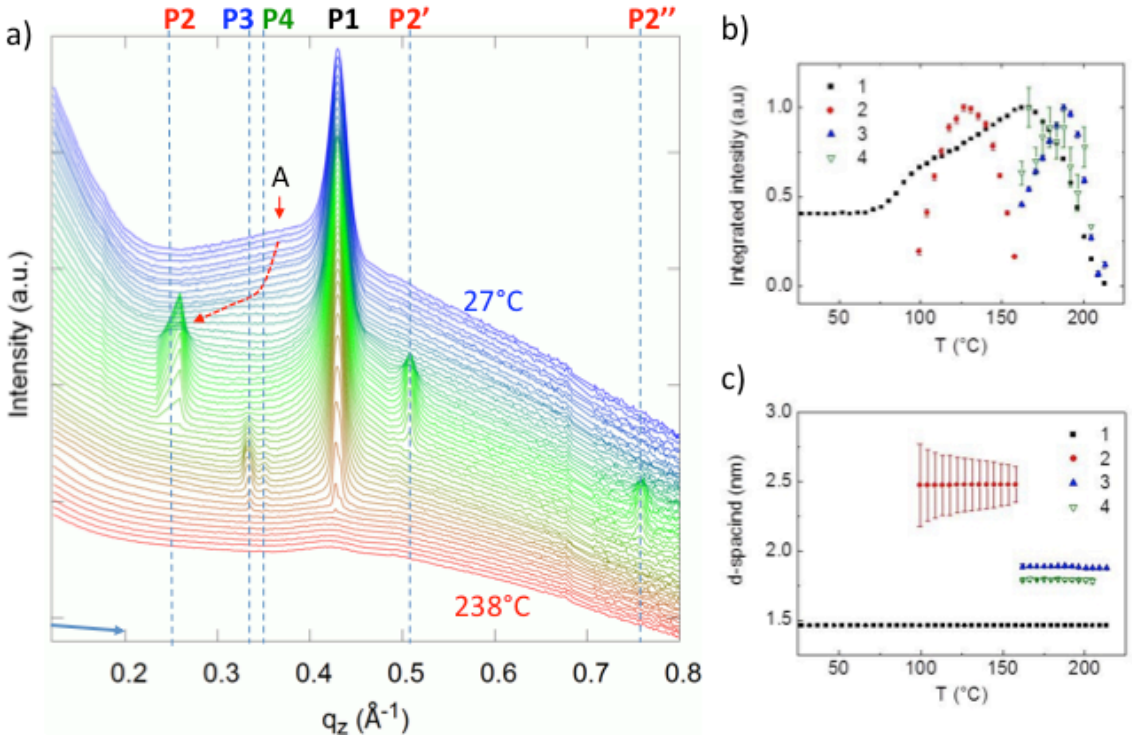

Fig 4.19 a) Intensity integrated along the out-of-plane direction of GISAXS images collected in-situ and real time during thermal ramp. Integrated intensity (b) of peaks 1-4 and (c) related *d*-spacing.

4.3.1. XPS/Auger measurements

XPS were performed on the Ag NP crystals and nanoclusters. The spectrum, shown in Fig. 4.20, confirms the changing in the chemical nature of the building block of the highly ordered structures. XPS was an interesting tool to understand how silver atoms inside the crystals lattice rearrange chemically theirself in response to the raising of temperature.

For the first step, XPS spectra shows the presence of the atomic species: Ag, F, C and S. Although the XPS spectrum of the ligand is currently not available in literature, we assumed that the electronic properties of the 4FTP are similar to the Fluorobenzene[17] and the Thiopenol,[18] as confirmed by measured binding energies (B.E.) in good agreement with the values reported in literatures.

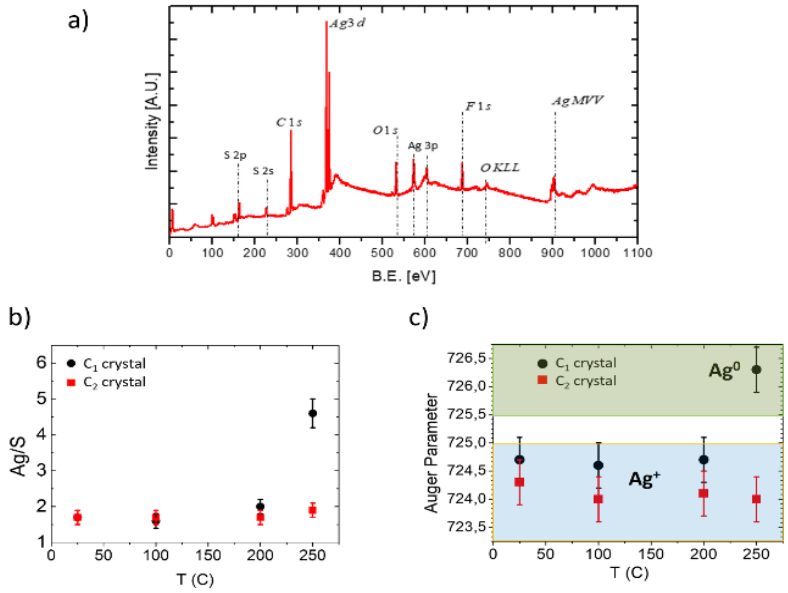

Fig 4.20 a) XPS spectrum of Ag NPs. b) Ratio between Silver and Sulfur atoms, as measured by XPS spectra and c) Auger parameters measured at different annealing temperature, from RT to 250 °C.

Where C 1s (285.5±0.1 eV) is compatible with C 1s emission in Fluorobenzene (285.5±0.4 eV); F 1s (687.6±0.1 eV) is compatible with a C-F bond, i.e. Poly(vinyldene fluorinde) (688.1±0.3 eV),[19] while the S $2p_{3/2}$ (162.9±0.1 eV) has a similar energy position of the Thiopenol (163.3 eV).

The Auger modified parameter[20] is very sensitive to the chemical state and in the case of silver, the measured Binding Energy of the Ag $3d_{5/2}$ (368.8±0.1 eV) and the Auger parameter (AP-$3d_{5/2}$, $M_4N_{45}N_{45}$ = 724.7±0.4 eV) can be unambiguously attributed to a non-metallic Silver being 368.7±0.1 (Ag^+) eV and AP-$3d_{5/2}$, $M_4N_{45}N_{45}$ is the range 723.0-724.9 eV ($Ag^{+/2+}$),[21] respectively.

4.3.2. Thermal annealing – C_1 crystal

The degradation of the nanocluster was monitored inside the crystals by looking at the Ag/S ratio. Due to the presence of Siver inside the metal core of the cluster and sulfur normally present externally, ligands, using Ag/S ratio was the right choice to investigate the degradation mechanism. At room temperature the Ag/S ratio was 1.7±0.2 compatible with the stoichiometric ratio (Ag/S = 1.47).

T [C]	Ag/F	Ag/S	S/F	Auger modified parameter
25	2.1 ± 0.3	1.7 ± 0.3	1.2 ± 0.3	724.7 ± 0.4
100	2.3 ± 0.2	1.6 ± 0.4	1.4 ± 0.3	724.6 ± 0.5
200	2.9 ± 0.2	2.0 ± 0.2	1.4 ± 0.3	724.7 ± 0.8
250	7.4 ± 0.2	5.4 ± 0.4	1.4 ± 0.5	726.3 ± 0.3

Table 2 C_1 crystals. Atomic species ratio, as measured by XPS at different annealing temperature

By heating up to ≈ 250°C, C_1 crystals began to melt following the desorption of ligands, as observed by Mass Spectroscopy. In particular, Auger spectroscopy analysis monitors the chemical state of silver atoms at increasing temperature. Auger parameter AP-$3d_{5/2}$, $M_4N_{45}N_{45}$ remains constant in the non-metallic Ag region until 250° C, confirming the Ag^+ state at low temperature, due to the confinement in the nanometric core and as well as the Ag-S bond. Only at 250 °C, a difference was observed (Ag^0) with a corresponding transition to metallic silver strongly indicating the melting of the Ag NP nanoparticles. The measured binding energy of Ag $3d_{5/2}$ (368.1±0.1 eV) is in good agreement with the expected binding energy value for bulk (368.20-368.30 eV) and in excellent agreement with the reported value for the Ag metallic nanoparticle (368.1±0.1 eV).[7]

4.3.3. Thermal annealing – C_2 layered crystal

XPS analysis performed on C2 layered structures, Table 3, showed the same chemical composition and electronic structure of the nanocluster in the C_1 crystals: S/F and Ag/S ratios were respectively 1.3±0.3 and 1.6±0.2; also the Ag was in non-metallic state, as observable from Auger parameter AP-$3d_{5/2}$, $M_4N_{45}N_{45}$ equal to 724.3±0.5 eV.

T [C]	Ag/F	Ag/S	S/F	Auger modified parameter
25	2.1 ± 0.3	1.6 ± 0.2	1.3 ± 0.3	724.7 ± 0.4
100	2.3 ± 0.2	1.6 ± 0.2	1.4 ± 0.3	724.6 ± 0.5
200	2.9 ± 0.2	2.0 ± 0.2	1.4 ± 0.3	724.7 ± 0.8
250	7.4 ± 0.2	5.4 ± 0.4	1.4 ± 0.5	726.3 ± 0.3

Table 3 C_2 crystals. Atomic species ratio, as measured by XPS at different annealing temperature.

The stability of IBAN and the role of ligands were investigated combining Auger spectroscopy analysis and residual gas analysis (RGA) at increasing temperature in vacuum environment.

RGA (in the next paragraph) showed that the system changed at T>200 °C. This evidence can be ascribed to the desorption of 4-FTP ligands and/or counterions (a similar behavior was also reported for gold NP).[22]

Since the RGA technique was unable to distinguish between the two chemical systems, Auger analysis was used to monitor the chemical state of silver atoms. The IBAN were stable up to T=250°C, and Auger data showed only the Ag+ chemical state, due to the atomic confinement in the nanometric silver nanocluster core and the Ag-S bond.[23] At T ≥200 °C, a different state was observed in C1 crystals due to the transition to metallic silver (Ag0).

The data observed shows that IBAN assemble in triclinic crystals to form C1 structures; while at T=200°C they undergo a melting transition, with no chemical modification of the IBAN. At ≥250°C chemical degradation of the IBAN takes place, due to the desorption of ligands.

C2 layered structures displayed a better thermal stability than C1 crystals in high vacuum (10-7 mbar) as well as in air, also confirmed by RGA measurements.

The main chemical difference between the two crystals were the chemical state of silver, as observed by Auger parameter. Samples obtained by SVA in dichloromethane, featuring only C2 crystals, showed a significant fraction of oxidized Ag+ up to 250 °C, where above the melting point of the crystal which can be ascribed to the pristine IBAN. Conversely, samples obtained in acetone showed only the presence of metallic silver Ag (0), due to complete degradation and melting of the IBAN, already at 250°C, as discussed before.

4.3.4. RGA analysis

Residual Gas Analysis was performed in combination with XPS. Inside the same chamber, RGA gives interesting and usefull information about the degradation mechanism of silver nanoclusters inside highly ordered structures. A degradation mechanisms was noticed at 170°C in the nanoclusters, also confirmed by optical spectroscopy, XRD and residual gas analysis. From in situ XPS analysis (see the paragraph 4.3.1 for the spectra and the silver/sulfur ratio trend) thermal treatments, in UHV, shows that 4-FTP molecule does not degrade up to 300°C. The S/F ratio remains constant within experimental error, while a desorption phenomenon is observed by the decreasing of S or F respect the Ag, which gives an increase of the Ag/S ratio from 200 °C.

A more accurate evidence of desorption dynamics was given by Mass Spectroscopy of the residual gas, the 4-FTP molecule, identified by m/z = 128, $FC_6H_4SH^+$, 127 $FC_6H_4S^+$ and 108 $C_6H_4S^+$, was desorbed from the NP surface when the temperature overcome 170°C, as showed in Fig. 4.21. Literature data report a similar desorption temperature (187 °C) for 4-FTP on Au (SEM).[8]

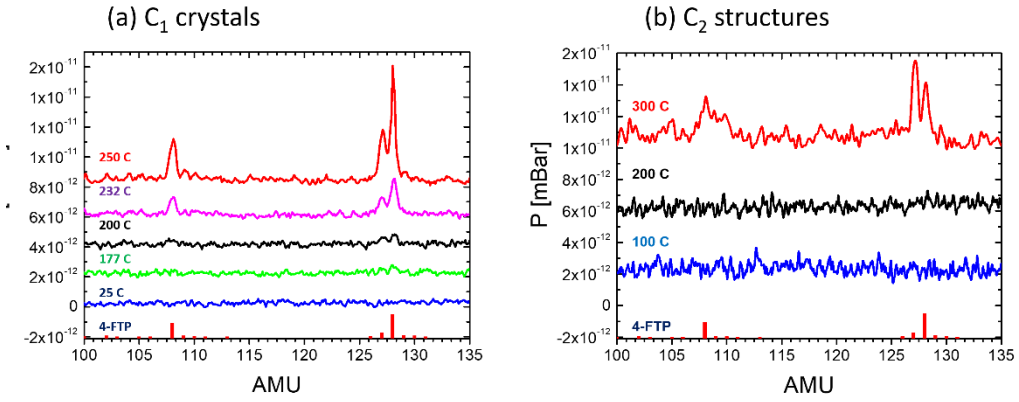

Fig 4.21. Mass spectra acquired during RGA at different temperatures on (a) C_1 crystals and (c) C_2 structures. RGA spectra of pure 4-FTP ligand (red columns in the lower part of the graphs) are shown as reference.

4.4. Conclusions

In summary in the first part of this PhD thesis was reported a study for the preparation of robust, macroscopic and ordered self-assembled structures of core-shell nanoclusters by using solvent vapor annealing.

IBANs, having 44 silver atoms and 30 external S-R ligands were used as ideal building block, due to their uniform dispersity and high processability. Such nanoclusters are chemically stable in the right solvent, and can be stored for months or processed easily from solution, forming large crystals of pristine IBANs, similarly to normal molecules. Such crystals are held together by weak, reversible supramolecular forces, allowing them to be re-dispersed in solution to give single IBAN again. However, when exposed to suitable solvents (in particular DCM) the IBAN undergo a structural and chemical change, forming layered structures of oxidized silver atoms, bound together to form a continuous covalent structure protected on the upper and lower side by the thiol molecules. Such covalent 2D structures show a better order and thermal stability than the 3D supramolecular crystals, and have been characterized using microscopic, spectroscopic and diffraction techniques.

5. Azobenzenes

5.1. Self assembling of azo molecules on solid substrate with weak interaction forces

5.1.1. Azobenzene in solution

Azobenzene is the common name given to a wide class of compounds able to perform movements induced with a photo stimulus. Changing the donor and the acceptor group and tuning the dipole moment of the molecule is possible to change the reactivity of the molecule respect the light. Mechanical movement performed in microsecond to seconds is what azobene are able to do just with the changing of the dipole moment. The knowledge got in IBAN study was applied to the manipulation and morphological fuctionalization of surfaces without the use of covalent bonds using azobenzene.

Acid yellow 9 (4-Amino-1,1′-azobenzene-3,4′-disulfonic acid monosodium salt) and Disperse Orange 3 (4-(4-Nitrophenylazo)aniline) were chosed as ideal candidates to perform study in the surface modification.

The first step was the comprehension of the switching beviour of azomolecule models in solution. Two solutions were prepared, one in water and the other one in DMF.

In fig. 5.2 are presented the beviour of the molecules to the monocromator light at 365 nm (UV) before and after irradiation.

a)

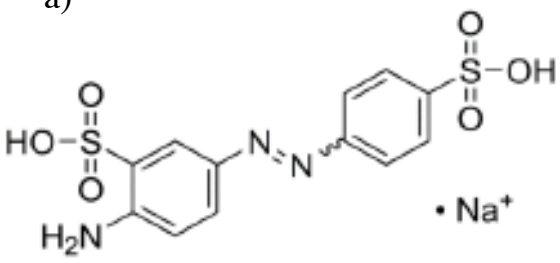

b)

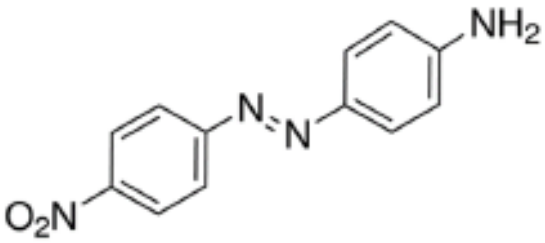

Fig. 5.1 a) Chemical formula of the Acid yellow 9 (4-Amino-1,1′-azobenzene-3,4′-disulfonic acid monosodium salt); b) chemical formula of Disperse Orange 3 (4-(4-Nitrophenylazo)aniline).

The interaction of the molecule with the UV radiation is showed in the figure, respect to the classical switching azo spectra, the first molecule showed an overlapping of the two peaks (Trans and cis). In this configuration possible estimation in regards the photoswitching is difficult to have, mainly due to the strong dipole moment of the molecule which guarantee a fast movement of the photoswitching, microsecond in case of acid yellow 9 and millisecond for disperse orange 3.

- Possible explaination respect to the classical trend: due to the black box in the spectrophotometer and with the very fast photo switching of the molecule the molecule were mainly in the trans form.
- Although the presence of the classical two peaks, the trend of the intensity in the absortion in function of the wavelength is totally opposite to the classical trend.

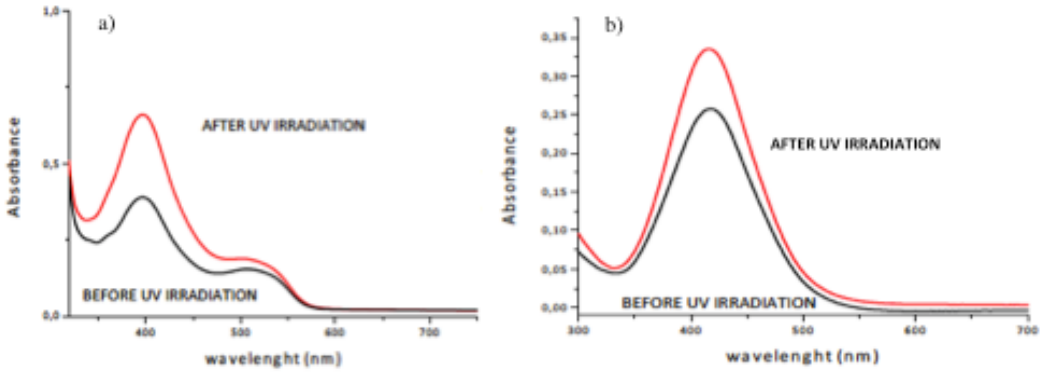

Fig. 5.2 UV-Vis spectra absorbtion of the Acid yellow 9 solution a) and Disperse Orange 3 b) upon irradiation with 365 nm UV light.

5.1.2. SAM formation of azomolecules

Build an ordered structures on a flat platform without any type of covalent functionalization is a challenge, in particular to generate islands of ordered molecule with the same height. The system chosen were commercial small molecules that switch between trans and cis isomers when they are illuminated by ultraviolet light (λ = 365 nm), with the corresponding change of the direction of the electric dipole vector.

Acid yellow 9 and Disperse Orange 3 were found to be ideal molecules with the use of drop casting. With a diluted solution (0,01g/l) in water, for the first molecule, and DMF for the second one, were generated a good population of self assembled islands with the same height, as are possible to observe in Fig. 5.3. The drop deposisted on silicon oxide 300 nm was left 8h to dry in a petri dish.

Analysing it with atomic force microscope were found islands with an average height of 2 nm (value calculated by hundreds of islands). The average value of 2 nm for acid yellow 9 confirm a not correct deposition in a monolayer of material but probably in bi layer of material, interconnected between the molecules.

Acid yellow 9 shows a height of 1,4 nm calculated with ChemDraw software, it is difficult to imagine, in our case, a disposition of a monolayer of molecules.

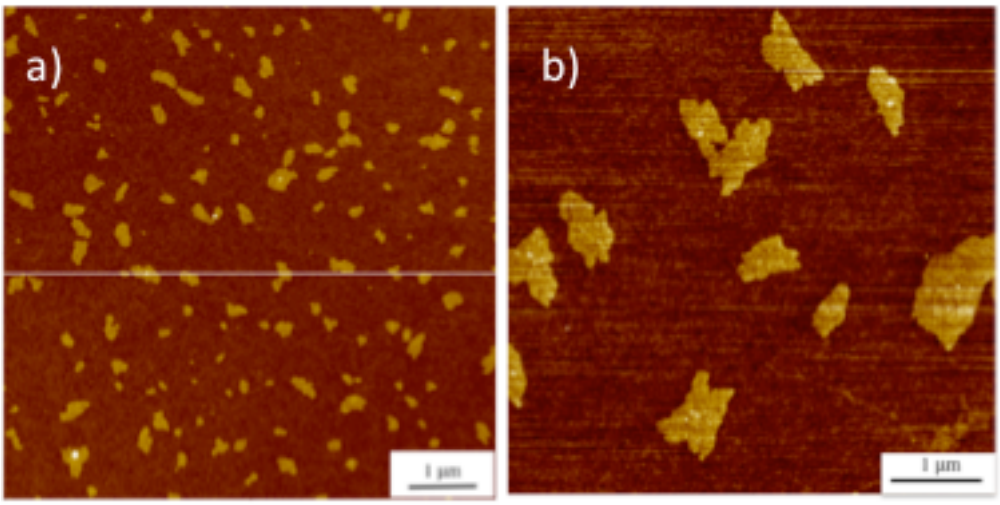

Fig. 5.3 Atomic force microscopy analysis of Acid yellow 9 molecules self assembled on silicon oxide 300 nm. b) magnification analysis of the previous image.

Acid yellow 9 was deposited also by spin coatin, where the low concentration of the material joined with short time of interaction with the substrate avoid any type of rearrangement. In the other hand solvent vapour annealing showed much time for the molecule for being organized in ordered

structure making it difficult to tune. In fact SVA was the main method to generate ordered 3D structures.

The study of photoswitch in solid-state and for micrometric self-assemblies was performed by measuring the surface potential (SP) using KPFM. UV Led light (365 nm) was directed on the self assembled molecules on silicon with native oxide in situ, inside the microscope chamber. With an irradiation time of 1h was possible to see the photoswitching of the SAMs.

Using the Helmholtz equation, the SP was given by electrical molecular-dipole moment normal to the substrate. A rotation of the vector due to the photoisomerization corresponds to a variation in the measured potential.

Azobenzene molecules self-aggregated on silicon substrate forming (A) mono- and (B) bilayers 2D islands of a few microns size, as evinced by AFM analysis reported in Fig. 5.4b. The height of each layer was 1.6 ± 0.2 nm, suggesting that the molecules are roughly packed perpendicular to the substrate. Also the corresponding electric dipole vectors of the packed molecules are aligned, as confirmed by KPFM measurements. KPFM measurements are performed in situ and Fig. 5.5c reports the map of the surface potential difference between the sample before and after the UV illumination $\Delta SP = SP_{light} - SP_{dark}$. The substrate was not affected by the UV light and no potential variation was measured. A negative variation was only measured in the case of bilayer islands (marked with B) while monolayers (A) did not show remarkable changes. Quantitative analysis revealed that the potential shift was not uniform in the bilayer. In the central region of the island, the measured shift amounts $\Delta SP \approx -30$ mV while is zero close to the boundaries. This behavior cannot be ascribed to experimental artifacts, which can affect the KPFM measurements leading to an underestimation of the measured potential of objects with lateral size smaller than very few hundreds of nm, as calculated using semi-quantitative methods previously developed.

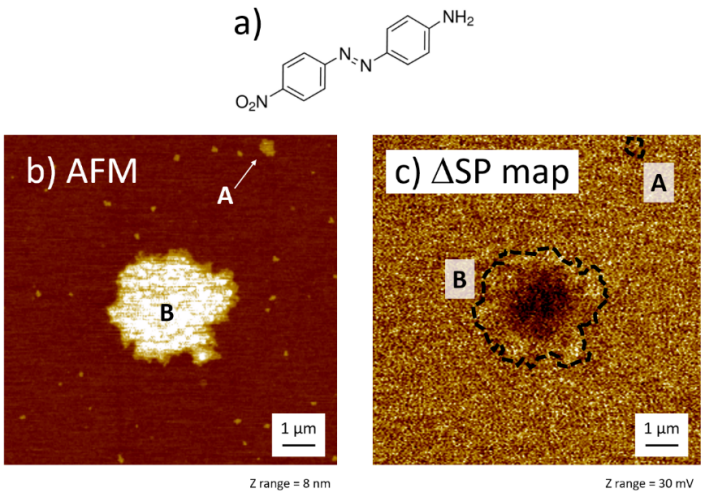

Fig 5.4 Azobenzene molecule: (a) Chemical formula of Disperse Orange 3, (b) AFM image of self-aggregates and (c) corresponding map of the surface potential variation (DSP) between sample illuminated and under dark.

It is noteworthy to point out that if the plane of rotation of the dipole vector is parallel to the substrate surface, the variation of the measured potential is equal to zero. For this reason, the non-uniformity of the measured ΔSP reveals the presence of a complex morphological arrangement of the molecules that can pack in different configurations.

Moreover, the presence of high dipole moment in azobenzene molecuses induce an high velocity switching, speed rate around nano seconds (in case of very high dipole moment, refered to Acid yellow 9). Due to the high switching speed of the azo molecules visualize the SAM in KPFM was trigger and difficult. The photoswitching noticed was sometimes inside the instrumental error of the instrument (less that 5 mV) and any possible explaination of the mechanism was difficult to define. On the other hand thanks to a weaker dipole moment respect Acid yellow 9, Disperse Orange 3 was clearly visible in Kelvin Probe microscopy (Fig5.4 and Fig 5.5). Respect to the classical value of photoswitching of a Azobenzene SAM covalently functionalized to gold surfaces ≈ 100 mV,[24] islands of material showed a photoswitching of ≈ 10-20 mV. This is well explained by the non covalent functionalization with the substrate which produce a randomly distribution of the molecules. The value found as ΔSP was averaged of the general dipole moments of the molecules randomly distributed in all the directions.

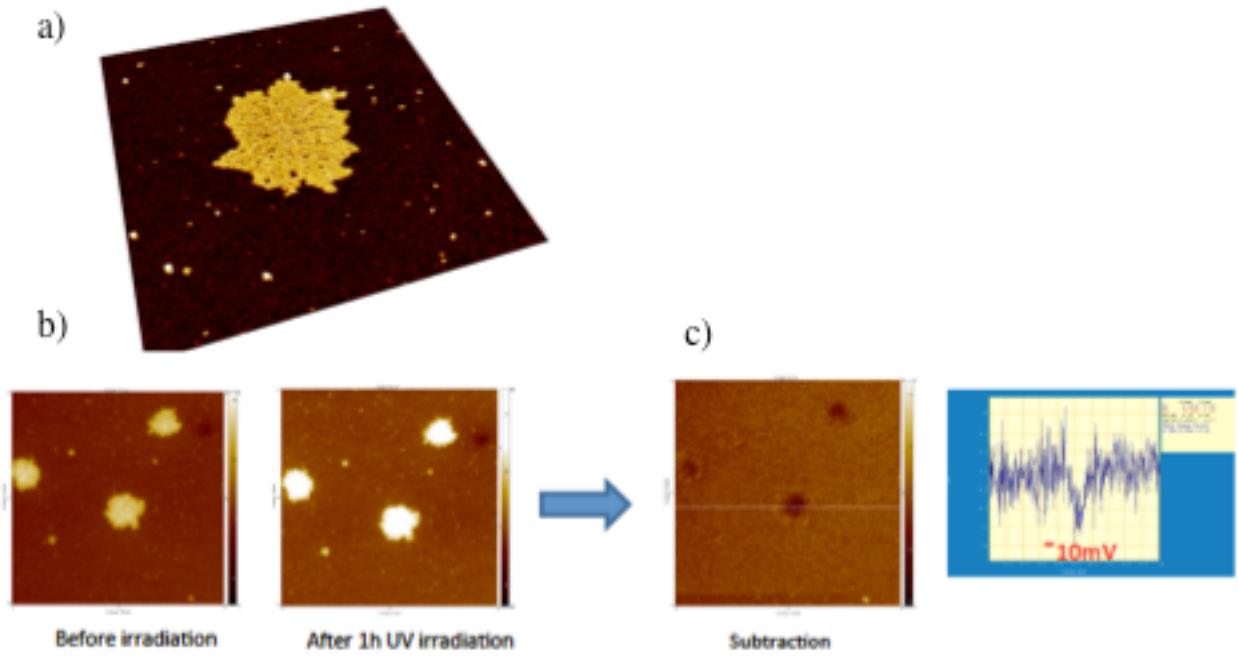

Fig 5.5 a) 3D rendering of an atomic force image of Disperse orange 3. b) Kelvin Probe Force analysis before and after irradiation with 365 UV light, in situ. c) Image manipulation with metrology software SPIP 6.

The data were treated with image metrology software Spip 6. The surface potential images were recorded before and after irradiation. The raw data were subtracted to avoid any contribution of the doping of the substrate. The final image was the result of the photoswitching contribution of the SAMs organized on the surface.

5.1.3. Self assembling of 3D structure of azobenzene

Using the right approach in solvent vapour annealing, with the right time was possible to tune the formation of big ordered assemblies which gave information how molecules arrange in macroscopical structures.

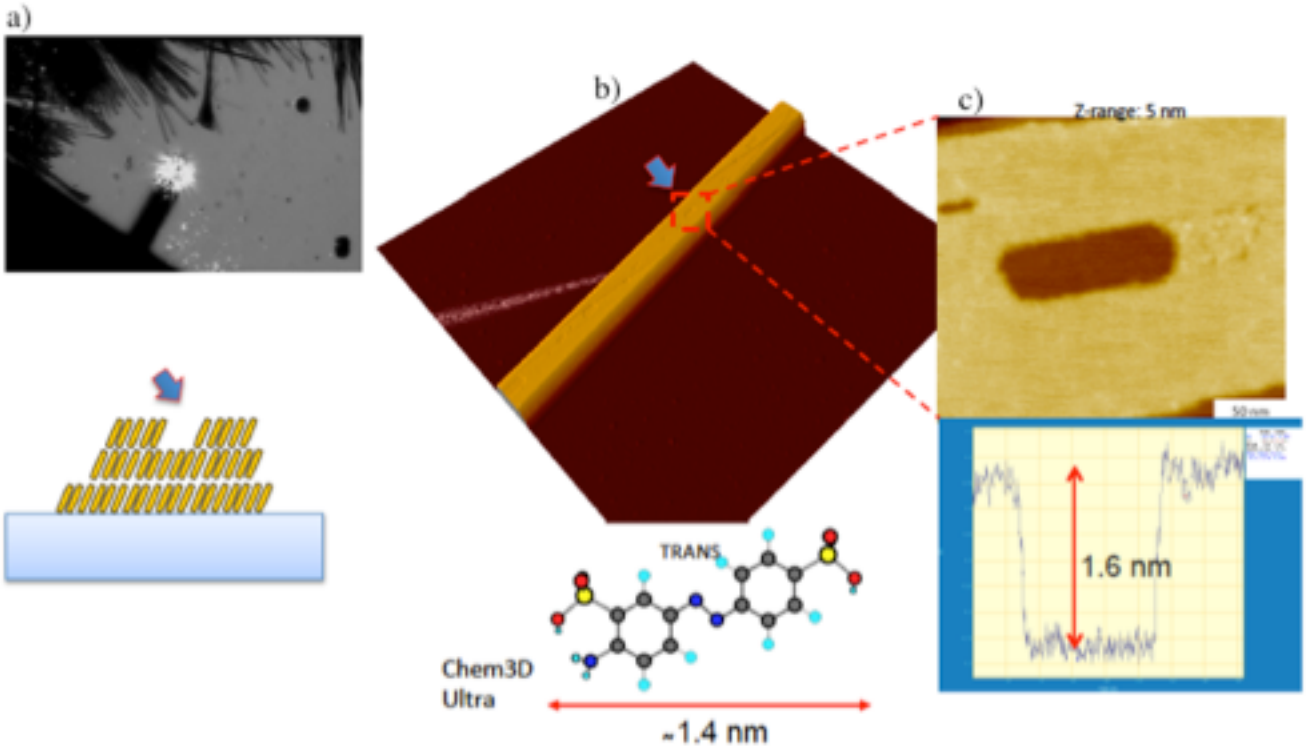

Fig 5.6 a) Optical image of Acid yellow 9 crystals obtained in solvent vapour annealing. b) 3D rendering of the needle like structure obtained in SVA with atomic force microscopy. c) AFM image and profile of Acid yellow 9 crystal of a formation hole with a deep in agree with the length of the molecule.

Crystals of Acid yellow 9, were obtained in water with a concentration of 1 gr/ml with an exposure time of 48h inside the box for solvent vapour annealing. The analysis of the crystals were performed to obtain informations about the displacement of molecules in highly ordered structure. In particular in Fig 5.6c) is shown a hole having a dept of 1,6 nm quitly in according with the total length of the molecules as calculated in Chem3D Ultra (1,6 nm respect to 1,4 nm). Probably the disposition of one row of molecules or a second row on the top of the prevois can give a good picture of how molecules self assembly in 3D structure.

5.2. Conclusions

In the second part of this PhD thesis were used as candidates azobenzenes to understand and manipulate molecules to produce ordered structures and surface modification. Thanks to the strong knowledge behind this molecules, strongly studied since decades, azobenzene were chosen to understand how the systems developed in our lab as Solvent Vapour Annealing could be applied to re-arrange azomolecules without any possible covalent functionalization. Unfortunately due to the non covalent functionalization was, in one way, easy to self assemble molecules to produce ordered island and highly ordered crystalline systems. In the second way, it was difficult to observe the photoswitching of the molecules. As in case of Acid yellow 9 where, the high dipole moment of the molecule, prevented the possibility to be seen in kelvin probe microscopy (due to the long time of image aquisition). Disperse orange 3 on the other hand was instead easier than the Acid yellow 9 to be seen in KPFM but without any type of covalent functionalization the switching trend of the molecules was always closely to the instrumental error of the microscope.

6. Experimental methods

6.1. Sinthesis of Silver nanocluster (IBAN) $Ag_{44}(4FTP)_{30}^{4-}$

The nanoclusters were prepared inside the SUNMIL group at EPFL in the Prof. Stelllacci group, whereby we collaborate with an European network "ISwitch".

Sinthesis of silver nanoclusters, "IBAN" intensely and broadly absorbing nanoparticle were synthesized as described by Bakr and coworkers.

The NP were prepared with a reduction of the silver trifluoroacetate solution with the presence of the capping ligand and PPh^{4+} counterions. We used as organic ligand a 4-fluorothiophenol (4FTP), which gives nanoclusters highly uniformly dispersed, which are stable in solution for years, at - 4° degree. 4FTP was stirred with the molar ratio 2:1 respect to the silver trifluoroacetate in N,N-dimethylformamide (DMF) for 15 min. Then a solution of NaBH4 in DMF was added with molar ratio 4:1 respect to the silver, the solution was stirred for 4h after a few amount of water was added to increase the reduction power of the NaBH4 and left in the fridge at -4°C for some days.

IBANs working solution were prepared using 5 mg of nanoclusters powder dissolved in 2 ml of solvent, in general acetone and dichloromethane. Stirred and sonicated for 30s.

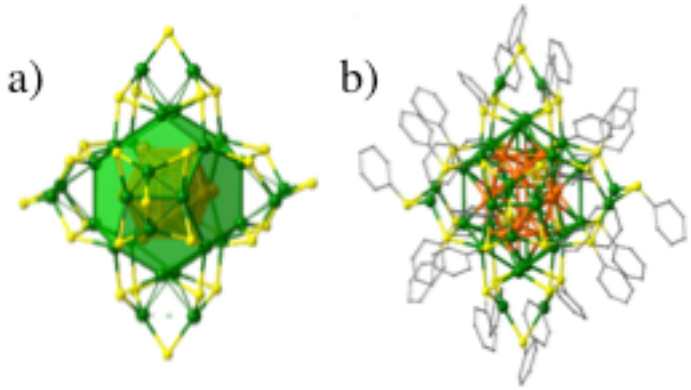

Fig 6.1 3D structure of $Ag_{44}(4FTP)_{30}^{4}$. a) Representation of the silver and sulphur displacement inside the IBAN. b) 3D structure surrounded by thiol ligands.

6.2. Acid yellow 9 and Disperse Orange 3

Acid yellow 9, 4-Amino-1,1′-azobenzene-3,4′-disulfonic acid monosodium salt, CAS number 2706-28-7, purity grade 95% was purchased from Sigma Aldrich.

Disperse Orange 3, 4-(4-Nitrophenylazo)aniline, CAS 730-40-5, purity grade 90 % was purchased from Sigma Aldrich.

Azobenzene solutions were prepared using 1 mg of powder in 100 ml of H_2O dist. and DMF stirred and sonicated for 30s.

6.3. Solvent Vapour Annealing apparatus

The solvent vapour annealing apparatus was created as described in [1,2]. A glass crystallizator with a volume of 300 ml was carefully cleaned and placed in a plane. Inside the vessel was inserted a platform with an height of 2 cm above the solvent front. Was added around 70 ml of solvent, in general dichloromethane or acetone. On the platform was deposited a silicon or silicon oxide square (1 x 1 cm). The whole box close in pressure and maintained closed for 30 min. After a drop of solution was deposited on silicon or silicon substrate ready for the macromolecular growth. The apparatus remain closed for 12 hours.

Solvent vapour annealing (SVA) was used to assemble the crystals, as described in referencence 2. 5 mg of IBAN were added in 2 ml of solvent, acetone or dichloromethane, and placed in the sonicator bath for 30s. SVA procedure was performed using a closed glass crystallizer. A drop of the solution previously prepared was positioned on a silicon wafer and deposited on a platform in the crystallizer, then the crystallizer was filled with 30 ml of solvent (acetone or dichloromethane). After 7 h, all samples were left to dry one day in atmosphere, to remove the solvent.

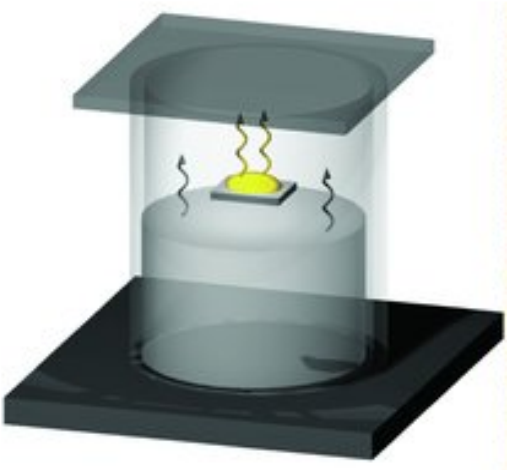

Fig 6.2 Schematic representation of the solvent vapour annealing apparatus and work of principle.[3]

6.4. Other methods

UV-vis spectroscopy measurements were performed using Perkin Elmer LAMBDA 650 spectrophotometer (deuterium and tungsten light sources), a high-performance double-beam dualmonochromator spectrometer with microcomputer electronics. Its wavelength range extends from 900 to 190 nm. Spectral band width in the UV-vis range is from 0.17 to 5.00 nm.

Wavelength range tested was 300-900 nm. The 24h solution monitoring were performed with Agilent CARY 100, double beam, dual chopper, ratio recording, Czerny-Turner 0.278 m monochromator UV-vis spectrophotometer, controlled by a computer.

Resonance light scattering spectroscopy (RLS) was performed using FLS920 Edinburg Instruments spectro fluorimeter with 450W Xenon lamp probe used for steady state experiments.

Signal detection was given by a photo-multiplier tube and a Time Correlated Single Photon Counting (TCSPC) with a MicroChannel plate.

Atomic Force Microscopy measurements were performed with a Digital Instruments AFM (Aura NT-MDT), using cantilevers in semi-contact mode (Bruker RTESP tips, material: 1-10 Ω▪cm phosphorus (n)- doped Si, f0 = 27–309 kHz, k = 20–80 N▪m-1). Raw AFM data were treated by using histogram flattening procedures[26] to remove the experimental artifacts due to the piezo-scanners.

Imaging: Data analysis was typically performed with SPIP (Image Metrology) software.

X-ray Photoemission Spectroscopy measurements were performed with a Phoibos 100 hemispherical energy analyser (Specs), using Mg Kα excitation source (XR-50, Specs) (photon energy = 1253.6 eV). The X-ray power was 250 W. The base pressure in the analysis chamber during analysis was $2*10^{-10}$ mbar.

Residual Gas Analysis (RGA) was done in the preparation HUV chamber of the XPS spectrometer (10^{-9} mbar) while heating the crystals from 25°C to 350 °C (5 °C/min). A quadrupole mass spectrometer was used (RGA 200, Stanford Research Systems), with an operative range of 0-200 amu.

X-ray Diffraction (XRD) measurements (out-of-plane geometry) were performed using SmartLab-Rigaku diffractometer equipped with a rotating anode (Cu λα = 1.5405 .), followed by a parabolic mirror to collimate the incident beam, and a series of variable slits (placed before and after the sample position)

Single Crystal X-ray Diffraction measurements were performed at the X-ray diffraction beamline (XRD1) of the Elettra Synchrotron, Trieste (Italy),[27] with a Pilatus 2M hybrid-pixel area detector.

Complete datasets were collected on the same crystal at 298 K and 400 K (nitrogen stream supplied through an Oxford Cryostream 700) with a monochromatic wavelength of 0.700, through the rotating crystal method. The crystal of $Ag_{44}(4FTP)_{30}$ was dipped in N-paratone and mounted on the goniometer head with a nylon loop. The diffraction data were indexed, integrated and scaled using X-ray Detector Software (XDS),[28] merging two datasets collected with different crystal orientations, at each temperature. The structures were solved using the dual space algorithm implemented in the SHELXT code.[29]

In-situ real time GISAXS measurements were performed at the beamline SAXS of ELETTRA synchrotron facility (Trieste, Italy) by using a wavelength of 1.54 Å and an incident angle, αi of 0.4°. GISAXS images were recorded for 30 seconds every minutes during the thermal annealing in nitrogen atmosphere and after the cooling. Different thermal ramps were carried out from room temperature up to 120°C, 180°C and 300°C. 2D camera (Pilatus detector) were placed normal to the incident beam direction at 600 mm from the sample.

Ex-situ XRD measurements. 2D-GIWAXS images were collected on the pristine and annealed samples at the beamline XRD1 of ELETTRA synchrotron facility by using awavelength of 1.542 αi was chosen slightly larger than the critical angle for total reflection of the crystals (0.3°), in order to penetrate through the full crystals depth. The diffraction patterns were recorded using a 2D camera (Pilatus detector) placed normal to the incident beam direction at 200 mm from the sample. XRD measurements, both in specular and grazing incidence geometries, were performed using a SmartLab Rigaku diffractometer in parallel beam geometry equipped with a CuKα (λ = 1.5418 .) rotating anode followed by a parabolic mirror to collimate the incident beam and a series of variable slits (placed before and after the sample position) to obtain an acceptance of 0.02° and 0.114°, respectively.

DFT simulations were carried out with the program CASTEP version 16.11.[17] Ultrasoft pseudopotentials were used in combination with a plane wave cutoff energy of 280 eV and the Perdew-Burke-Ernzerhof generalised gradient-corrected functional[30] to compute the ground-state wavefunction. In order to compensate for the known underestimation of Van deer Waals interactions, a semi-empirical dispersion-interaction correction[31] was used in DFT calculations. A Monkhorst-Pack grid[32] with a density of 0.05 $Å^{-1}$ was used for the sampling of k-points.

References

1. De Luca, G. *et al*. Solvent vapour annealing of organic thin films: controlling the self-assembly of functional systems across multiple length scales. *J. Mater. Chem.* **20,** 2493–2498 (2010).
2. Treossi Emanuele *et al*. Temperature-Enhanced Solvent Vapor Annealing of a C3 Symmetric Hexa-peri-Hexabenzocoronene: Controlling the Self-Assembly from Nano- to Macroscale. *Small* **5,** 112–119 (2009).
3. Wang Suhao *et al*. Self-Assembly and Microstructural Control of a Hexa-peri-hexabenzocoronene–Perylene Diimide Dyad by Solvent Vapor Diffusion. *Small* **7,** 2841–2846 (2011).
4. AbdulHalim, L. G. *et al*. A scalable synthesis of highly stable and water dispersible Ag44(SR)30 nanoclusters. *J. Mater. Chem. A* **1,** 10148–10154 (2013).
5. Bakr Osman M. *et al*. Silver Nanoparticles with Broad Multiband Linear Optical Absorption. *Angew. Chem.* **121,** 6035–6040 (2009).
6. Yang, H. *et al*. All-thiol-stabilized Ag44 and Au12Ag32 nanoparticles with single-crystal structures. *Nat. Commun.* **4,** 2422 (2013).
7. De Luca, G. *et al*. Orthogonal self-assembly and selective solvent vapour annealing: simplified processing of a photovoltaic blend. *Chem. Commun.* **49,** 4322–4324 (2013).
8. Spek, A. L. PLATON SQUEEZE: a tool for the calculation of the disordered solvent contribution to the calculated structure factors. *Acta Crystallogr. Sect. C Struct. Chem.* **71,** 9–18 (2015).
9. Kitaigorodskii, A. I. & Bureau, C. Organic chemical crystallography. (1961).
10. Landman, U. & Luedtke, W. Small is different: energetic, structural, thermal, and mechanical properties of passivated nanocluster assemblies. *Faraday Discuss.* **125,** 1–22 (2004).
11. Dance, I. G., Fisher, K. J., Banda, R. M. H. & Scudder, M. L. Layered structure of crystalline compounds silver thiolates (AgSR). *Inorg. Chem.* **30,** 183–187 (1991).
12. Boles, M. A., Engel, M. & Talapin, D. V. Self-assembly of colloidal nanocrystals: From intricate structures to functional materials. *Chem. Rev.* **116,** 11220–11289 (2016).
13. Hu, L. *et al*. Synthesis and Characterization of Single-Layer Silver–Decanethiolate Lamellar Crystals. *J. Am. Chem. Soc.* **133,** 4367–4376 (2011).
14. Baena, M. J., Espinet, P., Lequerica, M. C. & Levelut, A. M. Mesogenic behavior of silver thiolates with layered structure in the solid state: covalent soaps. *J. Am. Chem. Soc.* **114,** 4182–4185 (1992).
15. Hartmann, U. MAGNETIC FORCE MICROSCOPY. *Annu. Rev. Mater. Sci.* **29,** 53–87 (1999).
16. The GDIS Home Page. Available at: http://gdis.seul.org/. (Accessed: 4th October 2018)
17. Clark, D. T., Kilcast, D. & Musgrave, W. K. R. Molecular core binding energies for some monosubstituted benzenes, as determined by X-ray photoelectron spectroscopy. *J. Chem. Soc. Chem. Commun.* 516b – 518 (1971). doi:10.1039/C2971000516B
18. Lindberg, B. *et al*. Molecular spectroscopy by means of ESCA II. Sulfur compounds. Correlation of electron binding energy with structure. *Phys. Scr.* **1,** 286 (1970).
19. Hantsche, H. High resolution XPS of organic polymers, the scienta ESCA300 database. By G. Beamson and D. Briggs, Wiley, Chichester 1992, 295 pp., hardcover,£ 65.00, ISBN 0-471-93592-1. *Adv. Mater.* **5,** 778–778 (1993).
20. Gaarenstroom, S. & Winograd, N. Initial and final state effects in the ESCA spectra of cadmium and silver oxides. *J. Chem. Phys.* **67,** 3500–3506 (1977).
21. Ferraria, A. M., Carapeto, A. P. & do Rego, A. M. B. X-ray photoelectron spectroscopy: silver salts revisited. *Vacuum* **86,** 1988–1991 (2012).

22. Kang, H., Ito, E., Hara, M. & Noh, J. Formation of Ordered 4-Fluorobenzenethiol Self-Assembled Monolayers on Au (111) from Vapor Phase Deposition. *J. Nanosci. Nanotechnol.* **16,** 2800–2803 (2016).
23. Ramstedt, M. & Franklyn, P. Difficulties in determining valence for Ag0 nanoparticles using XPS—characterization of nanoparticles inside poly (3-sulphopropyl methacrylate) brushes. *Surf. Interface Anal.* **42,** 855–858 (2010).
24. Crivillers, N. *et al.* Large work function shift of gold induced by a novel perfluorinated azobenzene-based self-assembled monolayer. *Adv. Mater.* **25,** 432–436 (2013).
25. De Luca, G. *et al.* Non-conventional Processing and Post-processing Methods for the Nanostructuring of Conjugated Materials for Organic Electronics. *Adv. Funct. Mater.* **21,** 1279–1295 (2011).
26. Liscio, A. Scanning probe microscopy beyond imaging: a general tool for quantitative analysis. *ChemPhysChem* **14,** 1283–1292 (2013).
27. Lausi, A. *et al.* Status of the crystallography beamlines at Elettra. *Eur. Phys. J. Plus* **130,** 43 (2015).
28. Kabsch, W. Integration, scaling, space-group assignment and post-refinement. *Acta Crystallogr. Sect. D* **66,** 133–144 (2010).
29. Sheldrick, G. M. SHELXT–Integrated space-group and crystal-structure determination. *Acta Crystallogr. Sect. Found. Adv.* **71,** 3–8 (2015).
30. Perdew, J. P., Burke, K. & Ernzerhof, M. Generalized gradient approximation made simple. *Phys. Rev. Lett.* **77,** 3865 (1996).
31. McNellis, E. R., Meyer, J. & Reuter, K. Azobenzene at coinage metal surfaces: role of dispersive van der Waals interactions. *Phys. Rev. B* **80,** 205414 (2009).
32. Monkhorst, H. & Pack, J. Special points for Brillouin-zone integrations. (2005).

Conclusions

The supramolecular approach provides easy access to complex architectures holding several interesting properties useful in the frame of the emerging technologies, e.g. in the area of optoelectronics. The fabrication of self assembled species at surfaces is a prerequisite for the realization of working devices prototypes. Thus it is crucial to achieve a full control over the interplay between intramolecular, intermolecular and interfacial interactions in order to tailor complex 2D and 3D arrangements at will.

The PhD work concerned the study of self-assembled architectures at multiple length scales using a wealth of techniques spanning from nano- to microscale in order to correlate the local physico-chemical properties and their spatial distributions in films and nanostructures.

Tuning the molecule–molecule interactions, were produced organised assemblies with different size, dimensionalities (1D, 2D and 3D) and physico-chemical properties. In such cases, the self-assembly mechanisms were not assisted by the surface, being only governed by the geometry and the chemistry of the building block.

Two different monodisperse building-block model systems were exploited with a well-defined shape:

- Spherical nanoparticles (IBANs);
- Planar molecules (i.e. azobenzene molecules).

The highly symmetric structure of the IBAN allowed to realised layered (2D) and bulk (3D) superstructures with a lateral size up to several hundreds of microns having thermal stability (up to 300 °C) higher than the analogue superstructures colloidal assemblies.

In the thesis period was applied a particular technique act to manipulate molecules and aggregates, well established in our group, solvent vapour annealing, where tuning the solvent, time, temperature and pressure was possible to pilot the different morphologies.

We used as first model molecule IBAN, constituted by 44 silver atoms and surrounded by 30 external S-R ligands as an ideal building block. Different batches were tested showing always high stability in powder form (at -4°C in the freeze) as well as good monodispersity but when dissolved in acetone or dichloromethane the degradation start to begin. Although the good processability in the two solvents, silver nanoclusters were found lack in time life in solution, less in acetone than

dichloromethane. To know in the best conditions how these silver nanoclusters rearrange and degradate is the key factor for manipulate in order to create highly oriented structures with specific properties.

Triclinic and layered structures were obtained. Triclinic structure obtained also in previous articles[1,2], confirm the not denaturation of the silver nanoclusters without any chemical change of the silver core. However, when exposed to suitable solvents (in particular DCM) IBANs undergo a structural and chemical change, forming layered structures of oxidized silver atoms, bound together to form a continuous covalent structure protected on the upper and lower side by the thiol molecules. Such covalent 2D structures show a better order and thermal stability than the 3D supramolecular crystals.

2D structure that since the beginning[3] of the study of silver thiolates looked like an error, an impurity, but today with the great effort to graphene related materials, seems a promising new route to produce a new chemical 2D platform useful in particular for heterojuctions.

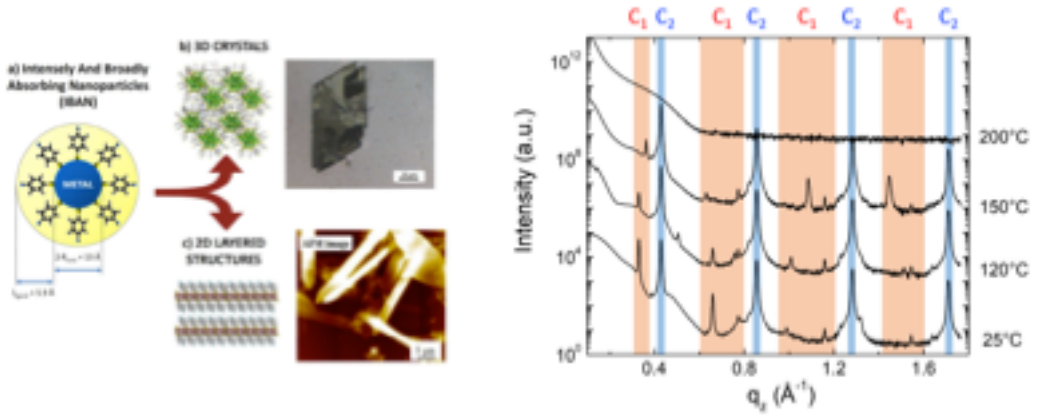

Fig 7.1 . a) Cartoon of Silver Nanocluster, b) rearrangement in 3D structure in optical microscopy, c) 2D self assembly in AFM image and molecular simulation. On the Right side: XRD measurements acquired at different annealing temperatures.C_1 triclinic structures, C_2 layered structures.

Supramolecular chemistry was also used to manipulate azobenzene molecules tuning the morphology and the electrostatic interactions on the surfaces. The removing of the thiol groups from the molecules allowed to neglect the interaction of the substrate allowing to realise self-assembled systems on different substrates such as gold, silicon, glass, etc. without any covalent functionalization. The increase of the degree of freedom in the molecular packing corresponded to more complex architectures of azobenzene compounds with respect to the case of the SAMs described before. This reflected on a wider behaviour of the switching response of the self-assembly when illuminated by UV light. AFM and KPFM directly showed that such architectures are polycrystalline and only some clusters photoisomerised.

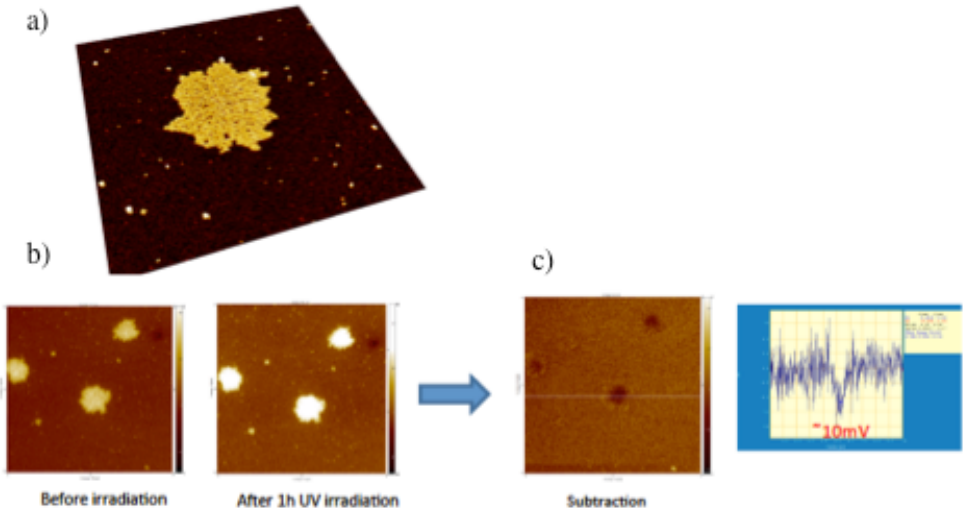

Fig 7.2 a) 3D AFM of Azobenzene Disperse Orange 3; b)c) KPFM images before and after UV irradiation and subtracted image with histogram.

References

1. Yang, H. *et al*. All-thiol-stabilized Ag44 and Au12Ag32 nanoparticles with single-crystal structures. *Nat*. *Commun*. **4,** 2422 (2013).
2. Harkness, K. M. *et al*. Ag44(SR)304–: a silver–thiolate superatom complex. *Nanoscale* **4,** 4269–4274 (2012).
3. Dance, I. G., Fisher, K. J., Banda, R. M. H. & Scudder, M. L. Layered structure of crystalline compounds silver thiolates (AgSR). *Inorg*. *Chem*. **30,** 183–187 (1991).

Acknowledgements

The journey towards the thesis completion has not always been smooth and easy and, without the help of many people who deserve my gratitude, I would never have reached the final goal.

First of all, I want to thank Dr. Andrea Liscio for helping me during my PhD period in the Nanochemistry Lab at ISOF CNR of Bologna. I want to thank him for his advices… a lot, in particular for the nanoworld of Scanning Probe Microscopy, for his patience and support during my PhD inside the European project ISwitch. Really Thank you Andrea.

I would like to thank Prof. Vincenzo Palermo for his precious help and for stimulating scientific discussion and for helping me to find the right way to follow. Thank you Enzo.

I wish to thank Prof. Loris Giorgini, for supervising me during my PhD period during these three years and for the useful discussions and help. Thank you Loris.

To my group at ISOF CNR inside the Nanochemistry Lab I want express all my gratitude, for encouraging me during these years and for the beautiful moments spent togheter inside and outside the lab. Thanks to Vanesa Quintano Ramos, Nicola Mirotta, Kostas Agalou, Jeffrey Xia, Alessandro Kovtun, our super project manager Maria del Rosso, Alessandra Scidà and Emanuele Treossi, without your help would not have been the same. Thanks ragazzi!!

A special thanks goes also to all the guys met during the ISwitch project, that have created a fantastic atmosphere rich of friendship and right competition. Thanks to Jasmin Santoro, Thomas Mosciatti, Giovanni Cotella, Aurelio Bonasera, Sergio Allegri, Vitalij Parkula, Anna Murello, Agostino Galanti, Marco Cairoli, Maria Serena Maglione, Ana Margarida Santiago da Silva, Urszula Cendrowska, Qiankun Wang, Ian Yi Hou and Valentin Cabanes.

A special mention to Simone Ligi and Cristian Trevisanut for helping and bearing me during the writing period, in particular with the new job at Graphene-XT. Grazie mille ragazzi.

A special thanks also goes to my family because without them I would never have been here. From my hearth Grazie.

Finally I would say thank you to all the guys who contribute actively to the project: Fabiola Liscio, Roberta Chiodini, Enrico Leoni, Filippo Monti, Francesco Manoli, Massimo Cocchi, Francesco Stellacci, Heinz Amenitish, Cristiano Albonetti, Manuela Meluc